Scalable Distributed Networked Haptic Cooperation

by

Ramtin Rakhsha

B.Sc., University of Tabriz, Iran, 2004

M.Sc., University of Tehran, Iran, 2007

A Dissertation Submitted in Partial Fulfillment of the

Requirements for the Degree of

DOCTOR OF PHILOSOPHY

in the Department of Mechanical Engineering

Scalable Distributed Networked Haptic Cooperation

by

Ramtin Rakhsha

B.Sc., University of Tabriz, Iran, 2004

M.Sc., University of Tehran, Iran, 2007

Supervisory Committee

Dr. Daniela Constantinescu, Co-supervisor

(Department of Mechanical Engineering)

Dr. Yang Shi, Co-supervisor

(Department of Mechanical Engineering)

Dr. Afzal Suleman, Departmental Member

(Department of Mechanical Engineering)

Dr. Panajotis Agathoklis, Outside Member

(Department of Electrical and Computer Engineering)

Supervisory Committee

Dr. Daniela Constantinescu, Co-supervisor
(Department of Mechanical Engineering)

Dr. Yang Shi, Co-supervisor
(Department of Mechanical Engineering)

Dr. Afzal Suleman, Departmental Member
(Department of Mechanical Engineering)

Dr. Panajotis Agathoklis, Outside Member
(Department of Electrical and Computer Engineering)

ABSTRACT

In cooperative networked haptic systems, some distributed distant users may decide to leave or join the cooperation while other users continue to manipulate the shared virtual object (SVO). Cooperative haptic systems that support interaction among a variable number of users, called *scalable* haptic cooperation systems herein, are the focus of this research. In this thesis, we develop distributed control strategies that provide stable and realistic force feedback to a varying number of users manipulating a SVO when connected across a computer network with imperfections (such as limited packet update rate, delay, jitter, and packet-loss).

We first propose the average position (AP) scheme to upper bound the effective stiffness of the SVO coordination and thus, to enhance the stability of the distributed

multi-user haptic cooperation. For constant and small communication delays and over power-domain communications, the effectiveness of the proposed AP paradigm is compared with the traditional proportional-derivative (PD) scheme via multi-rate stability and performance analyses supported with experimental verifications.

Next, in a passivity-based approach, the scalability is pursued by implementing the AP scheme over wave-domain communication channels along with passive simulation of the dynamics. By constructing a passive distributed SVO in closed-loop with passive human users and haptic devices, we guarantee the stability of the distributed haptic cooperation system. However, energy leak at joining/leaving instances may compromise the passivity of the SVO. We examine the preservation of passivity of the proposed SVO scheme for such situations. A switching algorithm is then introduced in order to improve the performance of the cooperative haptic system. Experiments in which three users take turn in leaving or joining the cooperation over a network with varying delay and packet-loss will support the theoretical results.

Contents

List of Tables

List of Figures

ACRONYMS

VE	Virtual environment
SVE	Shared virtual environment
VO	Virtual object
SVO	Shared virtual object
AP	Average-position
PD	Proportional-derivative
LTI	Linear time-invariant
TDPC	Time-domain passivity control
PO	Passivity observer
PC	Passivity controller
PH	Port Hamiltonian
EBA	Energy bounding algorithm
LAN	Local area network
MAN	Metropolitan Area Network
WANem	Wide area network emulator
RDP	Remote dynamic proxy
PSPM	Passive-set position modulation
PCDC	Passive continuous-discrete time connector
SISO	Single input single output
MIMO	Multi input multi output

DEDICATION

Words fail to express my sincere love and appreciation to my family for their unconditional love and support. Baba, you set a unique role model in my life with your kindness and dedication to family. Ashi, you have always been a source of inspiration, forgiveness, and determination for me. Ramin, thanks for being an encouraging and supportive brother.

ACKNOWLEDGEMENTS

It is my pleasure to express my appreciation to my supervisors Dr. Daniela Constantinescu and Dr. Yang Shi for their continuous motivation and support throughout my PhD research. I also wish to extend my thanks to the members of my committee Dr. Afzal Suleman and Dr. Pan Agathoklis for their insightful comments during the course of my PhD program.

My sincerest gratitude goes to my beloved Mana, for her love, support, and devotions throughout the ups and downs of this period of my life. ♡

I owe my most gratitude to my dear friend, Dr. Naser Yasrebi - a source of friendship and inspiration. Thank you for making my way to UVic easy and pleasant.

I would like to make a special reference to Dr. Amirali Baniasadi, for his time and excellent guidances during the tough days. His precious role for Iranian students in UVic is undeniable.

And at last, to my friends and colleagues in UVic - thank you for the friendship that made it a joy to be in graduate school. Abbas Khorram, thank you for being a good listener and supporter. Nima Khadem-Mohtaram, thank you for the laughter.

Chapter 1

Introduction

In the late 80's and early 90's, teleoperation and virtual reality researchers started to provide touch and kinesthetic sensations to users interacting with remote and virtual environments. These sensations have been conveyed to users via vibration and force feedback applied through robotic computer interfaces called haptic devices (or displays). Depending on whether they measure position or force, haptic devices can be categorized into: (i) impedance interfaces, which measure position and apply force; and (ii) admittance interfaces, which measure force and display position. Impedance haptic displays are far more common than admittance haptic devices. Therefore, this work focuses on force feedback provided to users through impedance haptic interfaces.

Remote touch, provided through bilateral teleoperation, offers physical access to hazardous worksites where human health is threatened by fire, radiation, etc. Virtual touch, provided through haptic rendering of virtual environments (VEs), is beneficial in virtual reality applications like: surgical training with force feedback from a physically accurate virtual human organ; feeling virtual textures and objects in video games; therapy and rehabilitation programs that apply forces to patients to guide them along desired motions. Among these applications, haptic interfaces have

already been commercialized as medical training interfaces. On-line video gaming with force feedback is another important potential market for haptic technologies and motivates the work proposed of this thesis.

A single-user haptic system comprises a human user, a haptic display, a VE simulation and control algorithms [1] (Figure 1.1). The haptic interface senses the user's action, sends it to the VE, receives the reaction of the VE and applies it to the user. The simulation computes the motion/deformation of the VE in response to the user's action. The control algorithm maintains the interaction stable and renders the VE reaction to the user as faithfully as possible. The realism of the user's kinesthetic perception in the VE depends on the physical accuracy of the simulation algorithms and on the stability and transparency of the haptic feedback loop. Because unstable haptic feedback may injure the users and damage the haptic system, stability is critical in haptics. Yet, guaranteeing the stability of the haptic interaction with the VE is not trivial. This is because the haptic feedback loop includes the user (whose continuous-time dynamics are often time-varying and uncertain), coupled via the continuous-time haptic device and the VE (whose dynamics are simulated in discrete-time and may be non-linear) and, thus, forms a sampled-data system with variable and uncertain parameters [24]. Transparency measures how accurately the controller applies the simulated interaction forces to the user. Transparency is important for the user's sense of presence in the VE, i.e., their sense of interacting with a real environment. Guaranteed stability and transparency are conflicting requirements for haptic systems [53] - a perfectly transparent haptic system is not guaranteed stable.

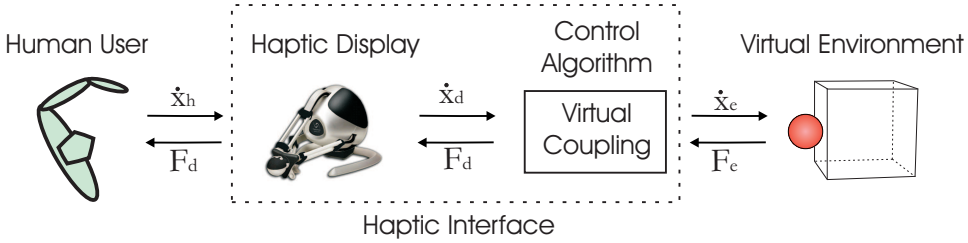

Figure 1.1: Single user haptic system.

A multi-user cooperative haptic system comprises several single-user haptic systems connected over a computer network via a coordination control algorithm. The coordination controller permits the users to share a VE haptically, i.e., to interact through forces with each other directly and to touch and manipulate virtual objects together. Multi-user haptic systems rely on: (i) client-server communications and centralized coordination control strategies (Figure 1.2a); and (ii) peer-to-peer communications and distributed coordination control architectures (Figure 1.2b). When connected via client-server communications, users send their motion information to a central server which simulates the centralized virtual environment and sends interaction forces back to all users. When connected via peer-to-peer communications, each user simulates a local copy of the shared virtual environment (SVE) and sends their motion information to other peers. Peer-to-peer architectures are often preferred since they can support haptic cooperation in much stiffer VEs because they suffer only half the communication delay of client-server architectures [28].

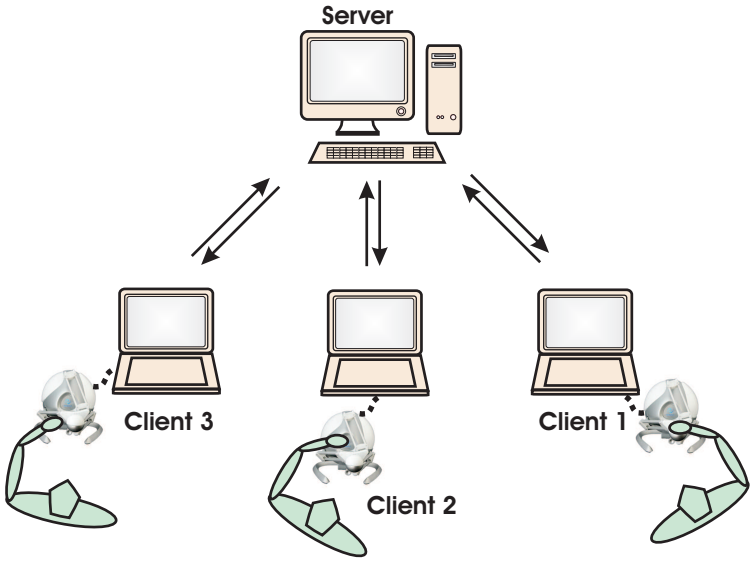

(a) Centralized

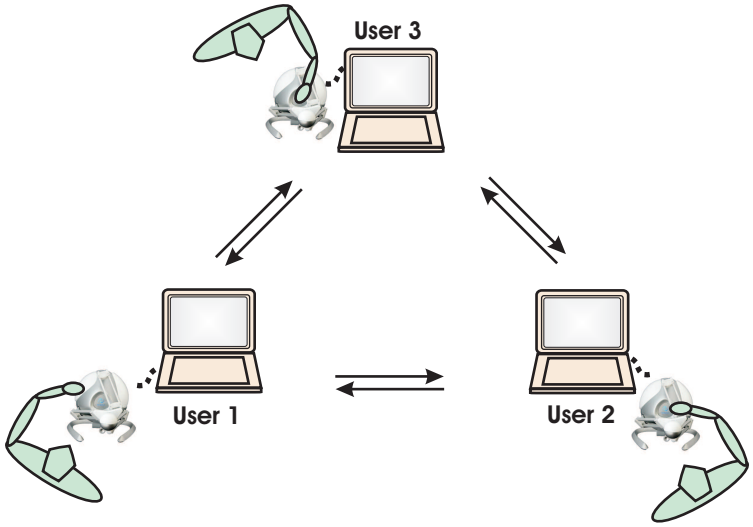

(b) Distributed

Figure 1.2: Networked haptic interaction supported through: (a) client-server communications and centralized coordination control; (b) peer-to-peer communications and distributed coordination control.

Cooperative networked haptic interaction is important in applications like: teletherapy [98], where it permits medical personnel to provide physical assistance to remote patients; collaborative surgical training [9], where it allows expert surgeons to remotely supervise medical interns; haptically-enabled multi-user on-line computer games [51], where it enhances the sense of presence in the virtual environment through

kinesthetic sensations. However, network communications introduce delays, jitter and packet-losses in the multi-user haptic feedback loop, and can easily destabilize the cooperation. Significant research effort has been dedicated to stabilizing the haptic cooperation among networked users. Mostly two-users cooperative haptic systems have been reported to date [28, 48]. The stability of multi-user cooperative haptic systems has only recently started to be studied [39, 46, 47]. In cooperative networked haptics applications, some distributed distant users may decide to leave or join the cooperation while other users continue to manipulate the shared virtual object (SVO) (see Figure 1.3).

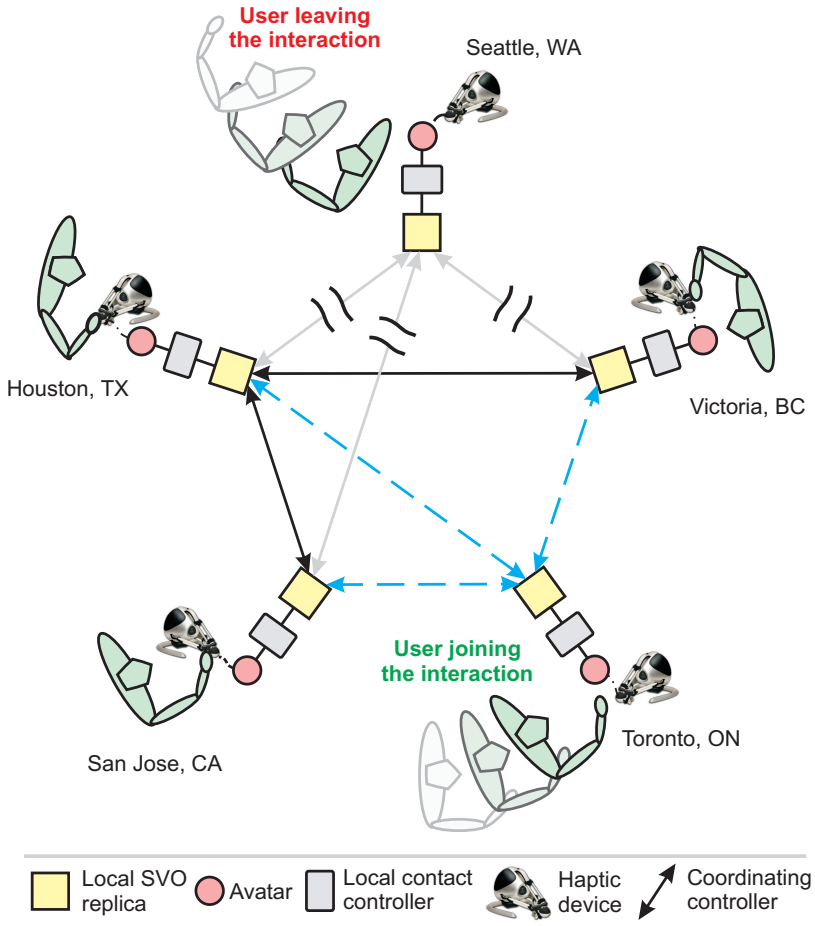

Figure 1.3: Distributed haptic cooperation among a varying number of users. The virtual object is shared among geographically distributed distant peers some of whom may join or leave the cooperation.

For instance, in a haptically-enabled online video game with haptic feedback, players may want to join their teammates in a battlefield. Little research [39] focuses on permitting users to join or leave the interaction. Cooperative haptic systems that support interaction among a variable number of users, called *scalable* haptic cooperation systems herein, are the focus of this research.

1.1 Challenges

In recent years, shared virtual environments implemented over the Internet have attracted great interests because they can potentially support force-based interactions among a large group of users. However, the non-deterministic nature of the Internet (such as jitter, delay, and packet-loss) adversely affects the stability and transparency of the distributed networked-based multi-user haptic cooperation. Delay causes the feedback force to lag behind the operator command, which results in unwanted oscillations and instability [3,17,42,65]. Furthermore, delay prompts discrepancy between different copies of the SVO which degrades transparency [15, 28, 91]. The variation of the network delay (i.e. jitter) poses stability and fidelity challenges on cooperative haptics over the Internet [36, 77]. Packet-loss threatens stability [37, 43] and also impairs the users' perception of the shared virtual environment [64, 65]. Packet-loss can be treated with the techniques developed for varying delays and thus, all theoretical conclusions arising from the treatment of varying delays apply to packet-loss.

In the haptic cooperation, the number of participants varies when: operators log-in/depart the network; or communication blackout or device failure occurs. For distributed haptic cooperation systems with a varying number of users, despite the difficulties due to the characteristics of the communication channels, there are key challenges that the proposed work needs to overcome. A change of the number of

users may lead to:

- *changes in the communication network topology*[1]: Establishment/deletion of the communication channels endangers stability [16,39,61]. In fact, the coordinating controller (often of PD-type) is built on the top of the communication topology (see Figure 1.3) that makes design of the coordination architecture dependent to the network topology;

- *modification of coordination controller gains*: The impedance of the coordination controllers may exceed the Z-width[2] [23] of the haptic displays. The variation of the coordination gains of the SVO may exceed the stable upper bound [80], resulting in instability of the SVO;

- *variations in the dynamics of the SVO copies*: As the number of operators increases, the division of the VO mass among users' copies may result in instability if the mass of the local SVO copies becomes smaller than the minimum mass [14]. Besides, the variation of the mass is directly reflected in the dynamics of the SVO copies at the leaving/joining instances which brings up performance concerns.

Hence, for safe and effective operation, it is desirable to develop a scalable control strategy that can guarantee the stability of the haptic cooperation with a varying number of participants.

[1]Network topology is a mathematical model that defines how the distributed agents (e.g, SVO copies) are arranged to interconnect and exchange information.

[2]The dynamic range of mechanical impedance exhibited by a haptic device (Its range may vary from next to zero in complete freedom to near infinity in full contact).

1.2 Objectives

The goal of this research is to develop a distributed control strategy that can provide stable and realistic force feedback to a varying number of users manipulating a SVO when connected across a computer network with imperfections (such as limited packet update rate, delay, jitter, and packet-loss). Specifically, scalability will be pursued via relaxing the dependency of the controller and of the VE on the participant count.

1.3 Contributions

The contributions of this thesis are two-fold:

- In Chapter 3, the average position (AP) scheme is proposed to upper bound the effective stiffness of the SVO coordination and thus, to enhance the stability of the distributed multi-user haptic cooperation. Over power-domain communications with limited update rate, the conventional proportional-derivative (PD) may destabilize distributed multi-users force interactions because its effective coordination gain increases with the participant count. For constant and small communication delays, the effectiveness of the proposed AP paradigm is compared with the PD scheme via multi-rate stability and performance analyses supported with experimental verifications.

- In Chapter 4, the AP scheme is developed for wave-based communications with time-varying delays and packet-losses, leading to a passive framework for SVOs. The proposed passive architecture decouples the design of the coordinating controllers from the communication network and thus, allowing for the selection of coordination gains independent of the number of cooperating peers. However, passivity may not be maintained when the cooperating participants leave

or join the network since, energy quanta may be extracted from or injected in the reaming SVO system via temporary open ports. Chapter 5 examines the preservation of passivity of the proposed SVO scheme for such situations. A switching algorithm is then introduced in order to improve the performance of the cooperative haptic system. Experiments in which three users take turn in leaving or joining the cooperation over a network with varying delay and packet-loss will support the theoretical results.

1.4 Outline

A literature review of the existing related research to this thesis is presented in Chapter 2. In Chapter 3, a distributed coordination architecture (i.e, the average position (AP) strategy) is proposed which lets to upper bound the effective stiffness for SVO and thus, allowing for the selection of the controller gains independent of the number of distributed users. However, when implemented on unreliable communication networks, the haptic cooperation with the proposed AP architecture can easily become unstable. In a passivity approach in Chapter 4, we introduce an n-port passive SVO which in close-loop with passive human users and haptic devices guarantees the overall stability over uncertain communication networks. In Chapter 5, we investigate the passivity maintenance of the proposed architecture in Chapter 4 when the number of cooperating users varies. This is followed by concluding remarks and future works in Chapter 6.

Chapter 2

Networked Haptic Cooperation - Literature Review

In teleoperation systems, users (residing at master side) can touch, manipulate and explore the remote environment (slave side). In haptics, virtual objects (VOs) in virtual environment (VE) are in analogous role with remote sides in teleoperation systems. Figure 2.1 depicts an analogy between teleoperation and haptic systems. Operators

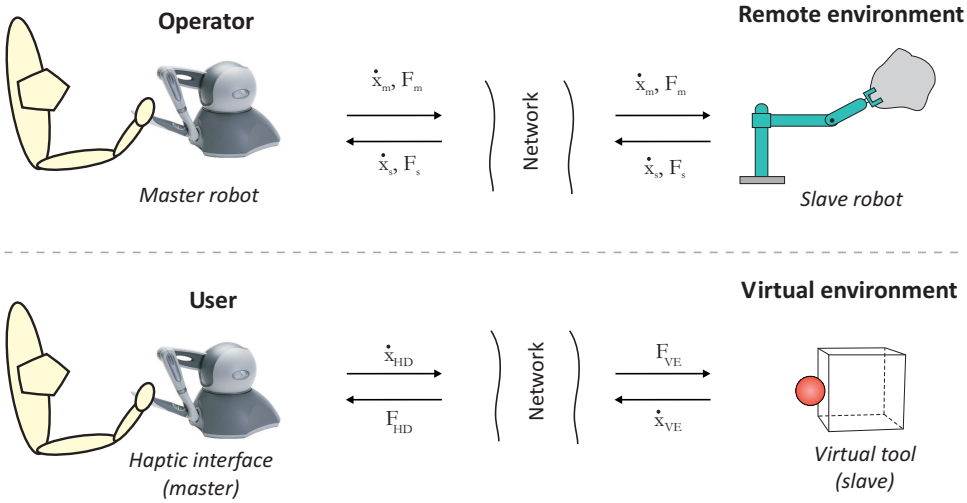

Figure 2.1: Analogy between a teleoperation and a haptic system.

and remote/virtual environments are interconnected in a feedback loop through the

communication medium. Forces from remote/virtual environments are fed back to the human operators to provide the sense of touch. However, the feedback forces may be affected by communication limitations (e.g: latency, jitter, and packet-loss) that result in unwanted oscillations and ruin the sense of telepresence. From the control point of view, the foremost and primary goals in haptic/teleoperation systems are to satisfy two conflicting requirements: *stability* and *transparency*. In a transparent system, the human user should be able to feel the contact force as if they were manipulating the virtual/remote object directly. Transparency is a measure to evaluate the performance of the control architectures via the assessment of how truthfully the impedance of the real/virtual environment is transferred to the human users. Different control techniques have been utilized to stabilize the time-delayed teleoperation systems. Relevant literature can be categorized as: (i) *Conventional controllers* such as Lyapunov approach [22,78,105] and, proportional-derivative (PD) controllers [45,75]; (ii) *Robust controllers* in which scattering [31,32], sliding mode [76], and H_∞ frameworks [90] are used for robust control of bilateral teleoperators over Internet; and (iii) *Adaptive controllers* as alternative to trade-off between stability robustness and performance [21,34,62,95,105] and; (iv) *Passivity-based controllers* [11,49,56,72,87,97] in which, passivity techniques are employed to provide sufficient conditions for stability. All these control paradigms for bilateral teleoperators are mostly applicable to haptic systems too. Next, we firstly review the state of the art of passivity-based bilateral teleoperation systems and then, after a brief introduction on multi-rate haptics, will focus on multilateral teleoperation and mutli-user cooperative haptics over Internet and the possibility of employing passivity approaches for such systems.

2.1 Passivity-based controllers

Passivity-based controllers monitor and control the flow of energy between different system components. They benefit from the fact that the feedback interconnection of passive systems is passive and thus stable [100]. Passivity is a sufficient condition for stability which does not require the models of operators and remote environments and is also applicable to linear and nonlinear systems. In literature, the remote environments and human users are assumed to be passive systems and hence, ensuring the passivity of the telemanipulation controller guarantees the overall stability. However, how to maintain the passivity of the telemanipulation over unreliable communication channel remains a challenging issue.

Scattering theory was firstly used by Anderson and Spong [5] to build a passive communication channel to cope with constant time-delay impairments on bilateral teleoperation systems. Reformulating the scattering theory, the *wave variable*-based approach was introduced by Niemeyer and Slotine [72] to make the communication channel a passive network element. These architectures guarantee the stability of teleoperation systems independent of constant transmission delay, presupposing the passivity of the rest of the system. However, since no explicit position signal is transmitted via wave-based communications, the original wave method results in position drift due to the mismatched position/force information between the master and slave sides. Remedies to improve the performance include: the transmission of the explicit position signal and drift error by employing *wave integrals* and adjusting the wave command [73] and; the use of Smith predictors [18]. The wave method was also extended for varying delays and packet-losses in [19, 94].

In time domain, a passivity approach was proposed in [87] by Ryu *et al.* in which, the time domain passivity control (TDPC) paradigm [33] was applied to bilateral teleoperation. The TDPC algorithm detects the active behaviour of the system through

an on-line passivity observer (PO) by monitoring and measuring the energy flow into the communications. The passivity controller (PC) adapts the injected damping to dissipate the excess of energy when observed by PO. This algorithm requires simultaneous information about the exchange of energy at the master and the slave sides which makes such approach not applicable to systems with time-delayed communication line. An energy reference algorithm was later introduced by Artigas *et al.* in [11] to estimate the energy of the communication channel based on the locally exchanged power variables at master/slave sides. According to the active behaviour observed by PO at each side, PC maintains the passivity. For unreliable communication channel with time-varying delays and packet-losses, Ryu *et al.* [85, 88] split the energy flow into the communication channel at each port side to incoming (E_{in}) and outgoing (E_{out}) energy flow. At each side, the passivity is maintained by a PC if the difference between E_{out} and E_{in} shows energy generation. Generally, TDPC approach suffers from the lack of an analytical performance (transparency) measurement method. Besides, the time domain approach is a "watch-and-act" policy in which, PO detects non-passive behaviour and then PC strives to compensate for it. This may create noisy behaviour specially when the haptic device's motion is small and PC needs to compensate for positive (i.e., active) values of PO.

The energy bounding algorithm (EBA) was proposed in [49] in which, the EBA limits the generated virtual energy to the physical dissipated energy in the master/slave robots. Since this technique requires models of viscous friction in the robots, deviation of the model from the actual physical friction can easily endanger the stability.

In a different approach, Lee *et al.* [56] introduced the passive set-position modulation (PSPM) framework in which, a virtual damper (i.e, derivative gain) stores the dissipated energy in an energy tank to limit the discrete jump of the potential energy

stored in the spring-like (i.e, proportional) controller. But, the PSPM design relies on a constant damping value to dissipate and extract energy into the energy tanks. This corresponds to always dampening the action, resulting to an over-damped response of the system. To improve the transparency, in a similar work, Franken *et al.* [30] combined the passivity and the transparency of the teleoperation system by defining two layers, i.e: *top layer* that implements the desired transparency and; *lower level* whose role is to maintain the passivity by employing energy tanks and ensuring that no virtual energy is generated. The design in their approach was independent of time delay in the communication channel.

In [97], it is shown how to preserve the passivity of interconnection of continuous- and discrete-time Port-Hamiltonian systems while matching the power-flow at their interface. In that approach, the passivity of telemanipulation was guaranteed independent of the sampling period. A strategy was introduced to maintain the passivity of the wave-based communication channel under variable time delays and packet loss. The proposed policy decides to pick null packets at the time instances when empty packets[1] are detected at the receiver side. The out of order packets get discarded and are replaced with null packets. However, the technique suffers performance downturn as the decoded zero-valued wave data result in energy dissipation and dampen the motion.

Passivity method has also been applied to the haptic systems in literature. Passivity condition presented by Colgate *et al* [23, 24] offers the largest achievable stiffness of the virtual object which is limited by the sampling rate and the device's inherent damping. Miller *et al* in [68] incorporated device damping to derive the sufficient conditions for passivity of haptic systems. Time domain passivity approach was used by Hannaford and Ryu for haptic systems [33]. Wave variable transformation was utilized

[1]Empty packets detected at the receiver sides are due to: varying delay; and/or packet drop-out

as a control strategy for single-user haptic systems [25, 26, 57]. The Port-Hamiltonian technique was employed to obtain passive haptic display for any physical virtual environment and for any sample period [97]. The major disadvantage of passivity-based method is its too conservative stability conditions that incurs poor performance in many cases.

2.2 Multi-rate haptics

In haptic systems, the servo-loop rate is typically set to 1 kHz to deliver high fidelity force feedback to human users. However, a fast haptic rendering rate may not be achievable when virtual environments are complex (such as deformable objects) and/or implemented over the network. The slow update rate of the VEs bounds the stable contact/coordination stiffness and thus, degrades the fidelity of haptic feedback. To address such issues, multirate simulation techniques have been introduced for:

- *slowly updated VEs* in which, the perceived contact stiffness by the users is enhanced either by increasing the sampling frequency of the VE [27, 50, 63] or, by dissipating the virtual generated energy via the following methods: frequency domain analysis [67], time-domain passivity-based multi-rate approaches [13, 56, 86, 89, 97], or multi-rate wave-domain schemes [41, 103];

- *networked-based VEs* for which, the multi-rate stability and transparency of haptic cooperation is studied in [28] for both centralized and distributed VEs when implemented over power-domain networks with constant time-delays and limited packet update rate. Passive multi-rate wave-domain communication was later introduced for centralized [102] and distributed haptic cooperation [81, 82].

2.3 Multi-user cooperative haptics

In recent years, teleoperation systems have been emerging into multiuser systems in which, single/multiple users cooperatively manipulate a remote environment via single/multiple remote users. Unlike traditional teleoperation systems with one single complex remote robot, multiple simpler robots collaborating as a group can accomplish tasks more efficiently. Such systems feature more robustness since they are easier to be repaired or replaced. Some recent research on collaborative teleoperation systems are discussed next. A multilateral shared control architecture for dual-master/single-slave teleoperation system is proposed in [47] in which, a dominance factor [74] defines the level of authority of the master users over the slave robot and the environment. Both force and position information are exchanged between the two master and slave robots, constructing a six-channel control architecture that not only allows for interaction with the slave robot, but also between the master users.

From the network prospective, any multiple-master/multiple-slave teleoperation system can be cast into an interconnection of smaller networks whose control design is analogous to the coordination/consensus problem of multiple agents (i.e, robots) exchanging information via a graph. In cooperative haptic systems, however, the continuous-time agents do not actually exist and instead, the SVO copies correspond to the agents whose second-order dynamics are modelled in discrete-time. Therefore, the problem of distributed haptic cooperation inherits challenges that demand different approaches than in multirobotic systems.

Passivity-based control has been proved to be a useful approach for the problem of motion coordination of multi-agent systems [10, 20, 29]. In particular, Arcak in [10] separated the dynamics of the agents from their kinematics reframing the system as two feedforward and feedback subsystems respectively. Storage functions for both subsystems were used to assess their level of passivity and in close-loop, ensuring the

overall stability. When applied onto the SVO system, the feedback path exhibits lack of passivity due the discrete-time forward-Euler integration. For close-loop passivity, however, it is not clear how to provide excess of passivity in feedforward subsystem to compensate the shortage of passivity of the feedback path. In a continuous-time settings, Chopra *et al.* in [20] used Lyapunov function candidates to investigate the passivity-based control for output-synchronization of multiple passive nonlinear agents over switching network topologies with communication delays. Yet, their work was built based on the assumption of passive agents which makes it inapplicable to the problem of SVO design. In a single-master/multi-slave teleoperation framework, Franchi *et al* [29] introduced a decentralized control scheme navigating a group of robots (treated as slave side) to avoid obstacles via maintaining a formation at the remote side. In a leader-follower like modality, the action of a single master robot is dispatched to one member of the remote robots (i.e, leader) whose motion is also influenced due to interacting with its neighbouring robots in the group. Arbitrary split/join of the mobile robots in the remote group is made possible via passivity-based control techniques. Interconnection of a passive master robot with a passive slave robot-group via passive communication channels can ensure the closed-loop stability. However, the technique preserves the passivity of the remote group with underlying switching topology only for fixed number of mobile robots. Besides, no transmission delay is considered for inter-agent interactions. In [99], a similar but simplified scenario to [29] was introduced in which splits/joins only occur in excessive inter-robot distances where as in [29], the algorithm allows for arbitrary split/join decisions at any time. Note the employment of the above mentioned techniques to design the SVO only results to a stable (not passive) SVO system as it uses passivity as a design tool to ensure stability. Indeed, a stable SVO in closed loop with haptic interfaces and operators is not necessarily stable.

In real world applications of cooperative haptic systems, the number of cooperating peers may vary due to the following reasons: communication blackout; hardware failure; or users' will to leave/join the cooperation. In this thesis, we propose a distributed control strategy that provides stable haptic cooperation with varying number of users, when manipulating a SVE across a network. The existing research on collaborative haptic systems can be categorized in two-fold: *experimental studies* [2–4, 15, 40, 58–60, 91–93, 96] and; *theoretical research* [12, 28, 39, 70, 71, 80–82, 102]. Most of the experimental studies have concentrated on application prospective and thus, they lack a thorough analysis of stability and/or performance. Therefore, in the following, a brief introduction on the latest theoretical findings in this discipline is overviewed.

2.3.1 Theoretical achievements on collaborative haptic systems

Fotoohi *et al.* in [28] presented the first systematic research covering many detailed aspects in collaborative haptic systems. For networks with constant delays but limited packet update rate (such as local area networks, LANs), [28] investigated the stability and transparency of both centralized and distributed control of haptic cooperation. The results confirmed that distributed controllers render stiffer virtual contacts than centralized control and thus, are more suitable for haptic interaction in rigid virtual environments. For performance evaluation, the admittance perceived by the users was introduced to compare the fidelity of each scheme. For distributed control architecture, Niakosari *et al.* [70, 71] later introduced a new fidelity index by measuring the discrepancy among local SVOs to quantify the transparency of the haptic simulation.

The analytical works mentioned above have focused on power domain communi-

cations exclusively. Passive multi-rate wave-domain communication was introduced in [102] for centralized haptic cooperation systems. The analysis revealed that the use of passive wave-domain communications can significantly increase the stiffness of the VE rendered to the users who manipulate a centralized virtual object together. This idea was later incorporated in a distributed haptic cooperation with two users [81]. The analysis predicted that larger coordination gains can be used when two users are connected via passive wave communications than when they are connected via power communications. Larger maximum coordination gain independent of the network delay provided increased and robust coherency of the SVO. The stability and performance of distributed multirate control of direct touch in networked haptic systems was investigated in [82]. In [82], remote dynamic proxies (RDPs) as physically-based avatars of remote peers in the local VE were employed in order to prevent the remote peer position discontinuities caused by the infrequent packet updates. Over both power-domain and wave-domain communication channels, the paper considers communication networks with fixed delay and with packet update rate smaller than the update rate of the users' local force feedback loops. Analysis and experiments were conducted to demonstrate that: over power-domain communication, RDPs allow for stiffer contact between users; and employment of passive wave-domain communications should make the distributed multirate control of direct touch stable regardless of the fixed communication delay.

Passivity-based design has also attracted researchers working in the field of cooperative haptic systems. Among the few decentralized studies, Bianchini *et al.* [12] employed state-space passivity conditions in the form of linear matrix inequalities (LMI's) to ensure the stability of multi-user haptic interactions. Virtual coupling parameters were computed to guarantee the stability of the cooperative haptic system for *em a priori* connectivity of a centralized SVO. However, their work neither

offered experimental validation nor performance analysis. Ansari *et al.* [7] implemented a modified PSPM [56] algorithm on a centralized haptic cooperation system. The PSPM approach incurs poor performance since it requires damping injection onto the dynamics of the SVO. Besides, the value of this damping depends on the controller gains and the sampling period. Recently, Huang *et al.* [39] introduced a discrete-time passivity framework to achieve asymptotic position consensus among discrete-time agents (i.e, SVO copies) with second-order dynamics. They cast the synchronization problem of shared virtual environment into the discrete-time second-order consensus problem and employed discrete-time passive integrators [55] to design a passive peer-to-peer control architecture. Their passivity condition relies on local damping injection at each user and thus, makes the technique conservative for virtual environments where little local SVO damping is of interest. Besides, *em a priori* knowledge of the communication conditions is a must in their design approach.

To our best knowledge, except [39] and [80], the stability of multi-user cooperative haptic systems with more than two users has not been pursued in literature. Our ultimate goal in this work is to develop a distributed control strategy that not only encapsulates the shortcomings of [39] and [80], but also provides stable and realistic force feedback to a varying number of users.

Over power-domain communications with constant time delay and limited packet update rate, next chapter will introduce the average position (AP) coordination strategy for distributed SVO. In Chapter 4, over wave-based communications with time-varying delays and packet-losses, the proposed architecture is developed to provide n-port passivity of the SVO. This idea is then extended in Chapter 5 for the case when the number of cooperating distributed peers varies.

Chapter 3

Average-position Coordination

Proportional-derivative (PD) control is often used to coordinate the two copies of the virtual environment (VE) in distributed two-user networked haptic cooperation. However, a PD controller designed to coordinate a VE shared by two users may destabilize distributed multi-user force interactions because its effective coordination gain increases with the participant count. This chapter proposes the average position (AP) strategy to upper bound the effective stiffness for the shared virtual object (SVO) coordination and thus, to increase the stability of distributed multi-user haptic cooperation. The chapter first motivates the AP strategy via continuous-time analysis of the autonomous dynamics of a SVO distributed among n users connected across a network with infinite bandwidth and no communication delay. It then investigates the effect of AP coordination on distributed multi-user haptic interactions over a network with limited bandwidth. For constant and small communication delays, the multi-rate stability and performance analyses are performed for cooperative manipulations of a SVO by three and four operators. Three-users experimental manipulations of a shared virtual cube validate the analysis.

3.1 Introduction

Conventional PD coordination places bounds on the maximum stable coordination gains, especially in the presence of limited update rate and communication delay of the connecting network [28]. When the number of interacting peers increases, the PD coordination of a distributed SVO destabilizes the haptic cooperation. The objective of this chapter is to introduce a distributed control architecture whose effective coordination gain does not depend on the number of cooperating participants. This work focuses on multi-user haptic cooperation across a computer network with limited bandwidth and constant communication delays. It supports fast sampling of the users' force feedback loops in the presence of slower network update rates by adopting a dual-rate control architecture. In the dual-rate architecture, users' local haptic rendering loops are sampled at the typical force control interval of $T_f = 0.001$ s and receive synchronized updates from the other local feedback loops every $T_s = \mathcal{M}T_f$ where $\mathcal{M} \in \mathbb{N}$. Like [28], this chapter employs the lifting technique [8] to model, and to investigate the stability and performance of, multi-user networked haptic cooperation with AP coordination. This chapter: (i) analyses the autonomous dynamics of SVO distribution among n users over a network with infinite bandwidth and no communication delay; (ii) investigates the stability and performance of distributed three- and four-user haptic cooperation with AP coordination over a network with limited bandwidth and small and constant communication delay; and (iii) validates the multi-rate stability and performance analysis via experiments in which three users manipulate a virtual cube together.

In the following, Section 3.2 motivates the proposed AP coordination of a distributed SVO, and shows that its effective stiffness is upper bounded by the coordination stiffness of a two-user cooperation. Section 3.3 derives the closed-loop state-space dynamics of dual-rate multi-user networked haptic interaction, and in-

vestigates the stability of force feedback with AP coordination for three and four operators. Section 3.4 presents the frequency-domain performance of three- and four-user networked haptic cooperation with AP coordination. Section 3.6 validates that AP coordination increases the stability and the performance of distributed multi-user networked haptic cooperation through experiments in which three networked users manipulate a shared virtual cube together. Section 3.7 concludes the chapter with suggestions for future work.

3.2 Average-position scheme

Distributed multi-user networked haptic cooperation is implemented via: (i) providing a local copy of the SVO to each peer user; (ii) coordinating all SVO copies through distributed coordination control; and (iii) rendering the dynamics and contacts of the local SVO to each user through haptic interaction control. Typically, virtual coupling is selected for haptic rendering and PD controllers are used to coordinate the distributed SVO copies to each other [28], as depicted in Figure 3.1. The mass of the SVO is equally distributed among, and the SVO damping is inherited by, all its copies. Such conventional distributed PD coordination of the SVO is straightforward to implement, but its effective stiffness grows with the number of users. Therefore, controller gains designed for two-user haptic cooperation may destabilize force interactions among multiple operators. Here, we propose the AP coordination strategy to upper bound the effective SVO coordination gain to the stiffness of the two-user coordination.

The gain dependency of the conventional PD coordination scheme on the number of cooperating peers can be derived from the autonomous dynamics of SVO distribution across a network with infinite bandwidth and no communication delay. These

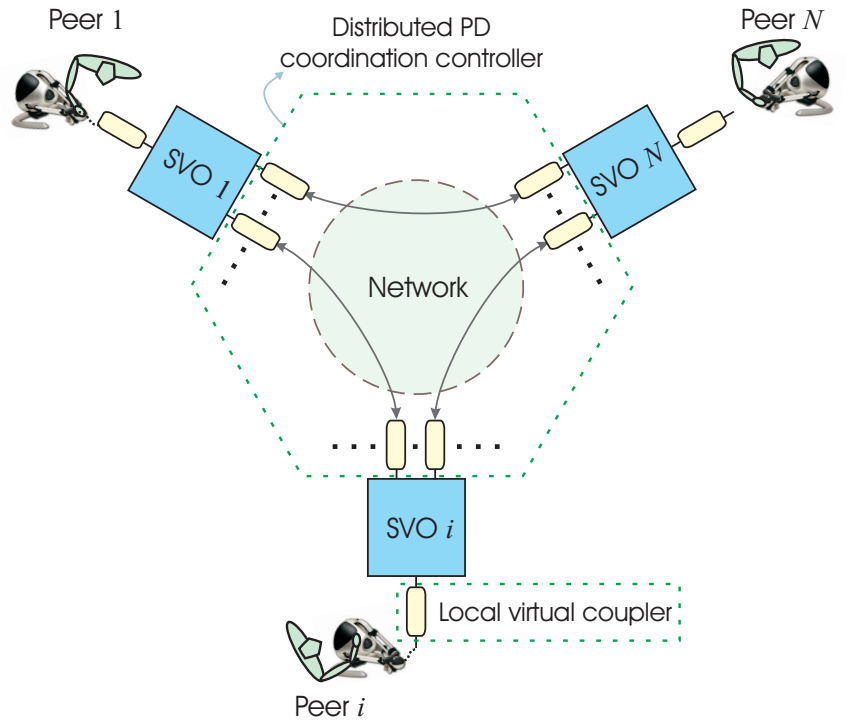

Figure 3.1: Conventional PD coordination of distributed haptic cooperation among n networked users.

dynamics are obtained starting from the dynamics of the i-th local copy of the distributed SVO:

$$\frac{M}{n}\ddot{x}_i + b\dot{x}_i = \sum_{j=1,j\neq i}^{n} \left(K_T\left(x_j - x_i\right) + B_T\left(\dot{x}_j - \dot{x}_i\right)\right), \tag{3.1}$$

where M and b are the mass and damping of the SVO, n is the number of users among which the SVO is distributed, K_T and B_T are the stiffness and damping gains of the coordinating PD controller, and x_l, $\dot{x}_l$, $\ddot{x}_l$ are the position, velocity and acceleration, respectively, of the l-th SVO copy, with $l = 1, \ldots, n$. Together, the n local SVO dynamics in Equation (3.1) yield the autonomous dynamics of the distributed SVO

with PD coordination:

$$\begin{aligned} \frac{M}{n}\mathbf{I}_{n\times n}\ddot{\mathbf{x}} &+ \left(\left(b+nB_T\right)\mathbf{I}_{n\times n} - B_T\mathbf{1}_{n\times 1}\mathbf{1}_{1\times n}\right)\dot{\mathbf{x}} \\ &+ \left(nK_T\mathbf{I}_{n\times n} - K_T\mathbf{1}_{n\times 1}\mathbf{1}_{1\times n}\right)\mathbf{x} = \mathbf{0}\,. \end{aligned} \tag{3.2}$$

In Equation (3.2), $\mathbf{x}$, $\dot{\mathbf{x}}$ and $\ddot{\mathbf{x}}$ are n-dimensional vectors which collect the positions, velocities and accelerations of all SVO copies, respectively, $\mathbf{I}_{n\times n}$ is the n-dimensional unity matrix and, $\mathbf{1}_{i\times j}$ is an $i \times j$ matrix with all entries 1. The stiffness matrix of PD coordination of the SVO in Equation (3.2) is:

$$\mathbf{K}_{PD} = K_T\left(n\mathbf{I}_{n\times n} - \mathbf{1}_{n\times 1}\mathbf{1}_{1\times n}\right), \tag{3.3}$$

and has one zero eigenvalue, which corresponds to the rigid body motion of the SVO, and one eigenvalue with geometric multiplicity $(n-1)$, which is called effective coordination stiffness herein and grows with n (see Figure 3.3). To bound the effective coordination stiffness, we propose the AP coordination strategy.

In the AP scheme, each SVO copy is locally coordinated to the average position of all other remote SVO copies, as schematically depicted in Figure 3.2 for the SVO copy of Peer i. In this figure: m_{HD_i} and b_{HD_i} are the mass and damping of the haptic device; $m_i = \frac{M}{n}$ and $b_i = b$ are the mass and damping of the SVO copy; K_{C_i} and B_{C_i} are the stiffness and damping of the local contact coupler; and K_T and B_T are the stiffness and damping of the distributed AP coordination controller, all at Peer i. The autonomous dynamics of the i-th local copy of the distributed SVO with AP coordination are:

$$\frac{M}{n}\ddot{x}_i + b\,\dot{x}_i = K_T\left(\frac{\sum_{j=1,j\neq i}^{n} x_j}{n-1} - x_i\right) + B_T\left(\frac{\sum_{j=1,j\neq i}^{n} \dot{x}_j}{n-1} - \dot{x}_i\right), \tag{3.4}$$

and, combined with the dynamics of the other local copies, yield the autonomous dynamics of the distributed SVO with AP coordination:

$$\begin{aligned}\frac{M}{n}\mathbf{I}_{n\times n}\ddot{\mathbf{x}} &= \left(\left(b+\frac{nB_T}{n-1}\right)\mathbf{I}_{N\times N}-\frac{B_T}{n-1}\mathbf{1}_{n\times 1}\mathbf{1}_{1\times n}\right)\dot{\mathbf{x}} \\ &+ K_T\left(\frac{n}{n-1}\mathbf{I}_{n\times n}-\frac{1}{n-1}\mathbf{1}_{n\times 1}\mathbf{1}_{1\times n}\right)\mathbf{x}. \end{aligned} \tag{3.5}$$

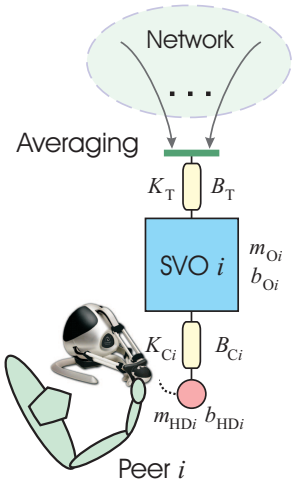

Figure 3.2: Average-position (AP) coordination of haptic cooperation among n users as applied at Peer i.

The stiffness matrix of AP coordination of the SVO is:

$$\mathbf{K}_{AP} = K_T\left(\frac{n}{n-1}\mathbf{I}_{n\times n}-\frac{1}{n-1}\mathbf{1}_{n\times 1}\mathbf{1}_{1\times n}\right), \tag{3.6}$$

and has one zero eigenvalue, which corresponds to the rigid body motion of the distributed SVO, and one eigenvalue with geometric multiplicity $(n-1)$ which decreases strictly monotonically to K_T as n grows (see Figure 3.3).

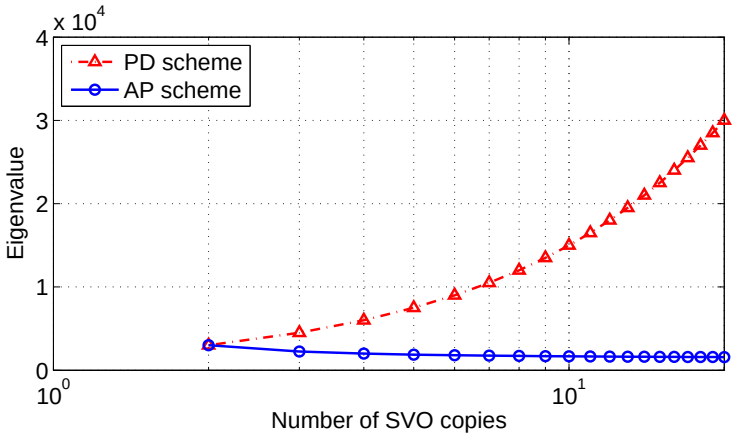

Figure 3.3: Effective coordination stiffness for up to $n = 20$ copies of SVO when, $K_T = 1500$ N/m for both AP and PD schemes.

Note that the distributed SVO dynamics are controlled by the eigenvalues of $\frac{n}{M}\mathbf{K}_{AP}$ and, therefore, the AP scheme needs to be coupled with inversely proportional scaling of K_T to guarantee stable SVO distribution for arbitrary n. Although not employed here, such coupling is straightforward to implement.

According to Figure 3.2, the dynamics of the distributed n-user networked haptic cooperation with AP coordination combine:

- the dynamics of the i-th haptic device:

$$m_{HD_i}\ddot{x}_{HD_i} + b_{HD_i}\dot{x}_{HD_i} = f_{h_i} - f_{C_i}, \tag{3.7}$$

- with the dynamics of the i-th SVO copy:

$$m_i\ddot{x}_i + b_i\dot{x}_i = f_{C_i} - f_{T_i}, \tag{3.8}$$

for all $i \in \{1, \ldots, n\}$. In Equations (3.7) and (3.8): f_{h_i} is the force applied by Peer i

to their haptic interface; f_{C_i} is the local contact force at Peer i:

$$f_{C_i} = K_{C_i}(x_{HD_i} - x_{_i}) + B_{C_i}(\dot{x}_{HD_i} - \dot{x}_{_i}); \tag{3.9}$$

and f_{T_i} is the force applied by the AP coordination controller on the i-th SVO copy:

$$f_{T_i} = K_T(x_{_i} - x_{_{i_d}}) + B_T(\dot{x}_{_i} - \dot{x}_{_{i_d}}), \tag{3.10}$$

with $x_{_{i_d}}$ and $\dot{x}_{_{i_d}}$ being the desired position and velocity of the i-th SVO copy, respectively. In the AP strategy, they are computed via:

$$x_{_{i_d}}(t) = \frac{\sum_{j=1,j\neq i}^{n} x_{_j}(t - T_d)}{n-1} \tag{3.11}$$

and

$$\dot{x}_{_{i_d}}(t) = \frac{\sum_{j=1,j\neq i}^{n} \dot{x}_{_j}(t - T_d)}{n-1}, \tag{3.12}$$

where T_d is the communication delay of the network. In this chapter, the analysis is performed when n distributed users are interconnected via a fully-connected graph; the network delay T_d is assumed constant, equal in all communication channels, and an integer multiple $\mathcal{M}$ of the network packet update interval T_s, $T_d = \mathcal{M}T_s$.

3.3 Stability of dual-rate three- and four-user haptic cooperation

Because the typical network update interval is longer than the sampling interval required for realistic haptic rendering, the distributed haptic cooperation among n networked users is a dual rate closed-loop system. Its stability is controlled by the eigenvalues of its multirate state transition matrix. This matrix is computed using

the lifting approach introduced in [8] and first applied to haptic cooperation in [28]. The derivations are succinctly overviewed in this section.

The open-loop continuous-time state-space dynamics of n-user networked haptic cooperation combine the dynamics of the users, of the haptic interfaces and, of the SVO copies, and group the system inputs and outputs into fast and slow sub-vectors, hereafter indicated with the f and s indices, respectively. The inputs comprise the local contact forces, updated at the fast haptic rate (Equation (3.9)), and the SVO coordination forces, with components updated both fast and slow (Equation (3.10)), grouped into:

$$\mathbf{u}^\top = (\mathbf{u}_f^\top \quad \mathbf{u}_s^\top)^\top, \tag{3.13}$$

where:

$$\mathbf{u}_f^\top = (f_{C_1} \quad f_{T_{1_f}} \quad \dots \quad f_{C_n} \quad f_{T_{n_f}})^\top, \tag{3.14}$$

$$\mathbf{u}_s^\top = (f_{T_{1_s}} \quad \dots \quad f_{T_{n_s}})^\top, \tag{3.15}$$

$$f_{T_{i_f}} = K_T x_i + B_T \dot{x}_i, \tag{3.16}$$

and,

$$f_{T_{i_s}} = -K_T x_{i_d} - B_T \dot{x}_{i_d}. \tag{3.17}$$

The state vector comprises the states of all haptic interfaces and SVO copies:

$$\mathbf{x}^\top = (\mathbf{x}_{peer_1} \quad \dots \quad \mathbf{x}_{peer_i} \quad \dots \quad \mathbf{x}_{peer_n})^\top, \tag{3.18}$$

where

$$\mathbf{x}_{peer_i}^\top = (x_{HD_i} \quad \dot{x}_{HD_i} \quad x_i \quad \dot{x}_i)^\top; \quad i \in \{1, \dots, n\}. \tag{3.19}$$

The output vector is:

$$\mathbf{y}^\top = (\mathbf{y}_f{}^\top \quad \mathbf{y}_s{}^\top)^\top, \tag{3.20}$$

where

$$\mathbf{y}_f{}^\top = \mathbf{x}^\top \tag{3.21}$$

and,

$$\mathbf{y}_s^\top = (\mathbf{y}_{peer_{1_s}} \quad \cdots \quad \mathbf{y}_{peer_{i_s}} \quad \cdots \quad \mathbf{y}_{peer_{n_s}})^\top \tag{3.22}$$

with

$$\mathbf{y}_{peer_{i_s}}{}^\top = (x_{i_d} \quad \dot{x}_{i_d})^\top; \quad i \in \{1, \ldots, n\}. \tag{3.23}$$

Hence, the open-loop continuous-time state-space dynamics of n-user networked haptic cooperation with AP coordination are:

$$\begin{aligned} \dot{\mathbf{x}}_{4n\times 1} &= \mathbf{A}_{4n\times 4n}\mathbf{x}_{4n\times 1} + \mathbf{B}_{4n\times 3n}\mathbf{u}_{3n\times 1} \\ \mathbf{y}_{6n\times 1} &= \mathbf{C}_{6n\times 4n}\mathbf{x}_{4n\times 1} \end{aligned}, \tag{3.24}$$

and their discretization is obtained by lifting [8], in the form:

$$\begin{aligned} \mathbf{x}_{D_{(\mathcal{M}.4n)\times 1}}[k+1] &= \mathbf{A}_{D_{(\mathcal{M}.4n)\times(\mathcal{M}.4n)}}\mathbf{x}_{D_{(\mathcal{M}.4n)\times 1}}[k] \\ &\quad + \mathbf{B}_{D_{(\mathcal{M}.4n)\times((2\mathcal{M}+1).n)}}\mathbf{u}_{D_{((2\mathcal{M}+1).n)\times 1}}[k] \\ \mathbf{y}_{D_{(2\mathcal{M}+1).2n\times 1}}[k] &= \hat{\mathbf{C}}_{D_{((2\mathcal{M}+1).2n)\times(\mathcal{M}.4n)}}\mathbf{x}_{D_{(\mathcal{M}.4n)\times 1}}[k] \\ &\quad + \hat{\mathbf{D}}_{D_{((2\mathcal{M}+1).2n)\times((2\mathcal{M}+1).n)}}\ \mathbf{u}_{D_{((2\mathcal{M}+1).n)\times 1}}[k] \end{aligned} \tag{3.25}$$

Note that in the above equation, all the sampling instances kT_f are replaced by k for brevity. The derivation of $\mathbf{A}_D$, $\mathbf{B}_D$, $\hat{\mathbf{C}}_D$ and $\hat{\mathbf{D}}_D$ and the incorporation of the communication delays, via augmenting the state with the delayed inputs, are detailed in Appendix A.1. The stability of the dual-rate distributed n-user networked haptic cooperation hinges on the eigenvalues of the closed-loop state transition matrix:

$$\mathbf{A}_D^{cl} = \mathbf{A}_{D_{aug}} + \mathbf{B}_{D_{aug}}\mathbf{F}_D(\mathbf{I} - \mathbf{D}_{D_{aug}}\mathbf{F}_D)^{-1}\mathbf{C}_{D_{aug}},$$

where $\mathbf{A}_{D_{aug}}$, $\mathbf{B}_{D_{aug}}$, $\mathbf{C}_{D_{aug}}$ and $\mathbf{D}_{D_{aug}}$ are the state transition matrices obtained after augmentation with computational and communication delays, and the feedback matrix $\mathbf{F}_D$ includes the contact coupling and SVO coordination forces and is computed using the approach introduced in [8]. Namely, the n-user haptic cooperation is stable iff all eigenvalues of $\mathbf{A}_D^{cl}$ are inside the unit circle. Note that the stability margins in this chapter account for the autonomous system in which, the dynamics of the operators are not included in the analysis. This, in fact, is the worst case scenario for the close-loop system since, the damping of the users' hand generally results to the dissipation of energy. Therefore, the analysis of the stability of the autonomous system is sufficient for the close-loop stability.

3.3.1 Stability regions

This section presents a numerical investigation of the stability regions of two-, three- and four-user haptic cooperation with AP and with PD coordination. In fact such stability regions lead to stable controller parameters. In the analysis presented in this section, the haptic device parameters are selected such that they match the inertial and damping properties of the Falcon Novint haptic interface used in the experiments. The specification of the Falcon Novint devices can be found in Appendix A.9.

The following parameters are used in the computations: $m_{HD_i} = 0.1$ kg, $b_{HD_i} = 5.0$ Ns/m; $M = 0.6$ kg, $b = 5.0$ Ns/m, $T_f = 0.001$ s, $T_s = 0.008$ s. Figure 3.4 depicts the stability regions for undamped control, i.e., $B_T = B_{C_i} = 0$ Ns/m. Figure 3.5 shows the stability regions for damped control with $B_T = B_{C_i} = 2$ Ns/m. In all of these analyses, the communication delay is on step of slow update interval, i.e, $T_d = 0.008$ s.

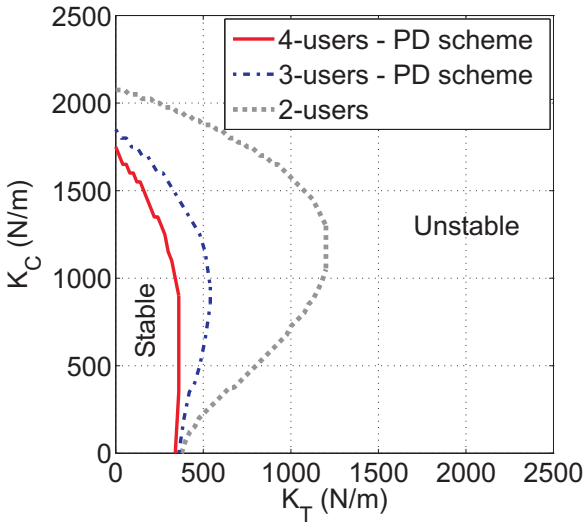

(a) PD coordination.

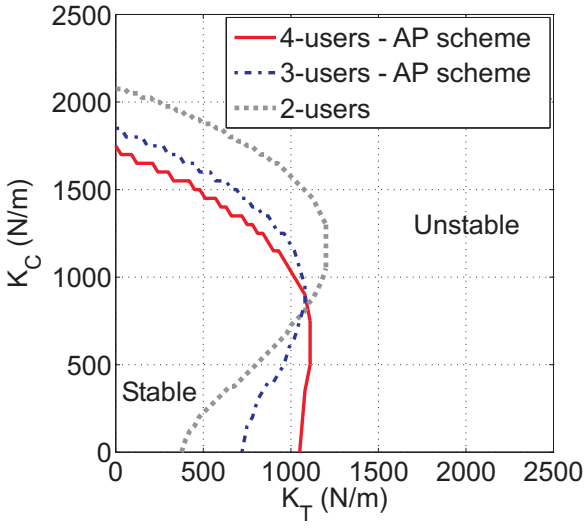

(b) AP coordination.

Figure 3.4: Stability region for two/three/four-user haptic cooperation ($B_T = 0$ Ns/m).

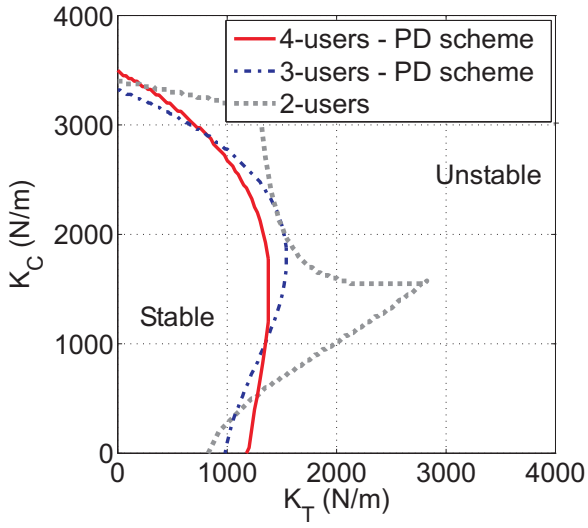

(a) PD coordination.

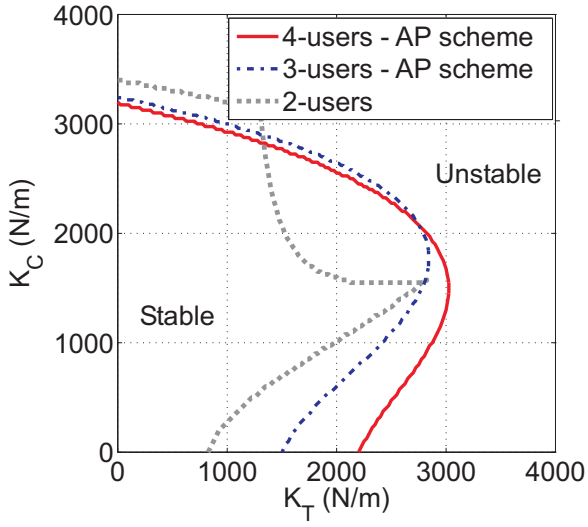

(b) AP coordination.

Figure 3.5: Stability region for two/three/four-user haptic cooperation ($B_T = 2$ Ns/m).

For both undamped and damped coordination, respectively, Figures 3.4 and 3.5 demonstrate that the proposed AP coordination expands the stability regions of haptic cooperation. This is in contrast to the PD coordination which decreases the stability region as the number of peers grows. The variations in the trend of the

stability regions, however, depend on different system parameters such as the mass of the SVO and communication delay, as reported in [84].

3.4 Performance evaluation

In distributed multi-user haptic cooperation, the position discrepancy among the SVO copies threatens the fidelity of the force interactions. For example, suppose that Peer i tries to move their local copy of the SVO while other users are not in touch with their local copies. If the coordination of the n distributed SVO copies is perfect, Peer i imposes the same motion on all SVO copies and feels the multiple SVO copies as rigidly attached to each other. However, for coordination with limited gains, Peer i feels the SVO copies as connected to each other with springs with finite stiffness and with slowly moving ends (due to the updated delays received across the network). This section uses the admittance $G_i(z) = \frac{\dot{x}_i(z)}{f_{h_i}(z)}$ of the SVO copies to compare users' perception of a distributed SVO with AP and PD coordination to user's perception of an "ideal" virtual object. Accordingly, the ideal admittance is the ratio of the VO velocity to the input hand force (see Figure 3.6). Let a SVO with mass M be distributed among n peers. Consequently, the mass of each SVO copy is $\frac{M}{n}$. In ideal conditions, we can assume that the SVO copies are connected and coordinated via massless rigid links. This, thus, imposes perfect synchronization between distributed SVO copies. Therefore, the ideal SVO can be considered as one single VO with mass M. Note that we assume no local damping on the SVO dynamics to account for the worst case scenario. The G_i-parameters are computed after lifting the dual-rate system to its unirate counterpart [28].

The frequency responses of a SVO distributed among two, three and four users and coordinated via the AP and PD schemes are depicted and compared with the ideal

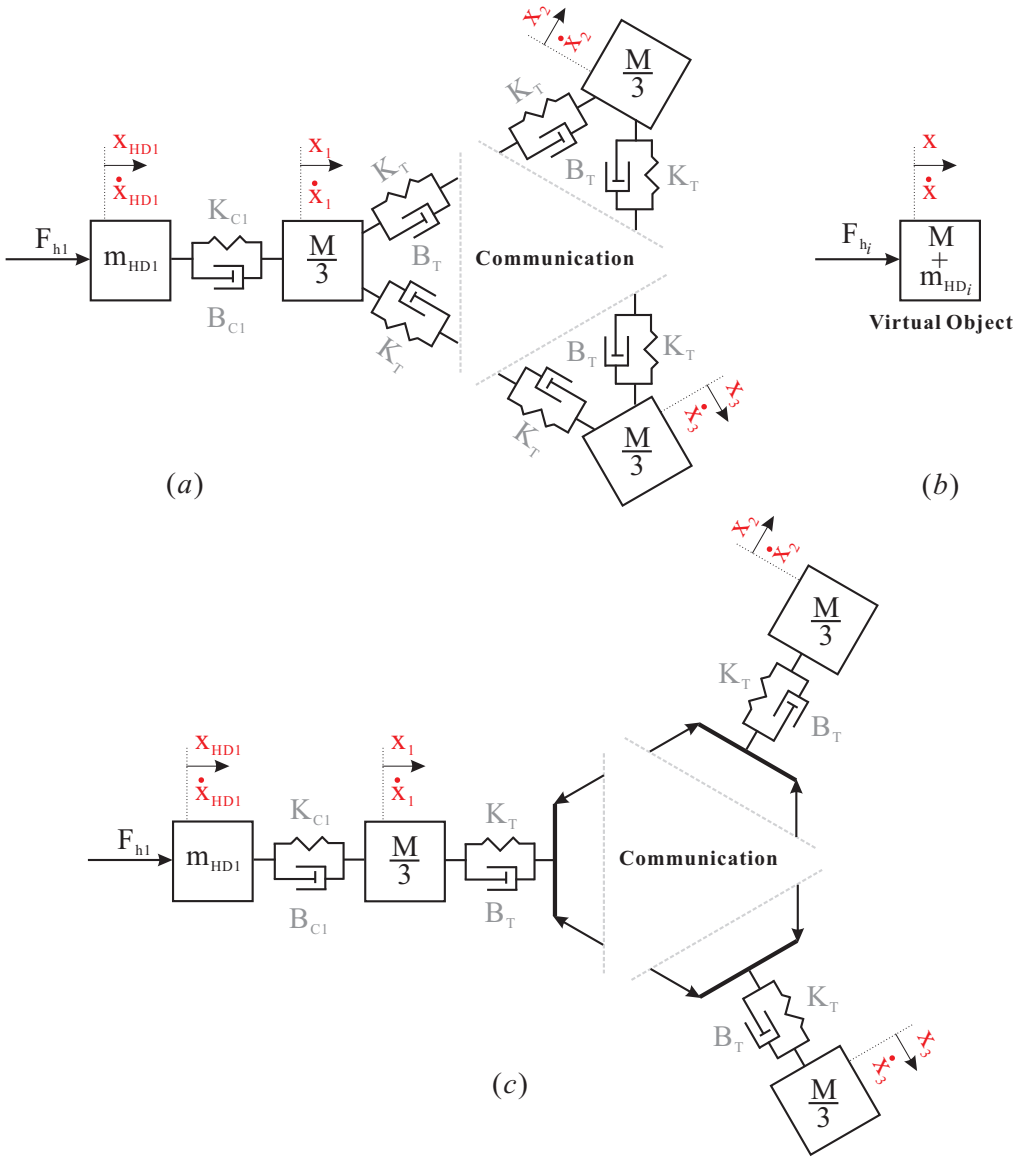

Figure 3.6: (a) Single user interacting with a virtual object shared among $n = 3$ users through PD scheme, (b) Ideal interaction, (c) Single user interacting with a virtual object shared among $n = 3$ users through AP scheme.

case in Figure 3.7. The empirical parameter values that guarantee the stability of the cooperative hatpic system are chosen as: $M = 0.45$ kg; $b = 0$ Ns/m; $K_T = 1000$ N/m; $B_T = 5$ Ns/m respectively; and $T_d = T_s = 0.008$ s in all communication links.

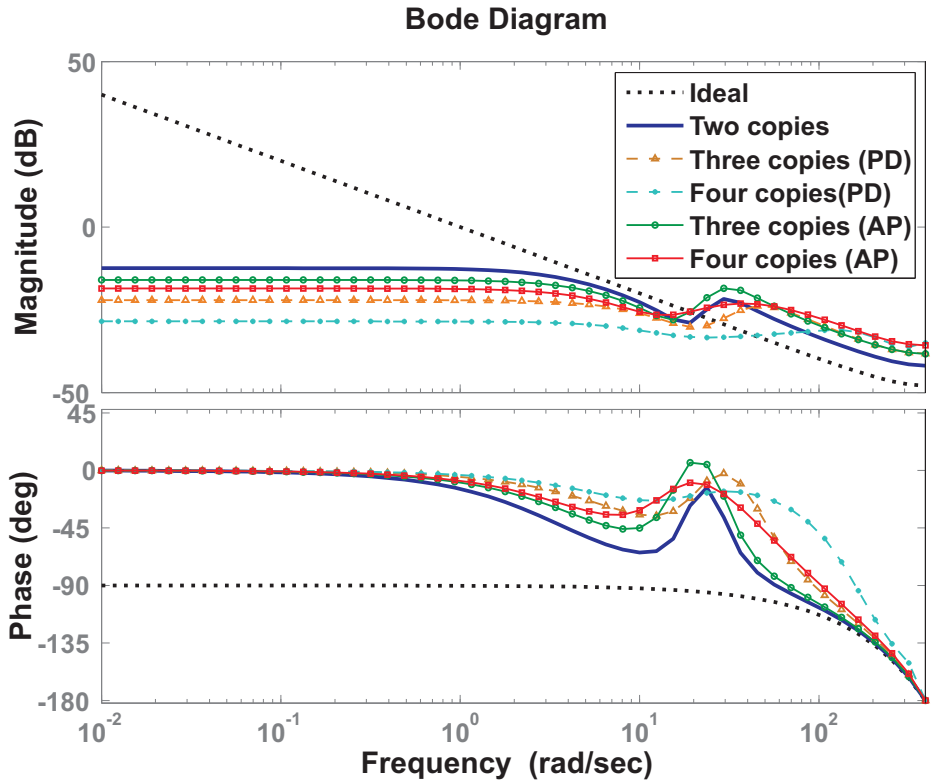

Figure 3.7: SVO admittance for two-, three- and four-user cooperation with AP and PD coordination, and with communication delay $T_d = T_s = 0.008$ s in all links.

In Figure 3.7, the deviations from the ideal frequency response show increased viscous behaviour, due to the low packet update rate, the delays in communication channel, and the damping of the coordination [28]. Nonetheless, Figure 3.7 confirms: (i) that a distributed SVO with AP coordination has admittance closer to the admittance of a pure mass than a distributed SVO with PD coordination; and (ii) that the perceived damping of the distributed SVO increases with the peer count. This is expected given that the number of communication links increases and that each link introduces additional damping in the cooperation.

3.5 Discussion: performance vs. stability

In can be mathematically shown that the AP coordination controller is in fact, the PD coordination controllers scaled by a factor of $(n-1)$. As the number of users increases, the AP offers stable cooperation at the expense of incorporating smaller coordination gains. This, in turn, degrades the position coherency of the distributed SVO. This issue can be addressed by employing passive multi-rate wave-based communication channel as reported in [81]. The analysis therein confirms that larger (one order of magnitude) stable coordination gain independent of the network delays can be used which, provides increased and robust coherency of the SVO.

3.6 Experimental validation

This section validates the results of the analysis in the sections above through experiments performed on a testbed which comprises three FALCON NOVINT haptic devices connected to three computers which all run Windows XP on an Intel Core 2 Duo CPU at 2.67 GHz with 2 GB RAM. The computers are in the same laboratory and communicate over the network via the UDP protocol over a local area network with data transmission rate of 125 Hz. The virtual environment is simulated at 1 kHz via a C^{++} console application and includes: a shared virtual cube constrained by a virtual enclosure to move along a single horizontal x-direction; and three virtual spheres representing the haptic devices. Given the proximity of the three computers, the actual network delay is negligible. Therefore, a Wide Area Emulator (WANem) is used to implement a desired network delay T_d, equal in all communication channels. Figure 3.8 depicts the experimental testbed with three cooperating users.

In all experiments, the parameter values are as follows: the mass and damping of the SVO are $M = 0.45$ kg; and $b = 0$ Ns/m, respectively; the coordination

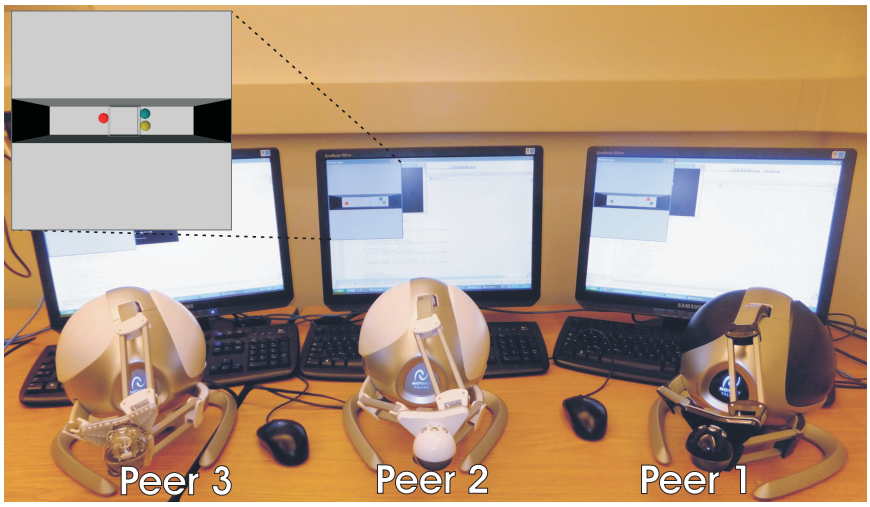

Figure 3.8: Experimental testbed.

damping is $B_T = 5$ Ns/m; the contact stiffness and damping are $K_C = 3500$ N/m and $B_C = 5$ Ns/m, respectively; $T_f = 0.001$ s; $T_s = 8T_f = 0.008$ s; and the round-trip network delay is $T_d = 6T_s = 0.048$ s.

3.6.1 Stability tests

In the experiments carried out in this section, two of the three users cooperatively manipulate the SVO along the enclosure. The coordination stiffness is selected $K_T = 2100$ N/m. The numerical analysis in Section 3.3.1 predicts that the three-user haptic cooperation is stable if AP coordination is used, and is unstable if conventional PD coordination is employed (see Figure 3.5). The analysis is confirmed by the experimental results in Figure 3.9.

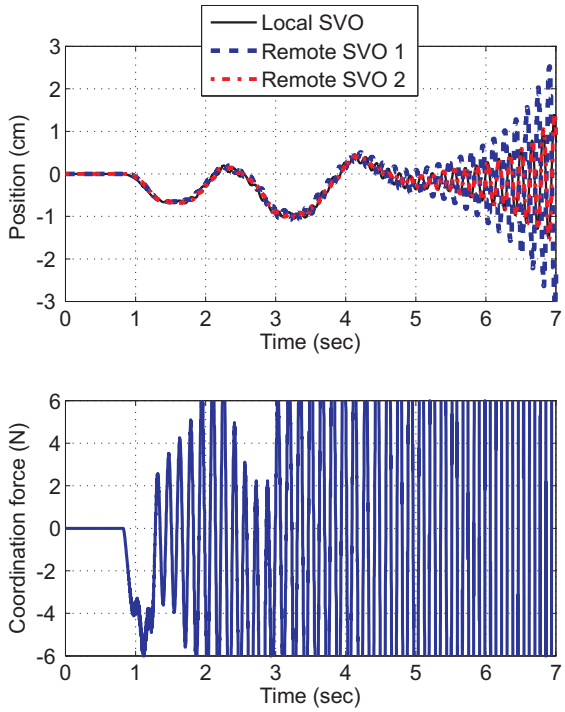

(a) PD coordination.

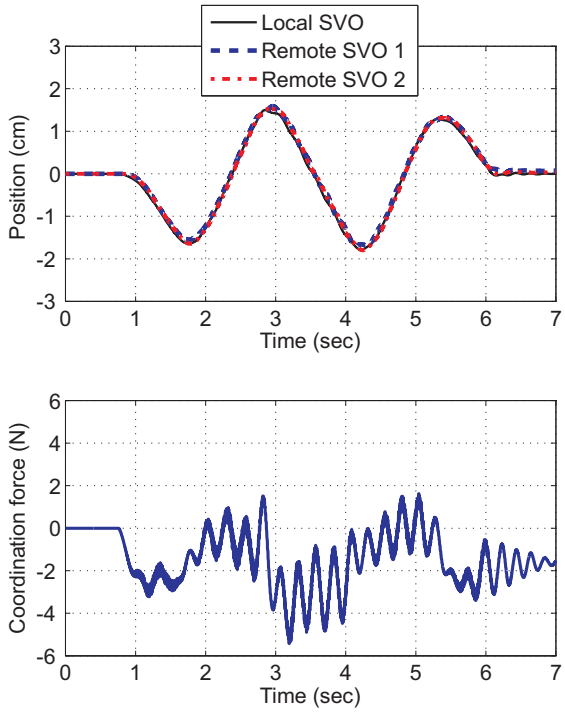

(b) AP coordination.

Figure 3.9: Experimental three-user haptic cooperation ($K_T = 2100$ N/m).

3.6.2 Perceived viscosity tests

This section contrasts the performance of AP coordination to the performance of conventional PD coordination through controlled experiments. The coordination stiffness is set to $K_T = 1000$ N/m, to ensure that the three-users haptic cooperation is stable regardless of the coordination scheme. To guarantee the same initial conditions during successive experiments, the users are replaced by forces applied to the haptic devices via commands sent to the servo motors.

The experiments start with Peer 1 at the right end of the virtual enclosure, pushing the SVO with a constant force $f_{h_1} = 1.5$ N, and with Peer 2 and Peer 3 not in contact with the SVO. Thus, the SVO travels along the enclosure to the left during the experiment. Figure 3.9 depicts the position of the SVO at Peer 1. It shows that the SVO moves a distance of 20 mm in 1.22 sec when AP coordination is used, and it moves 20 mm in 1.514 sec when PD coordination is employed. These experimental results confirm that AP coordination renders a less viscous SVO to users than PD coordination, as predicted analytically.

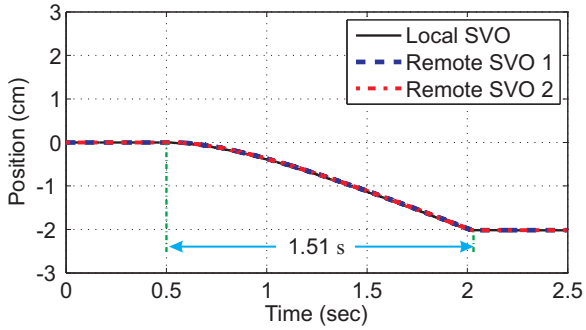

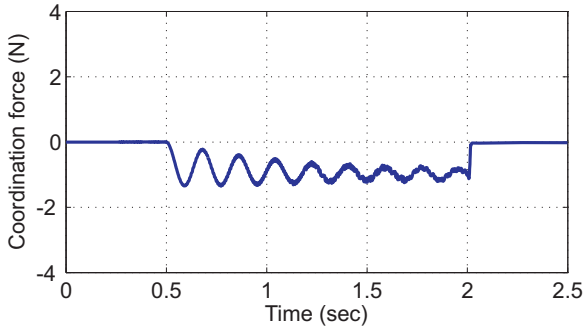

(a) PD coordination.

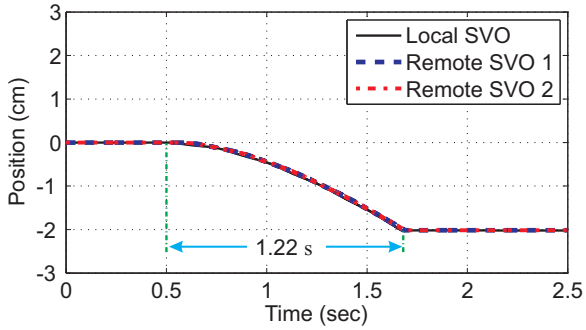

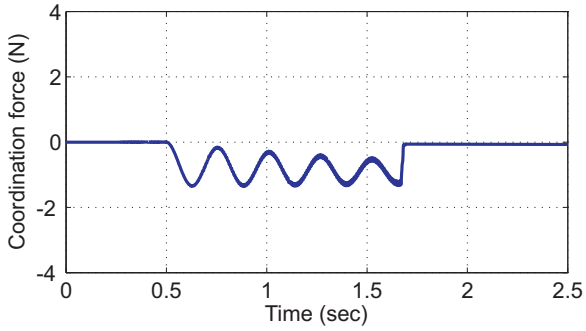

(b) AP coordination.

Figure 3.10: Experimental three-user haptic cooperation with communication delay $T_d = 6T_s = 0.048$ s. The experiments start with Peer 1 at the right end of the virtual enclosure, pushing the SVO with a constant force $f_{h_1} = 1.5$ N, and with Peer 2 and Peer 3 not in contact with the SVO.

3.7 Summary

This chapter has proposed the average position (AP) coordination for distributed multi-user networked haptic cooperation. Through continuous-time analysis of the autonomous dynamics of an SVO distributed among n users, as well as through multirate analysis of the closed-loop state-space dynamics of three- and four-user haptic cooperation, we showed that the AP strategy increases the stability of the interaction compared to conventional PD coordination. Using numerical analysis, it is illustrated that AP coordination is also beneficial to the SVO admittance rendered to the cooperating users. Namely, users perceive the distributed SVO as less viscous when it is coordinated using the AP scheme than when it is coordinated using the conventional PD scheme.

However, the main drawbacks of the multirate methodology [8] used here are:

- time-delays are presumed to be constant and very small[1];
- knowledge about the model of the haptic interfaces are crucial for the stability analysis;
- the analysis considers that the system runs on LAN or MAN which completely ignores jitter and packet-loss for real-world applications;
- the entire system is assumed to be linear time-invariant (LTI) and thus, it is unclear how the employed multirate control approach [28] can be extended to systems implemented on Internet where jitter and packet-loss are principal issues.

Besides, although the AP scheme allows for the selection of the controller gains independent of the number of distributed users, it does not facilitate for small values of

[1] In [81] and [82], we employed passive multirate wave based communication channels for a two-user haptic cooperation system. The analysis confirmed that the stability regions are extended of an order of magnitude independent of the value of constant communication delays.

the mass of SVO copies. In fact, as the number of operators increases, the division of the SVO mass among users' copies may result in instability if mass value becomes smaller that the minimum mass [14]. In the next two chapters, we aim to address the mentioned issues with the AP scheme by investigating techniques for guaranteeing the stability of distributed haptic cooperation among an arbitrary number of users, across networks with varying communication delays and packet-losses. In particular, scalability will be pursued by implementing the AP scheme for wave-based communication channels along with passive simulation of the dynamics.

Chapter 4

Passive Shared Virtual Environments

In practice, the model of human users and haptic devices are often unknown, uncertain, and time-variant. Conventional approaches for stability analysis of haptic systems assume that the human user does not inject energy into the system and behaves in a passive manner. The assumption of passive human operators and haptic interfaces [38] relaxes the need for their exact models for stability analysis. Feedback interconnection of multiple passive subsystems results in a passive and thus a stable system [69]. Therefore, construction of a passive SVO in closed-loop with passive human users and haptic devices can guarantee the stability of the distributed haptic cooperation system. This fact motivated us to develop a passive SVO whose copies are distributed among n users. Our main focus in this chapter is to construct a passive SVO (modelled as an n-port network element) in the presence of time-varying delay and packet-loss, and over a bidirectional and connected network topology. Next, we briefly overview the relevant research on this topic and then introduce the core idea of this chapter.

4.1 Introduction

Anderson and Spong in [5] employed scattering transformation to study the passivity of an n-port passive network. Built based on the singular values of the scattering matrix, to ensure passivity, their technique required the norm of the scattering operator to be less than or equal to one. However, such a condition is challenging to uphold as the model parameters of the robots are crucial for design. For multilateral teleoperation systems, Mendez *et al.* [66] proposed a passivity criterion to select the controller parameters. They extended the Raisbeck's [79] passivity criterion to general n-port networks. However, they ignored communication delays in their analysis. Nevertheless, their approach is only applicable to LTI systems and its extension for systems embedded with non-linear sources (such as uncertain data transmission channels) remains unclear. Kottenstette *et al.* in [52] employed power junctions [54] to construct an n-port passive wave-based network allowing to guarantee the stability of a networked system when coupled to multiple passive discrete-time agents (i.e, plants). Each distributed plant was equipped with a local controller to ensure their output-strict-passivity. This approach, however, is not suitable to use for cooperative haptic systems since the controller imposes extra dynamics to the SVO copies. Besides, the wave-based networked architecture introduced in [54] exhibits poor performance.

This chapter develops a passive framework for distributed virtual environments such that, the design of the coordinating controllers is decoupled from the network topology and the communication line issues. Preliminary results of this work have been presented in [83]. Yokokohji *et al.* in [44] introduced a lossless power distributor (i.e, wave node) in order to interconnect multiple teleoperators over a time-delayed computer networks using wave variables [72]. Here in this chapter, we construct an n-port passive communication architecture by implementing the node scheme introduced in [44], referred as *node scheme I*, on multi-lateral distributed networks under

unreliable data transmission channels. We then, connect n passive SVO copies and their corresponding coordinating controllers to the proposed communication network and thus, construct and n-port passive SVO. The discrete-time passivity of each local SVO copy and its corresponding coordination controller is ensured by employing the state modification technique [97]. Tailored for port-Hamiltonian systems, the approach in [97] allows the discrete-time dynamics of the system to evolve in such a way that it resembles the energetic properties of its corresponding continuous-time system and hence, guaranteeing its passivity. The n-port passive SVO introduced in this chapter is the foundation for Chapter 5, for which we study the proposed scheme when the number of SVO copies varies. Moreover, in this chapter, we performed both energetic and steady-state analyses of the proposed n-port passive network on a fully connected graph and compared it with a network architecture built based on the wave node scheme introduced in [54], referred to as *node scheme II*. The analyses predicted that the proposed network architecture implemented with *node scheme I*:

i) is lossless when subject to communications with no time delays;

ii) offers less dissipation in comparison to the network architecture built based on the *node scheme II*;

iii) and unlike *node scheme II*, results in bounded steady-state error as the simulation time grows.

The analytical findings are supported with simulations and experiments. The network architecture presented in this chapter enables us to separate the design of the coordination controllers from the communication network, and allows to achieve interaction stability without imposing extra damping injections on the dynamics of local SVO copies, regardless of unreliable communication channels.

In the remainder of this chapter, Section 4.2 reviews some preliminaries and definitions required throughout this chapter; The passivity properties of the two wave node schemes, i.e *node schemes I* and *II* are studied in Section 4.3. In Section 4.4, *wave node I* is implemented on multilateral wave-based network structure to construct an n-port passive communication network. In Section 4.5, port-Hamiltonian SVO copies along coordinating controllers are interconnected via the proposed control architecture and hence, the n-port passivity of the resulting SVO distributed among n peers is verified. The steady-state analysis for network architectures built based on both wave nodes is conducted in Section 4.6. Supporting simulations are presented in Section 4.7. Experimental 3-users haptic cooperation presented in Section 4.8 supports the theoretical findings.

4.2 Preliminaries and definitions

Passivity

A system is called passive only if it stores/dissipates or releases the energy which was supplied to it. By definition, a discrete-time system is n-port passive [33] if:

$$\sum_{i=1}^{n} \sum_{k=0}^{\bar{k}} f_i(kT)\dot{x}_i(kT)T \geq E(0) \tag{4.1}$$

where port i characterises a pair of power conjugated variables, force f_i and velocity $\dot{x}_i$, whose product represents power; T corresponds to T_f from previous chapter and stands for the discrete sampling period; $E(0)$ is a constant that depends on the initial conditions of the system; and $k, \bar{k} \in \mathbb{Z}^+$ where $\bar{k}$ is the final simulation time instant. Note, Equation (4.1) with equality implies the definition of an n-port lossless system for which, energy is neither dissipated nor generated. For brevity in the rest of this

thesis, all time instances kT are replaced by k.

Passive communication channel

Interconnected physical systems typically exchange energy over power-domain communications via which, the power variables (e.g, force and velocity) are transmitted. However, when power variables are subject to time delays, the communication channel acts as an active element that generates energy and leads to instabilities in closed-loop. Scattered [5] or wave-based [72] communications render the transmission channel passive in the presence of constant time delays. Scattering transformation encodes the power variables from power-domain into wave variables in wave-domain. The wave variables (u_i, v_i) can be calculated from the power variables ($\dot{x}_i$, f_i) using the following transformations [72]:

$$u_i(k) = \frac{b_w \dot{x}_i(k) + f_i(k)}{\sqrt{2b_w}}, \qquad v_i(k) = \frac{b_w \dot{x}_i(k) - f_i(k)}{\sqrt{2b_w}} \tag{4.2}$$

where b_w is the characteristic wave impedance. The communication channel can be considered as a 2-port network element (see Figure 4.1) via which, two interacting sides exchange information. Respectively, let u_{ij} and v_{ij} represent the incoming and outgoing waves of side i when interconnected to side j over a wave-based communication channel.

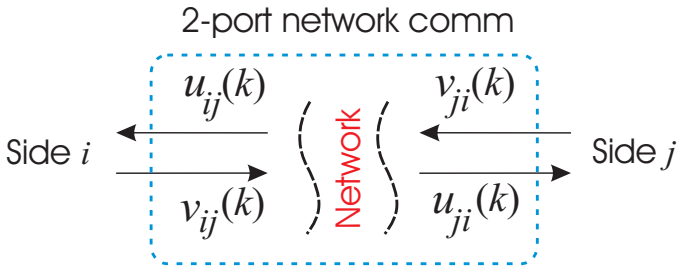

Figure 4.1: Wave-based communication channel as a 2-port network element.

The power entering the 2-port communication channel at time instant k is:

$$P_{ij}(k) = \frac{1}{2}\left(v_{ij}^2(k) - u_{ij}^2(k) + v_{ji}^2(k) - u_{ji}^2(k)\right) \tag{4.3}$$

It is straightforward to show that the passivity of the wave-based communication channel is guaranteed [72] since, the energy stored in the transmission channel upto time instant $\overline{k}$ is non-negative regardless of the magnitude of constant time delay (see Appendix A.2), that is:

$$E_{ij}(\bar{k}) = T\sum\nolimits_{k=0}^{\bar{k}} P_{ij}(k) \geq 0 \tag{4.4}$$

However, passivity might be endangered in unreliable communication networks due to empty packets detected at the receiver sides caused by time-varying delay. In this dissertation, we employ the queue management strategy introduced in [19] which maintains the passivity of the wave-based communication channel in the presence of varying time-delay and packet-loss.

4.3 Wave node

The *wave node* is a network element that interconnects multiple wave-based communication media [44, 54]. Let $\mathcal{N}_i$ define the set of node indexes of the neighbours of node i. The cardinality of the neighbours set $\mathcal{N}_i$ represents the number of neighbours (i.e, n_i) of the i-th node. With u_{ij} and v_{ij} denoting the incoming and outgoing waves of the j-th port of node i respectively, the passivity condition for node i in Figure 4.2 is [54]:

$$\sum_{j=0}^{n_i} u_{ij}^2(k) \geq \sum_{j=0}^{n_i} v_{ij}^2(k), \qquad \forall k \in \mathbb{Z}^+ \tag{4.5}$$

where n_i+1 stands for the number of the ports of wave node i. Equation (4.5) implies that the sum of the outgoing energy quanta should be less than or equal to the sum of the incoming ones. In this thesis, all the zero-indexed wave variables are assigned to the local ports via which, the local SVOs are connected to their corresponding wave nodes (see Figure 4.2). The zero-indexed wave variables can be then decoded to their corresponding desired power variables, that is, force and velocity. Note, unlike the previous chapter, the desired velocity ($\dot{x}_{i0}$) and force (f_{i0}) will no longer be indexed with subscript d.

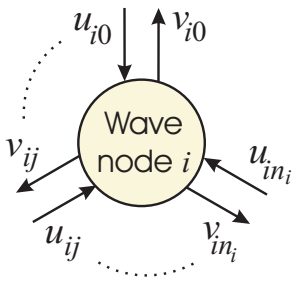

Figure 4.2: Wave-node i with $n_i + 1$ ports.

Each wave node as a power junction obtains a power distribution scheme which defines how the outgoing waves of the node are computed based on the incoming waves. In this chapter, two wave node schemes are studied:

- *Node scheme I*: Kanno *et. al* in [44] computed the outgoing waves for wave node i at port j using the following relation:

$$v_{ij}(k) = -u_{ij}(k) + \frac{2}{n_i + 1} \sum_{j=0}^{n_i} u_{ij}(k). \tag{4.6}$$

  The outgoing waves in Equation (4.6) are computed such that, if the wave variables were decoded into power variables, all decoded velocities would be equal and all decoded forces would sum up to zero. Note, the *node scheme I* is a power-preserving and lossless interconnection junction of wave channels [44]

as shown next.

Consider the wave node i shown in Figure 4.2 with n_i+1 ports. Using Equation (4.6) and summing up the power of all outgoing waves for the wave-node i gives:

$$\sum_{j=0}^{n_i} v_{ij}^2(k) = \sum_{j=0}^{n_i} \Big(- u_{ij}(k) + \frac{2}{n_i+1} \sum_{j=0}^{n_i} u_{ij}(k) \Big)^2 \tag{4.7}$$

With power variables f_{ij} and $\dot{x}_{ij}$, the corresponding encoded wave-variable u_{ij} can be calculated from Equation (4.2) and substituted into the last term of Equation (4.7) to give:

$$\begin{aligned} \sum_{j=0}^{n_i} v_{ij}^2(k) = \sum_{j=0}^{n_i} \Big(- u_{ij}(k) + \frac{2}{\sqrt{2b_w}(n_i+1)} \sum_{j=0}^{n_i} f_{ij}(k) \\ + \frac{\sqrt{2b_w}}{n_i+1} \sum_{j=0}^{n_i} \dot{x}_{ij}(k) \Big)^2 \end{aligned} \tag{4.8}$$

Following the physical law presented in [44], the corresponding decoded velocity for each wave-based transmission line connected to the wave-node i must be the same, i.e, $\dot{x}_{i0}(k) = \dot{x}_{ij}(k),\ \forall j \in \mathcal{N}_i$. Besides, the sum of all corresponding decoded forces applied onto the wave-node i must be zero, $f_{i0}(k) + \sum_{j\in\mathcal{N}_i} f_{ij}(k) = 0$. Therefore, Equation (4.8) can be written as:

$$\sum_{j=0}^{n_i} v_{ij}^2(k) = \sum_{j=0}^{n_i} u_{ij}^2(k) + 2\dot{x}_i(k) \sum_{j=0}^{n_i} \Big(b_w \dot{x}_i(k) - \sqrt{2b} u_{ij}(k) \Big) \tag{4.9}$$

By invoking Equation (4.2), Equation (4.9) turns to:

$$\sum_{j=0}^{n_i} v_{ij}^2(k) = \sum_{j=0}^{n_i} u_{ij}^2(k) - 2\dot{x}_i(k) \cancelto{0}{\sum_{j=0}^{n_i} f_{ij}(k)} = \sum_{j=0}^{n_i} u_{ij}^2(k), \tag{4.10}$$

which implies that Equation (4.6) is lossless and satisfies the passivity condition

in Equation (4.5) with equity.

- *Node scheme II*: LeBlanc *et. al* in [54] distinguished the local port of the wave node (i.e, zero-indexed) from the over-the-network ports by computing the outgoing waves of the wave node i as:

$$\begin{aligned} v_{i0}(k) &= \frac{1}{\sqrt{n_i}} \sum_{j=1}^{n_i} u_{ij}(k) \\ v_{ij}(k) &= \frac{1}{\sqrt{n_i}} u_{i0}(k) \end{aligned} \tag{4.11}$$

In fact, Equation (4.11) is similar to the local averaging of power variables [80] introduced in Chapter 3 but for wave-based communication networks. Note, the *node scheme II* is a passive interconnection junction of wave channels as shown next. By incorporating the node scheme in Equation (4.11), the outgoing power flow from the wave node i is:

$$\begin{aligned} \sum_{j=0}^{n_i} v_{ij}^2(k) &= \left(\frac{1}{\sqrt{n_i}} \sum_{j=1}^{n_i} u_{ij}(k) \right)^2 + n_i \left(\frac{u_{i0}(k)}{\sqrt{n_i}} \right)^2 \\ &= \frac{1}{n_i} \left(\sum_{j=1}^{n_i} u_{ij}(k) \right)^2 + u_{i0}^2(k). \end{aligned} \tag{4.12}$$

From Cauchy-Schwarz inequality we have:

$$\left(\sum_{j=1}^{n_i} u_{ij}(k) \right)^2 \leq n_i \sum_{j=1}^{n_i} u_{ij}^2(k). \tag{4.13}$$

Substitution of Equation (4.13) into Equation (4.12) gives:

$$\sum_{j=0}^{n_i} v_{ij}^2(k) \leq \sum_{j=0}^{n_i} u_{ij}^2(k), \tag{4.14}$$

which implies that the wave node scheme in Equation (4.11) obtains an input-

output passive mapping for all inputs u_{ij}'s into the wave node i. Note that Equation (4.13) turns into an equality if $v_{ij}(k)$ is constant for all $j \in \{1, \ldots, n_i\}$. However, such conditions rarely occur in practice. Therefore, unlike *node scheme I*, *node scheme II* dissipates energy for most of the times and its dissipative properties must be taken into account when it comes to designing the network structure.

4.4 n-port passive communication network

In this section, n wave nodes of type *node scheme I* are implemented on a multilateral wave-based communication network as shown in Figure 4.3. Each wave node i has

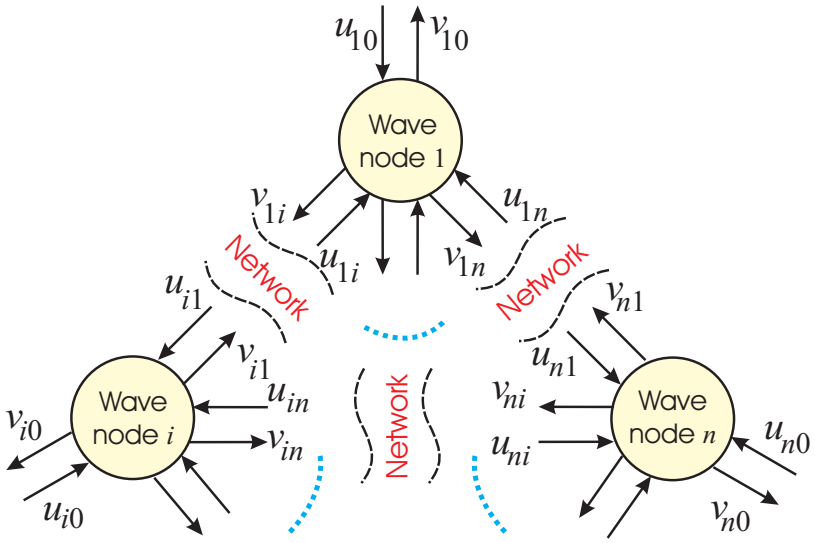

Figure 4.3: Multilateral wave-based communication architecture with n wave nodes.

one local port indicated with "0" that will be used to couple the local SVO copies to the network. The rest of the port indexes of wave node i correspond to the indexes of the nodes to which, the wave node i is connected (i.e, neighbours of node i). The network architecture (shown in Figure 4.3) including n wave nodes with *node scheme I* possesses n-port passivity as proved in the following.

The *node scheme I* is lossless and therefore the sum of all outgoing powers from node i is equal to the sum of all incoming power:

$$u_{i0}^2(k) + \sum_{j \in \mathcal{N}_i} u_{ij}^2(k) = v_{i0}^2(k) + \sum_{j \in \mathcal{N}_i} v_{ij}^2(k), \quad \forall i \in \{1, \ldots, n\} \tag{4.15}$$

Collectively, summing up the terms at both sides of the equity in Equation (4.15) for n nodes gives:

$$\sum_{i=1}^{n} \Big(u_{i0}^2(k) + \sum_{j \in \mathcal{N}_i} u_{ij}^2(k) \Big) = \sum_{i=1}^{n} \Big(v_{i0}^2(k) + \sum_{j \in \mathcal{N}_i} v_{ij}^2(k) \Big). \tag{4.16}$$

By taking the summation over time and rearranging Equation (4.16) we have:

$$T \sum_{k=0}^{\overline{k}} \sum_{i=1}^{n} \Big(u_{i0}^2(k) - v_{i0}^2(k) \Big) = T \sum_{k=0}^{\overline{k}} \sum_{i=1}^{n} \sum_{j \in \mathcal{N}_i} \Big(v_{ij}^2(k) - u_{ij}^2(k) \Big). \tag{4.17}$$

Let $T_d^{ij}(k) = d_{ij}(k)T$ be the time-varying delay with $d_{ij}(k) \in \mathbb{Z}^+$ from side i to side j. This dissertation employs the queue management policy introduced in [19] to maintain the passivity of the wave-based communication channel subject to time-varying delays and packet-losses. Therefore, regardless of time-varying delays and packet drop-out, the right hand side of Equation (4.17) is non-negative since each bidirectional communication channel, connecting sides i and j, satisfies the following:

$$\sum_{k=0}^{\overline{k}} v_{ij}^2(k) \geq \sum_{k=0}^{\overline{k}} u_{ji}^2(k) = \sum_{k=0}^{\overline{k}} v_{ij}^2(k - d_{ij}(k)). \tag{4.18}$$

Substitution of Equation (4.18) into Equation (4.17) gives:

$$T \sum_{k=0}^{\overline{k}} \sum_{i=1}^{n} \Big(u_{i0}^2(k) - v_{i0}^2(k) \Big) \geq 0, \tag{4.19}$$

which implies the n-port passivity of the multilateral communication network shown in Figure 4.3. In other words, the mapping from u_{i0} to v_{i0} for all $i \in \{1, \ldots, n\}$ is passive. It is worth mentioning that when subjected to perfect transmission lines with no delays, the right hand side of Equation (4.17) turns to zero and thus, implying losslessness of the multilateral network architecture built upon *node scheme I*. It is also straightforward to show that the network architecture including n nodes with *node scheme II* is n-port passive [54].

4.5 Passive shared virtual object

This section proposes an architecture for VOs such that the design of the coordinating controllers is decoupled from the communication network, allowing for the selection of coordination gains independent of the number of cooperating peers. The proposed architecture is schematically depicted in Figure 4.4. For fixed number of

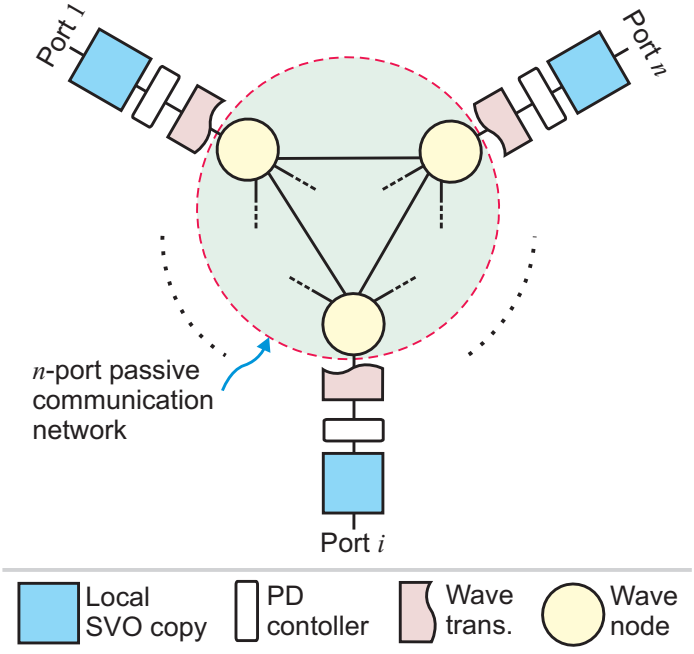

Figure 4.4: n-port passive shared virtual object (SVO).

participants, the discrete-time n-port passivity of the SVO with n copies is assured

by interconnecting the following passive subsystems: (i) local SVO copies; (ii) coordinating controller; and (iii) communication network architecture. Each local SVO and its corresponding coordinating controller is formulated in port-Hamiltonian framework and their discrete-time passivity is ensured by employing the state modification technique introduced in [97]. The passive network architecture introduced in Section 4.4 (shown in dashed circle in Figure 4.4) is composed of multiple wave nodes [44] whose role are to passively distribute power across the network while interconnecting multiple wave-based transmission lines.

4.5.1 Shared virtual object copy

A common means for the simulation of discrete-time dynamical systems is the forward Euler integration technique, mostly because of its low computational load for real time applications. However, such technique does not maintain the passivity of the systems due to energy injection [13]. The simulation of the SVO copies' dynamics and the coordinating controllers as two main elements of our system must preserve passivity in discrete-time setting. In this section, the local SVO copies and proportional-derivative (PD) coordinating controllers are modelled in port-Hamiltonian formalism [100]. We then employ a state modification framework presented in [97] simulate our discrete-time system such that the energetic evolution of its corresponding continuous-time system is resembled. In discrete-time setting, let $H(k)$ be the energy of the system at time instant k and, $\Delta H(K)$ defines the variation of energy during the time step $k \rightarrow k+1$. Hence, the new level of energy can be obtained by $H(k+1) = H(k) + \Delta H(k)$. The numerical algorithm introduced in [97] allows for computing the set of new sates $\mathtt{x}(k+1)$ whose associated energy is equal to $H(k+1)$ being consistent with the energetic evolution of the corresponding continuous-time system. Note, the energy

variation at the k-th time step can be calculated by [13]:

$$\Delta H(k) = T\Big(\mathbf{y}^{\top}(k)\mathbf{u}(k) - \frac{\partial^{\top}\mathtt{H}}{\partial \mathtt{x}}\, b\, \frac{\partial \mathtt{H}}{\partial \mathtt{x}}|_{\mathtt{x}=\mathtt{x}(k)}\Big) \tag{4.20}$$

where $\mathtt{x} \in \mathbb{R}^r$ is the state vector corresponding to r energy-storing elements of the system (e.g, momentum of a mass or elongation of a spring); $\mathbf{u}$ and $\mathbf{y}$ are the input and output vectors respectively; b is the damping; and Hamiltonian $\mathtt{H}(\mathtt{x}) : \mathbb{R}^r \rightarrow \mathbb{R}$ represents the total energy stored in the system.

Therefore, the discrete-time n-port passivity of a VO shared among n peers is made possible by formulating the SVO copies as port-Hamiltonian mass-spring-damper systems connected to the passive network architecture proposed in Section 4.4. Figure 4.5 demonstrates a local SVO copy at side i connected to its corresponding wave-node i via a port-Hamiltonian proportional-derivative (PD) coordinating controller. For local copies in Figure 4.5, each port comprises a pair of power conjugated variables, force f_{*_i} and velocity $\dot{x}_{*_i}$, whose product represents power respectively: at port C for the SVO-haptic device contact; at port T for the SVO-controller contact and; at port 0 denoting the network-PD controller interface.

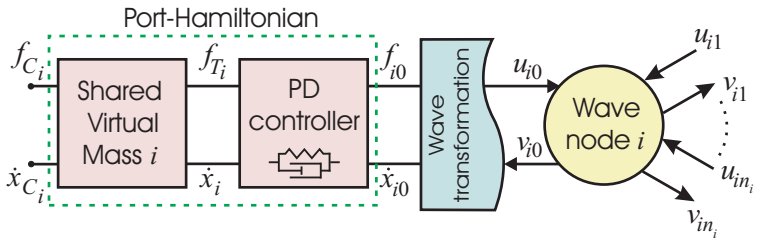

Figure 4.5: Local shared virtual object (SVO) copy i connected to its corresponding wave node at side i via the port-Hamiltonian PD coordinating controller.

Next, it is shown that the passivity condition in Equation (4.17) implies the n-port passivity of the network structure with respect to the power variables $\dot{x}_{i0_i}$ and f_{i0} for

$i = 1, \ldots, n$. From the wave transformation in Equation (4.2) we have:

$$u_{i0}(k) = \frac{b_w \dot{x}_{i0}(k) + f_{i0}(k)}{\sqrt{2b_w}}, \quad v_{i0}(k) = \frac{b_w \dot{x}_{i0}(k) - f_{i0}(k)}{\sqrt{2b_w}}. \tag{4.21}$$

Substitution of Equation (4.21) into Equation (4.19) yields:

$$T \sum_{k=0}^{\overline{k}} \sum_{i=1}^{n} \left(f_{i0}(k) \dot{x}_{i0}(k) \right) \geq 0. \tag{4.22}$$

where $f_{i0} = f_{T_i} = K_T q(k) + B_T \dot{q}(k)$; $q = x_i - x_{i0}$ is the position error corresponding to the elongation of the spring; and K_T and B_T are the proportional (stiffness) and derivative (damping) gains of the coordinating controller.

Port-Hamiltonian SVO and coordinating controllers

The discrete-time two-port passivity of each local SVO copy and PD coordinating controller is ensured through implementing the local SVO copy and its PD controller as two interconnected discrete-time port-Hamiltonian systems with states updated using the algorithm introduced in [94]. Therefore, the discrete-time two-port passivity condition of the i-th local copy of the SVO together with its coordinating PD controller (shown in the dashed box in Figure 4.3) with respect to the power variables pairs $(f_{C_i}, \dot{x}_{C_i})$ and $(f_{i0}, \dot{x}_{i0})$ is:

$$T \sum_{k=0}^{\overline{k}} \left(f_{C_i}(k) \dot{x}_{C_i}(k) - f_{i0}(k) \dot{x}_{i0}(k) \right) \geq -\frac{1}{2} K_T q_i^2(0) - \frac{p_i^2(0)}{2m}, \tag{4.23}$$

where m is the mass of the SVO copy, $q_i(0)$ is the initial spring elongation and $p_i(0)$ is the initial momentum of the i-th SVO copy. The right hand side of Equation (4.23) represents the initial potential and kinetic energy of the i-th PD controller and SVO mass, respectively (see Appendices A.5, A.6, and A.7 for the detailed derivations).

The interconnection of n discrete-time port-Hamiltonian SVO copies via local coordinating PD controllers and the network architecture shown in Figure 4.3 leads to an n-port passive discrete-time SVO. For n SVO copies, Equation (4.23) yields:

$$T\sum_{i=1}^{n}\sum_{k=0}^{\overline{k}}\Big(f_{C_i}(k)\dot{x}_{C_i}(k)-f_{i0}(k)\dot{x}_{i0}(k)\Big)\geq\sum_{i=1}^{n}\Big(-\frac{1}{2}K_Tq_i^2(0)-\frac{p_i^2(0)}{2m}\Big). \quad (4.24)$$

After substitution from Equation (4.22), Equation (4.24) becomes:

$$T\sum_{i=1}^{n}\sum_{k=0}^{\overline{k}}\Big(f_{C_i}(k)\dot{x}_{C_i}(k)\Big)\geq\sum_{i=1}^{n}\Big(-\frac{1}{2}K_Tq_i^2(0)-\frac{p_i^2(0)}{2m}\Big) \quad (4.25)$$

which implies discrete-time n-port passivity of the SVO with n copies. In this thesis the VO is characterised by impedance causality, that is, the contact controller accepts the position of the haptic device as the input and computes the interaction force as its output. Note, the interconnection of haptic interfaces (with position sensors) and passive VOs may not be power conserving. This is due to the fact that the velocity information of the continuous-time haptic device is not available and usually is computed from position information via forward Euler discrete derivation. In this work, we employ "Passive Continuous Discrete time Connector (PCDC)" [13] to assure that there is no energy generated at the analogue-digital converter. Therefore, it can be inferred that Equation (4.25) also accounts for the passivity of the system when human operators and haptic devices are in the loop. Also note that our proposed architecture neither requires damping injection on the dynamics of local SVO copies nor needs *em a priori* knowledge of network conditions. Therefore, unlike [39] it allows for less sluggish motion of the SVO in the presence of varying network delay and packet drop-out. Section 4.7 verifies the passivity of the SVO built based on *node schemes I* and *II* via simulations of four SVO copies connected across a network with varying time delays.

4.6 Steady-state analysis

In continuous-time setting, this section studies the steady-state response of both wave nodes implemented on the proposed multi-lateral wave-based communication architecture when the distributed SVO copies are interconnected over a fully-connected graph. With T_d^{ij} being the constant delay from side i to side j, for each wave-based transmission channel between sides i and j the following relation holds:

$$u_{ij}(t) = v_{ji}(t - T_d^{ji}) \tag{4.26}$$

Note, Equation (4.21) can be used to decode the wave variables u_{ij} and v_{ij} into their corresponding velocity $\dot{x}_{ij}$ and force f_{ij}. In the analysis presented in sections 4.6.1 and 4.6.2, the controller gains are selected such that the system remains stable.

4.6.1 Node scheme I

It is required to find a relation for the decoded velocity at the i-th site based on the encoded information of the rest of the sites, i.e $j \in \mathcal{N}_i$. Since in this section we assume the SVO copies are interconnected on a fully-connected graph, the cardinality of the neighbours set $\mathcal{N}_i$ is $n_i = n - 1$; $\forall i \in \{1, \ldots, n\}$, with n being the number of SVO copies. From Equation (4.21), the decoded velocity at port 0 of node i is:

$$\dot{x}_{i0}(t) = \sqrt{\frac{2}{b_w}} v_{i0}(t) + \frac{f_{i0}(t)}{b_w} \tag{4.27}$$

From Equation (4.6), v_{i0} can be written as:

$$\begin{aligned} v_{i0}(t) &= -u_{i0}(t) + \frac{2}{n_i+1}\Big(u_{i0}(t) + \sum_{j\in\mathcal{N}_i} u_{ij}(t)\Big) \\ &= \Big(\frac{1-n_i}{n_i+1}\Big)u_{i0}(t) + \frac{2}{n_i+1}\sum_{j\in\mathcal{N}_i} u_{ij}(t) \end{aligned} \tag{4.28}$$

Substitution of Equation (4.28) into Equation (4.27) along with Equation (4.26) gives:

$$\dot{x}_{i0}(t) = \sqrt{\frac{2}{b_w}}\left(\Big(\frac{1-n_i}{n_i+1}\Big)u_{i0}(t) + \frac{2}{n_i+1}\sum_{j\in\mathcal{N}_i} v_{ji}(t-T_d^{ji})\right) + \frac{f_{i0}(t)}{b_w} \tag{4.29}$$

From Equation (4.21), $u_{i0}(t)$ and $v_{ji}(t-T_d^{ji})$ in the above equation can be written in terms of their corresponding decoded power variables as,

$$\begin{aligned} \dot{x}_{i0}(t) = \sqrt{\frac{2}{b_w}}\Bigg(&\Big(\frac{1-n_i}{n_i+1}\Big)\frac{b_w\dot{x}_{i0}(t)+f_{i0}(t)}{\sqrt{2b_w}} + \\ &\frac{2}{n_i+1}\sum_{j\in\mathcal{N}_i}\frac{b_w\dot{x}_{ji}(t-T_d^{ji}) - f_{ji}(t-T_d^{ji})}{\sqrt{2b_w}}\Bigg) + \frac{f_{i0}(t)}{b_w} \end{aligned} \tag{4.30}$$

Given the fact that *node scheme I* represents equal velocities at all its ports, for node j we have $\dot{x}_{ji} = \dot{x}_{j0};\quad \forall i \in \mathcal{N}_j$. Therefore, Equation (4.30) can be further simplified to:

$$\dot{x}_{i0}(t) = \frac{1}{n_i}\Big(\sum_{j\in\mathcal{N}_i}\dot{x}_{j0}(t-T_d^{ji}) + \frac{f_{i0}(t)}{b_w} - \frac{\sum_{j\in\mathcal{N}_i} f_{ji}(t-T_d^{ji})}{b_w}\Big) \tag{4.31}$$

The dynamics of the i-th SVO copy with zero local damping $b = 0$ is:

$$m\ddot{x}_i(t) = f_{C_i}(t) - f_{T_i}(t) \tag{4.32}$$

in which,

$$f_{T_i}(t) = K\big(x_i(t) - x_{i0}(t)\big) + B\big(\dot{x}_i(t) - \dot{x}_{i0}(t)\big) \tag{4.33}$$

Hence, Equation (4.32) in Laplace domain turns to:

$$(ms^2 + Bs + K)X_i(s) = F_{C_i}(s) + (Bs + K)X_{i0}(s) \tag{4.34}$$

Besides, the Laplace transformation of Equation (4.31) gives:

$$X_{i0}(s) = \frac{1}{n_i}\Big(\sum_{j\in\mathcal{N}_i} e^{-sT_d^{ji}} X_{j0}(s) + \frac{F_{i0}(s)}{b_w s} - \frac{\sum_{j\in\mathcal{N}_i} e^{-sT_d^{ji}} F_{ji}(s)}{b_w s}\Big) \tag{4.35}$$

Replacement of $X_{i0}(s)$ from Equation (4.31) into Equation (4.34) yields:

$$\begin{aligned}(ms^2 + Bs + K)X_i(s) = F_{C_i}(s) \\ + \frac{Bs + K}{n_i}\Bigg(\sum_{j\in\mathcal{N}_i} e^{-sT_d^{ji}} X_{j0}(s) \\ + \frac{F_{i0}(s)}{b_w s} - \frac{\sum_{j\in\mathcal{N}_i} e^{-sT_d^{ji}} F_{ji}(s)}{b_w s}\Bigg).\end{aligned} \tag{4.36}$$

From Equation (4.34), similarly, $X_{j0}(s)$ for $j \in \mathcal{N}_i$ can be replaced in Equation (4.36) to give:

$$\begin{aligned}(ms^2 + Bs + K)X_i(s) = F_{C_i}(s) \\ + \frac{Bs + K}{n_i}\Bigg(\frac{\sum_{j\in\mathcal{N}_i} e^{-sT_d^{ji}}\Big((ms^2 + Bs + K)X_j(s) - F_{C_j}(s)\Big)}{Bs + K} \\ + \frac{F_{i0}(s) - \sum_{j\in\mathcal{N}_i} e^{-sT_d^{ji}} F_{ji}(s)}{b_w s}\Bigg),\end{aligned} \tag{4.37}$$

which can be further simplified to:

$$\begin{aligned} X_i(s) = & \frac{\sum_{j\in\mathcal{N}_i} e^{-sT_d^{ji}} X_j(s)}{n_i} \\ & + \Big(\frac{F_{C_i}(s) - \frac{\sum_{j\in\mathcal{N}_i} e^{-sT_d^{ji}} F_{C_j}(s)}{n_i}}{ms^2+Bs+K}\Big) \\ & + \frac{Bs+K}{(n_i)b_w s(ms^2+Bs+K)}\Big(F_{i0}(s) - \sum_{j\in\mathcal{N}_i} e^{-sT_d^{ji}} F_{ji}(s)\Big). \end{aligned} \tag{4.38}$$

Because the local contact forces are considered constant in this section, their dependency on time is dropped in the subsequent derivations. To derive the steady-state solution, let the following relation hold:

$$f_{C_i} + \sum_{j\in\mathcal{N}_i} f_{C_j} = 0, \qquad \forall i \in \{1,\dots,n\} \tag{4.39}$$

Therefore, using the Laplace transform of Equation (4.39), Equation (4.38) turns to:

$$\begin{aligned} X_i(s) = & \frac{\sum_{j\in\mathcal{N}_i} e^{-sT_d^{ji}} X_j(s)}{n_i} + \Big(\frac{\frac{f_{C_i}}{s} - \frac{\frac{-f_{C_i}}{s}\sum_{j\in\mathcal{N}_i} e^{-sT_d^{ji}}}{n_i}}{ms^2+Bs+K}\Big) \\ & + \frac{Bs+K}{(n_i)b_w s(ms^2+Bs+K)}\Big(F_{i0}(s) - \sum_{j\in\mathcal{N}_i} e^{-sT_d^{ji}} F_{ji}(s)\Big). \end{aligned} \tag{4.40}$$

Application of $\lim_{s\to 0} s$ on both sides of the Equation (4.40) gives:

$$\begin{aligned} \lim_{s\to 0} sX_i(s) = & \lim_{s\to 0} \frac{\sum_{j\in\mathcal{N}_i} e^{-sT_d^{ji}} sX_j(s)}{n_i} \\ & + \lim_{s\to 0} s\Big(\frac{\frac{f_{C_i}}{s} - \frac{\frac{-f_{C_i}}{s}\sum_{j\in\mathcal{N}_i} e^{-sT_d^{ji}}}{n_i}}{ms^2+Bs+K}\Big) \\ & + \lim_{s\to 0} \frac{Bs+K}{(n_i)b_w(s^2+Bs+K)}\Big(F_{i0}(s) - \sum_{j\in\mathcal{N}_i} e^{-sT_d^{ji}} F_{ji}(s)\Big) \end{aligned} \tag{4.41}$$

Knowing the fact that $\lim_{s\to 0} e^{-sT_d^{ij}} = 1$, Equation (4.41) is simplified to:

$$\begin{aligned}\lim_{s\to 0} sX_i(s) = \lim_{s\to 0} \frac{\sum_{j\in\mathcal{N}_i} sX_j(s)}{n_i} + \frac{(n_i+1)f_{C_i}}{(n_i)K} \\ + \lim_{s\to 0} \frac{Bs+K}{(n_i)b_w(s^2+Bs+K)}\Big(F_{i0}(s) - \sum_{j\in\mathcal{N}_i} F_{ji}(s)\Big)\end{aligned} \tag{4.42}$$

As detailed in Appendix A.3, the following relation holds,

$$\lim_{s\to 0} F_{ij}(s) = -\lim_{s\to 0} F_{ji}(s). \tag{4.43}$$

Therefore, substitution of Equation (4.43) into Equation (4.42) results in:

$$\begin{aligned}\lim_{s\to 0} sX_i(s) = \lim_{s\to 0} \frac{\sum_{j\in\mathcal{N}_i} sX_j(s)}{n_i} + \frac{(n_i+1)f_{C_i}}{(n_i)K} \\ + \lim_{s\to 0} \frac{Bs+K}{(n_i)b_w(s^2+Bs+K)} \lim_{s\to 0}\Big(F_{i0}(s) + \sum_{j\in\mathcal{N}_i} F_{ij}(s)\Big) \to 0\end{aligned} \tag{4.44}$$

in which, the last term is zero since the sum of all decoded forces for *node scheme I* at node i is zero, i.e, $f_{i0}(t) + \sum_{j\in\mathcal{N}_i} f_{ij}(t) = 0$. Hence, from the final value theorem, Equation (4.44) in time domain yields,

$$e_{ss}(t\to\infty) = \lim_{t\to\infty}\Big(x_i(t) - \frac{\sum_{j\in\mathcal{N}_i} x_j(t)}{n_i}\Big) = \frac{(n_i+1)f_{C_i}}{(n_i)K} \tag{4.45}$$

where e_{ss} stands for the steady-state error. The above relation implies that the steady-state error of the distributed SVO implemented based *node scheme I* is bounded. □

4.6.2 Node scheme II

From the definition of wave transformation in Equation (4.21), the decoded velocity at port 0 of node i is:

$$\dot{x}_{i0}(t) = \frac{\sqrt{2b_w}v_{i0}(t) + f_{i0}(t)}{b_w} \tag{4.46}$$

From Equation (4.11), the arriving wave v_{i0} can be replaced in Equation (4.46) to give:

$$\begin{aligned} \dot{x}_{i0}(t) &= \sqrt{\frac{2}{b_w}}\Big(\frac{1}{\sqrt{n_i}}\sum_{j\in\mathcal{N}_i} u_{ij}(t)\Big) + \frac{f_{i0}(t)}{b_w} \\ &= \sqrt{\frac{2}{b_w}}\Big(\frac{1}{\sqrt{n_i}}\sum_{j\in\mathcal{N}_i} v_{ji}(t - T_d^{ji})\Big) + \frac{f_{i0}(t)}{b_w} \end{aligned} \tag{4.47}$$

in which, for the last line, we used Equation (4.26) to replace u_{ij}. From Equation (4.11), v_{ji} can be substituted into Equation (4.47) which yields:

$$\dot{x}_{i0}(t) = \sqrt{\frac{2}{b_w}}\Big(\sum_{j\in\mathcal{N}_i} \frac{u_{j0}(t - T_d^{ji})}{n_i}\Big) + \frac{f_{i0}(t)}{b_w} \tag{4.48}$$

From the definition of wave transformation in Equation (4.21), the corresponding power variables of u_{j0} are substituted into Equation (4.48) as:

$$\dot{x}_{i0}(t) = \sum_{j\in\mathcal{N}_i}\Big(\frac{b_w\dot{x}_{j0}(t - T_d^{ji}) + f_{j0}(t - T_d^{ji})}{(n_i)b_w}\Big) + \frac{f_{i0}(t)}{b_w} \tag{4.49}$$

Given the fact that $f_{T_j}(t) = f_{j0}(t)$ for the coupling force developed in the coordinating controller (see Figure 4.5), by using Equation (4.33) for side j we have:

$$f_{j0}(t) = K\big(x_j(t) - x_{j0}(t)\big) + B\big(\dot{x}_j(t) - \dot{x}_{j0}(t)\big). \tag{4.50}$$

The above equation in Laplace domain turns to:

$$F_{j0}(s) = (Bs + K)\big(X_j(s) - X_{j0}(s)\big) \tag{4.51}$$

Besides, Equation (4.49) in Laplace domain turns to:

$$sX_{i0}(s) = \sum_{j \in \mathcal{N}_i} e^{-sT_d^{ji}} \Big(\frac{b_w s X_{j0}(s) + F_{j0}(s)}{(n_i) b_w} \Big) + \frac{F_{i0}(s)}{b_w} \tag{4.52}$$

Hence, $F_{i0}(s)$ can also be obtained similar to Equation (4.51) and all together, plugged into Equation (4.52) to yield:

$$\begin{aligned} sX_{i0}(s) = \sum_{j \in \mathcal{N}_i} e^{-sT_d^{ji}} \Big(\frac{b_w s X_{j0}(s) + (Bs + K)\big(X_j(s) - X_{j0}(s)\big)}{(n_i) b_w} \Big) \\ + \frac{(Bs + K)\big(X_i(s) - X_{i0}(s)\big)}{b_w} \end{aligned} \tag{4.53}$$

which can be simplified to:

$$\begin{aligned} X_{i0}(s) = \frac{\big((b_w - B)s - K\big)}{(n_i)\big((b_w + B)s + K\big)} \sum_{j \in \mathcal{N}_i} e^{-sT_d^{ji}} X_{j0}(s) \\ + \frac{Bs + K}{(n_i)\big((b_w + B)s + K\big)} \Big((n_i) X_i(s) + \sum_{j \in \mathcal{N}_i} e^{-sT_d^{ji}} X_j(s) \Big) \end{aligned} \tag{4.54}$$

Substitution of $X_{i0}(s)$ from Equation (4.54) into the dynamics of the i-th SVO copy (i.e, Equation (4.34)) results in:

$$\begin{aligned} (ms^2 + Bs + K) X_i(s) = \frac{f_{C_i}}{s} \\ + \frac{\big((b_w - B)s - K\big)(Bs + K)}{(n_i)\big((b_w + B)s + K\big)} \sum_{j \in \mathcal{N}_i} e^{-sT_d^{ji}} X_{j0}(s) \\ + \frac{(Bs + K)^2}{(n_i)\big((b_w + B)s + K\big)} \Big((n_i) X_i(s) + \sum_{j \in \mathcal{N}_i} e^{-sT_d^{ji}} X_j(s) \Big) \end{aligned} \tag{4.55}$$

From the dynamics of the j-th SVO copy as in Equation (4.34), $X_{j0}(s)$ can be plugged into Equation (4.55) to yield:

$$\begin{aligned} X_i(s) = & \frac{\big((b_w+B)s+K\big)f_{C_i}}{sD_2(s)} \\ & + \frac{1}{(n_i)D_2(s)}\Bigg(D_1(s)\sum_{j\in\mathcal{N}_i} e^{-sT_d^{ji}}X_j(s) \\ & - \big((b_w-B)s-K\big)\sum_{j\in\mathcal{N}_i} e^{-sT_d^{ji}}\frac{f_{C_j}}{s}\Bigg) \end{aligned} \tag{4.56}$$

in which

$$\begin{aligned} D_1(s) &= (ms^2+Bs+K)\big((b_w-B)s-K\big)+(Bs+K)^2 \\ D_2(s) &= (ms^2+Bs+K)\big((b_w+B)s+K\big)-(Bs+K)^2. \end{aligned} \tag{4.57}$$

Since $\lim_{s\to 0} D_1(s)/D_2(s) = 1$ and $\lim_{s\to 0} e^{-sT_d^{ji}} = 1$, application of $\lim_{s\to 0} s$ on both sides of the Equation (4.56) gives,

$$\begin{aligned} \lim_{s\to 0}\Big(sX_i(s) - \frac{\sum_{j\in\mathcal{N}_i} sX_j(s)}{n_i}\Big) = \lim_{s\to 0}\Bigg(& \frac{\big((b_w+B)s+K\big)f_{C_i}}{D_2(s)} \\ & - \frac{(b_w-B)s-K}{(n_i)D_2(s)}\sum_{j\in\mathcal{N}_i} f_{C_j}\Bigg) \end{aligned} \tag{4.58}$$

By using Equation (4.39), the right hand side of Equation (4.58) can be rearranged as:

$$\begin{aligned} \lim_{s\to 0}\Bigg(& \frac{(n_i)\Big((b_w+B)s+K\Big)+\Big((b_w-B)s-K\Big)}{(n_i)D_2(s)}f_{C_i}\Bigg) \\ &= \lim_{s\to 0}\frac{\Big((n_i+1)b_w+(n_i-1)B\Big)s+(n_i-1)K}{(n_i)\Big(m(b_w+B)s^3+(mK+b_wB)s^2+b_wKs\Big)}f_{C_i} \\ &= \frac{(n_i-1)k}{0}f_{C_i} \equiv \infty; \qquad\qquad \forall n_i > 1. \end{aligned} \tag{4.59}$$

Therefore, Equation (4.58) turns to:

$$\lim_{s\to 0}\Big(sX_i(s) - \frac{\sum_{j\in\mathcal{N}_i} sX_j(s)}{n_i}\Big) \to \infty. \tag{4.60}$$

From final value theorem, the above relation in time domain gives:

$$e_{ss}(t\to\infty) = \lim_{t\to\infty}\Big(x_i(t) - \frac{\sum_{j\in\mathcal{N}_i} x_j(t)}{n_i}\Big) \to \infty, \tag{4.61}$$

which implies that the steady-state error of the distributed SVO implemented using *node scheme II* is unbounded. □

4.7 Simulations

This section validates the theoretical findings presented in Section 4.5 through 1-DOF simulations of a VO with four distributed copies connected over bidirectional communications. Since this section only focuses on the passivity of the distributed SVO, simulations include the autonomous dynamics of the SVO with no haptic devices or users in the loop. Note, when the continuous-time electromechanical haptic displays and human operators are in the loop, the power conserving policy [13] for the interconnection of digital and continuous-time systems can be incorporated.

In all simulations, the initial positions of SVO copies are $[0.035, -0.01, 0.02, -0.04]^\top m$ and their initial velocities are set to zero. The sampling time is $T = 0.001\ s$ and the characteristic wave impedance is $b_w = 30\ Ns/m$. Each SVO copy has mass value of $0.15\ kg$ and is coordinated via a controller with proportional gain $K_T = 2000\ N/m$. The energy dissipation in the network is attributed to: (i) the wave node power distribution control law (i.e, *node scheme I* or *II*); and (ii) the communication imperfections. To energetically compare the two wave node schemes, a distributed VO

with minimal damping is simulated in SIMULATION I by setting the derivative gains of the coordinating controllers to zero ($B_T = 0$) and the time delay to a negligible value of $T_d = 0.001\ s$. In SIMULATION II and SIMULATION III, the derivative gain is $B_T = 0.2\ Ns/m$ and the time-delay varies as $0 \leq T_d \leq 0.06\ s$, as shown in Figure 4.6. Moreover, a fully connected and undirected network is used for communications in SIMULATION I and SIMULATION I, and connected and undirected network is used in SIMULATION III.

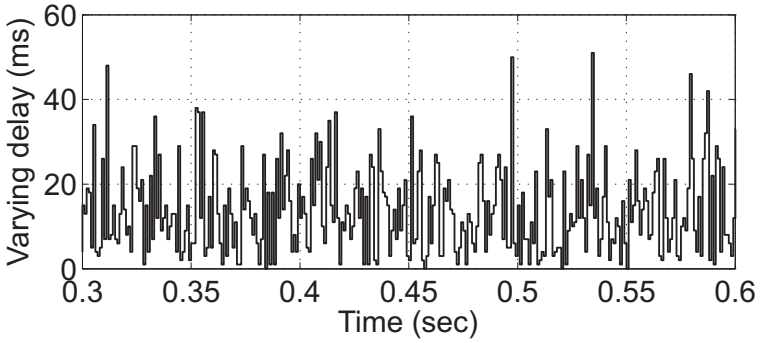

Figure 4.6: Time varying delay profile selected within the region $0 \leq T_d \leq 0.06$ s.

SIMULATION I: Figure 4.7a and Figure 4.7b depict the positions of four distributed SVO copies with wave communications when using *node scheme I* and in *node scheme II*, respectively. The wave node in *node scheme I* is lossless and therefore, the energy stored in the 4-port network is little compared to network with *node scheme II* (see Figure 4.7c in log-scale). The dissipation in the wave nodes in *node scheme II* leads to the settling of the SVO copies, whereas the lossless nature of the wave nodes with *node scheme I* can be observed in the continued oscillation of the SVO copies with constant amplitude.

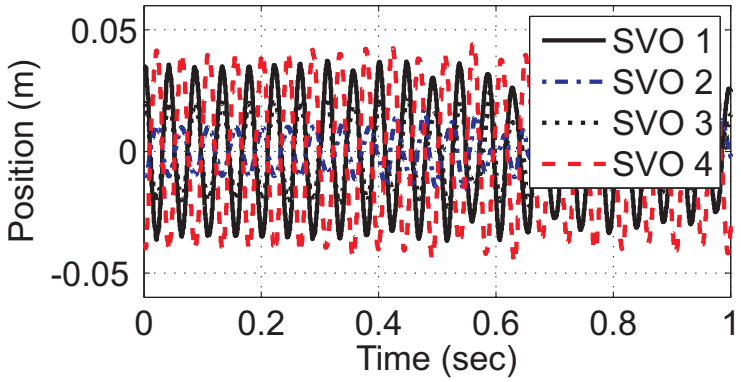

(a) Node scheme I.

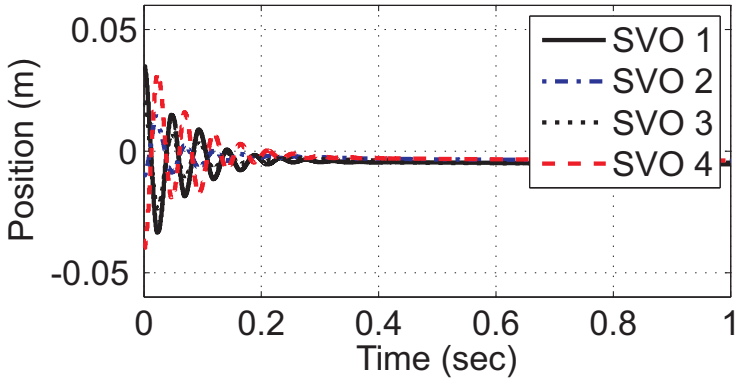

(b) Node scheme II.

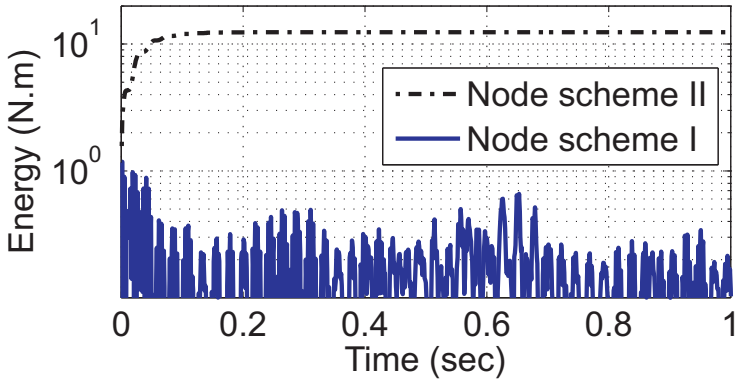

(c) Stored energy in the 4-port communication network.

Figure 4.7: Four SVO copies connected over a network with constant delay T_d = 0.001 s.

SIMULATION II: On a fully-connected network topology, Figure 4.8 compares the two wave-node schemes when the time-delay is varying and selected from the interval $0 \leq T_d \leq 0.06\ s$. The time varying delay is generated randomly in MATLAB/Simulink and a part of the simulation time is shown in Figure 4.6. The queue management strategy introduced in [19] is adopted to maintain the passivity of communication channels under varying time-delays. The dissipation caused by such algorithm results in the storage of energy in the network structure. However, network architecture build upon *wave scheme I* offers less dissipation resulting in longer settling time (see Figure 4.8a) and lower stored energy in the network structure (Figure 4.8c).

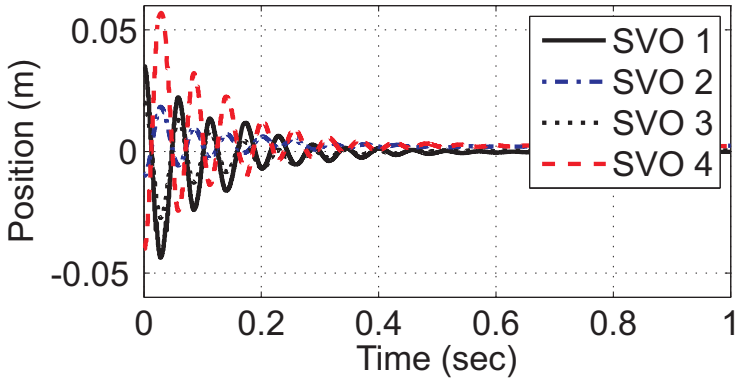

(a) Node scheme I on a fully-connected graph.

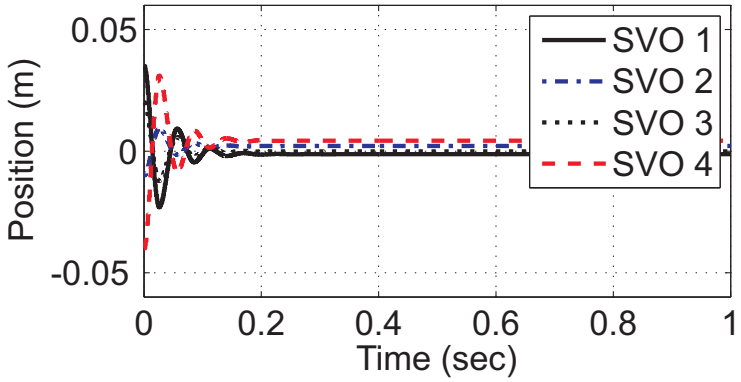

(b) Node scheme II on a fully-connected graph.

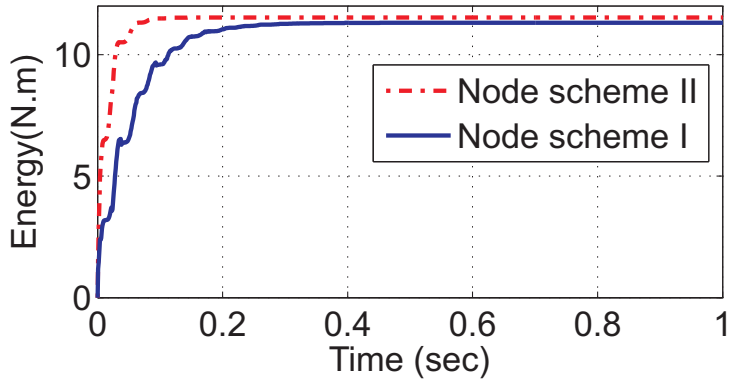

(c) Stored energy in the 4-port communication network.

Figure 4.8: Four SVO copies with varying network delay $0 \leq T_d \leq 0.06$ s.

SIMULATION III: In case of failure of a communication channel, as long as the connectivity graph stays connected, the peers can still interact through the remaining channels. In this simulation, the four SVO copies are interconnected via the connected graph for which SVO 4 losses its connections with SVO 1 and 2 as shown in Figure 4.9;

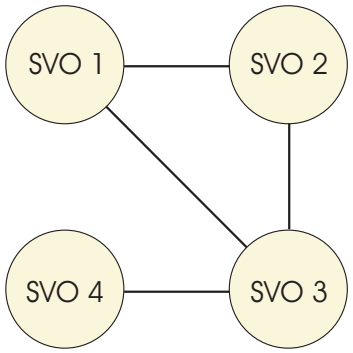

Figure 4.9: Four distributed SVO's on a connected graph.

The results in Figure 4.10 confirm that the 4-port passive SVO maintains its stability on a not necessarily fully-connected graph in the presence of time-varying delay.

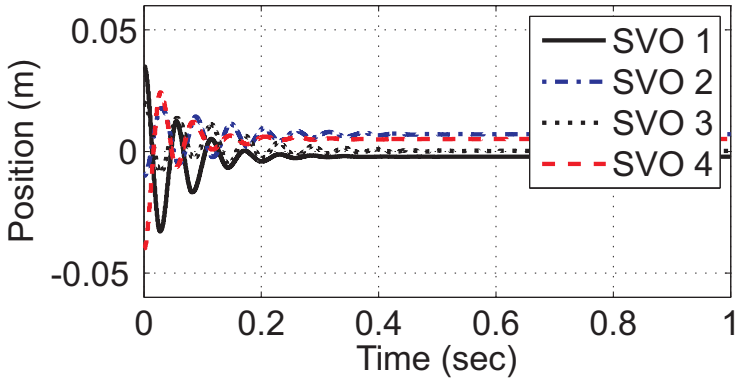

(a) Node scheme I on a connected graph.

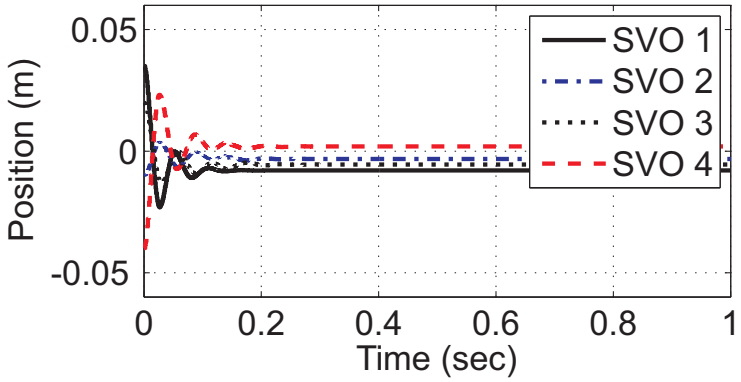

(b) Node scheme II on a connected graph.

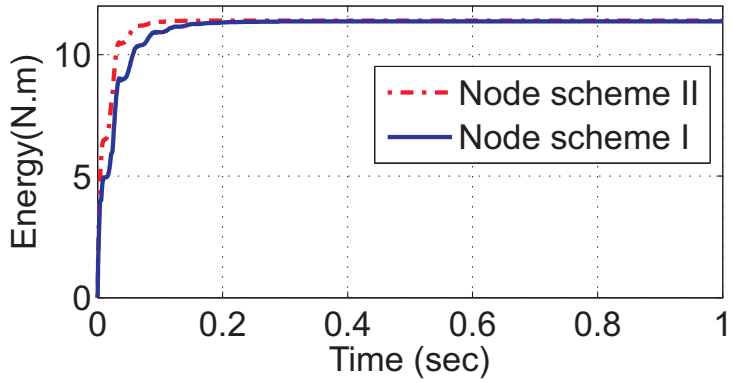

(c) Stored energy in the 4-port communication network with wave nodes implemented on a connected graph.

Figure 4.10: Four SVO copies with varying network delay $0 \leq T_d \leq 0.06$ s when SVO copies are connected via the graph shown in Figure (4.9).

4.7.1 Discussion

For the network structure built based on *node scheme II*, the stored energy in the network attains the value of 11.73 Nm on a fully-connected graph in Figure 4.8c where as on a connected communication topology, the energy value is 11.503 Nm as in in Figure 4.10c. This is because a dissipative element, i.e. a wave node, is dropped from the network. In fact, the wave node corresponding to the SVO 4 turns to a lossless element when $\mathcal{N}_4 = 1$ (see Equation (4.11). Also note that the dissipative effects of *node scheme II* cause faster settling time in Figures 4.8b and 4.10b comparing to *node scheme I* in Figures 4.8a and 4.10a. The storage of energy is attributed to the dissipation of energy due to: (i) *wave nodes constraints*: since the node law in Equation (4.11) implies passive distribution of power whereas Equation (4.6) represents a lossless one and/or; (ii) *varying time delay*: as the reordered packets, considered as dropped packets, result to a dampen motion due to the loss of the energy quanta. The steady-state position error is attributed to the transmission of velocity data across the wave communications. This issue can be mitigated by transferring wave integrals as suggested in [104]. Experimental validations are presented next.

4.8 Experiments

This section validates the the theoretical findings in Section 4.6 by performing experiments on a platform comprising three identical FALCON NOVINT haptic devices, each connected to a respective computer to provide 3DOF force feedback to the users. The setup is similar to the one we used in previous Chapter (as in Figure 3.8). Note that given the proximity of the three computers, the actual network delay over the LAN is negligible. The varying delay is modelled artificially to implement the network environment (see Figure 4.11). The VE is generated as a C++ console application

and comprises a virtual cube (shared among three users) in a rigid enclosure that constrains the cube to move horizontally along a single direction (i.e, x-axis). The parameters used in the experiments are selected as: $M = 0.5$ kg is the mass of the virtual cube; $b = 0$ Ns/m is the local damping; $b_w = 15$ denotes the wave impedance; the coordination stiffness and damping are $K_T = 6000$ N/m and $B_T = 5$ Ns/m respectively; and the varying communication delay 20 ms $\leq T_d(k) \leq$ 70 ms is implemented in all communications via programming.

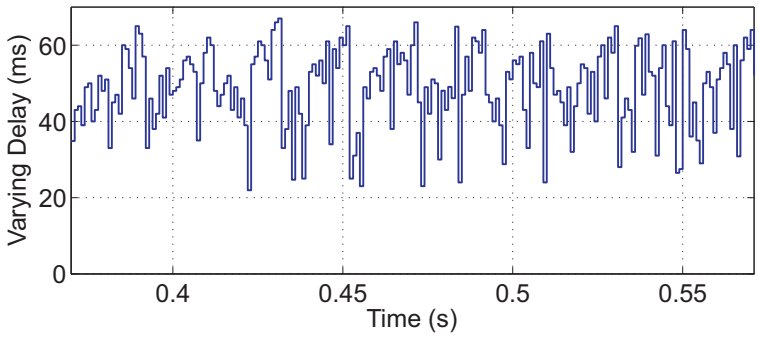

Figure 4.11: Experimental profile of the time varying delay selected from the interval 20 ms $\leq T_d(k) \leq$ 70 ms.

The experimental steady-state tests are categorized in twofold:

- Three-users Haptic cooperation when controlled forces are applied onto the SVO copies (Figures 4.13, 4.14, 4.15, & 4.16) - these sets of experiments allow for excluding the dynamics of the human hand from the results;
- Three-users Haptic cooperation when users are in the loop (Figures 4.17 & 4.18);

4.8.1 Haptic cooperation with controlled applied forces

This section presents the experimental three-users haptic cooperation when the controlled applied forces on the SVO copies i) are balanced and sum up to zero (Figures 4.13 & 4.15); and ii) are unbalanced (Figures 4.14 & 4.16)), resulting to the motion

of the shared virtual cube along the closure. The force profile of the balanced and unbalanced applied forces are respectively depicted in Figure 4.12a and Figure 4.12b.

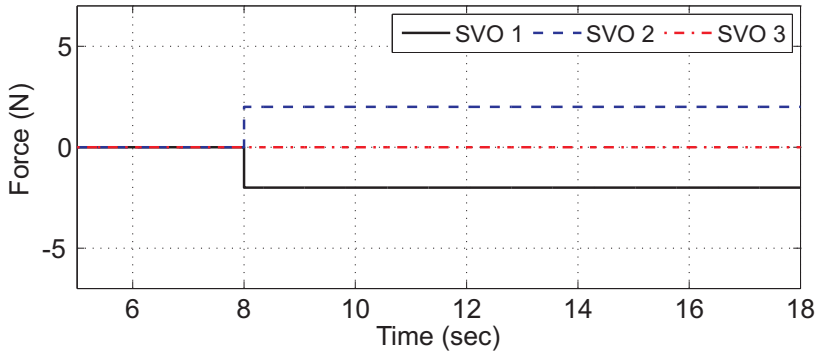

(a) Balanced forces.

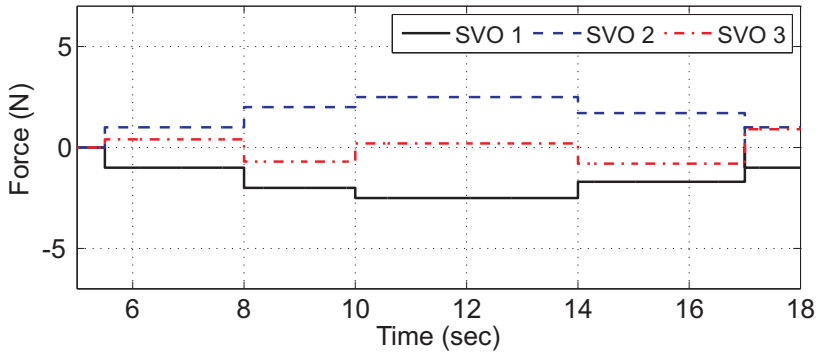

(b) Unbalanced forces.

Figure 4.12: External controlled forces applied on the local SVO copies.

Over communication channels with constant time delay of $T_d = 50$ ms, Figures 4.13 & 4.14 compare the performance of the three-users haptic cooperation implemented based on *node schemes I* and *node schemes II*. Note that the unbalanced controlled forces are chosen such the shared virtual cube remains within the closure designed in the VE (see Figure 4.12b). These Figures confirm the theoretical steady-state results in Section 4.6 by certifying that the implementation of *node scheme II* on the multi-lateral wave-based communication channel (shown in Figure 4.3) causes the SVO copies drift apart as the simulation time grows.

In a similar procedure but over communication channels with time-varying delay of 20 ms $\leq T_d(k) \leq$ 70 ms, the experiments are conducted for both balanced and

unbalanced controlled forces, respectively in Figure 4.15 and Figure 4.16. It is worth mentioning that since we employ the queue management algorithm [19] to maintain the passivity of the communication channels with varying time delay, the overall passivity of the cooperation is not violated and when *node scheme I* is implemented, the cooperation still does not suffer any position drift. However, the problem of position drift is apparent when the *node scheme II* is implemented. By comparing the Figures 4.13 & 4.14 with Figures 4.15 & 4.16, for each case, the haptic cooperation over communications with varying delay seems to be sluggish (i.e, with smaller velocity profiles). This issue is attributed to the dissipation of energy in communication links under varying time delay. In fact, the employment of queue management strategy [19] (to maintain the passivity of wave-based communication under varying time delay) enforces dissipative behaviour which results to dampened motion.

4.8.2 Haptic cooperation with users in-the-loop

In a more realistic scenario in this section, the three-users haptic cooperation experiments are performed when users are in-the-loop. When the experiments commence, users start interacting with their local SVO copies via the avatar of their haptic devices. Note that in all of these experiments, distributed peers managed to keep the shared virtual cube within the closure in the VE. Figure 4.17 and Figure 4.18 respectively present the haptic cooperation over communications with constant and varying time delays. The corresponding contact forces are depicted in Figure 4.19 and Figure 4.20.

4.9 Summary

In distributed haptic cooperation, passive virtual environments alongside passive haptic devices ensure the stability of the closed loop system. In this chapter, the discrete-time n-port passivity of the shared virtual object (SVO) with n copies is assured by interconnecting the following passive subsystems: (i) local SVO copies; (ii) coordinating controllers; and (iii) communication network architecture. Each local SVO copy and its corresponding proportional-derivative (PD) coordination controller is formulated in port-Hamiltonian framework and their discrete-time passivity is ensured by employing the state modification techniques introduced in [13, 97]. Wave nodes as passive network elements were implemented on multilateral wave-based communication architecture to passively distribute power across the network. In this chapter, the node scheme introduced in [44], referred as *node scheme I*, is employed to construct a passive wave-based network architecture over an undirected and connected network topology with unreliable data transmission lines. Both energetic and steady-state analyses of the proposed network architecture is performed and compared with a network architecture built based on the wave node scheme introduced in [54], referred as *node scheme II* in this work. The analyses predicted that the proposed network architecture: is lossless when subjected to communications with no time delay; offers less dissipation comparing to the network architectures built based on the *node scheme II*; and the implementation of *node scheme I* results in increasing drift as the simulation time grows. The analytical findings are supported with simulations and experimental results.

Next chapter will focus on algorithms for guaranteeing the passivity of the proposed distributed SVO scheme when users leave or join the cooperative interaction at run time.

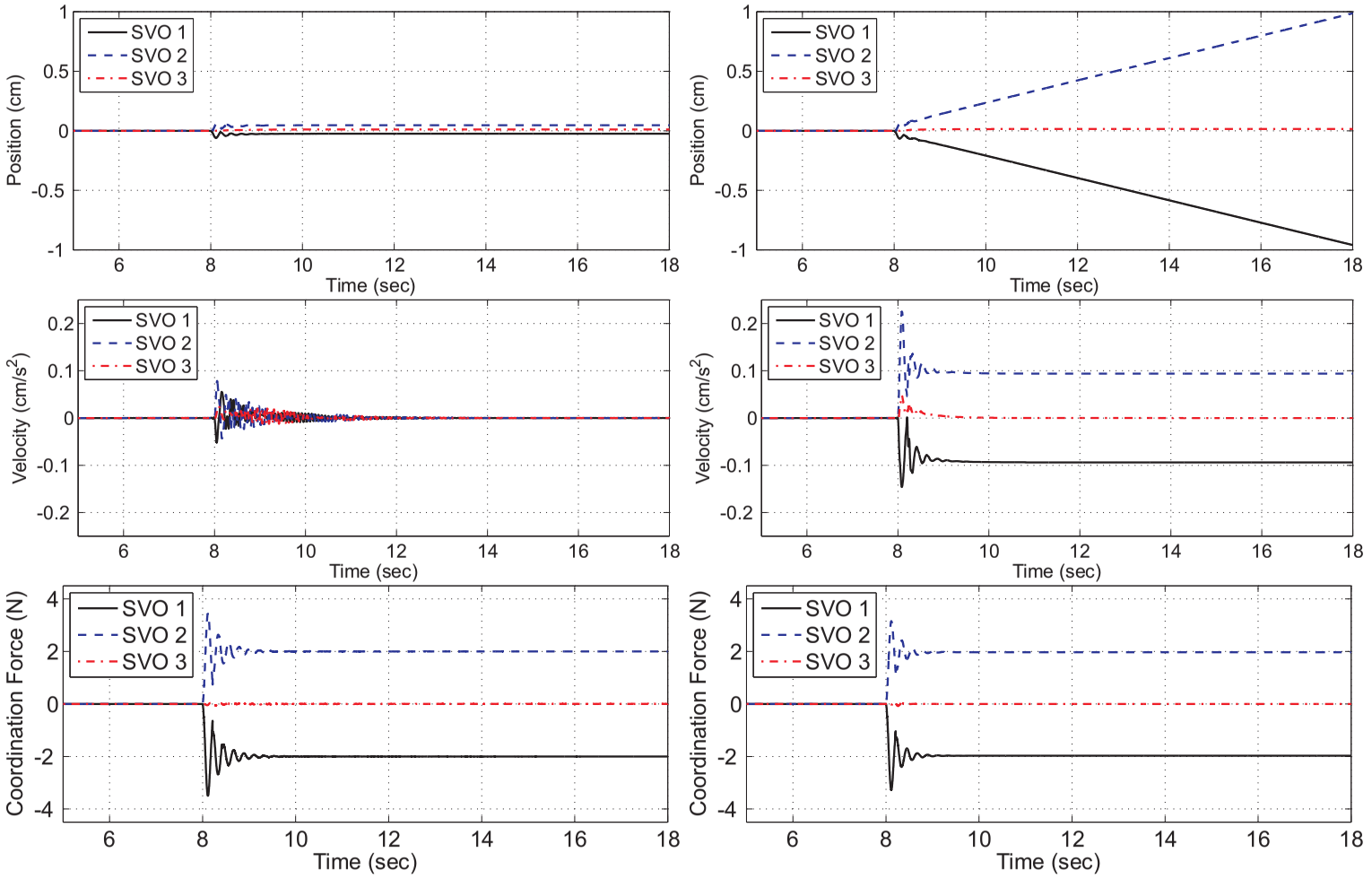

(a) *Node scheme I.* (b) *Node scheme II.*

Figure 4.13: Three-users haptic cooperation with controlled and balanced external applied forces on the SVO copies - The copies are interconnected via wave-based communication channels under constant network delay $T_d = 50$ ms.

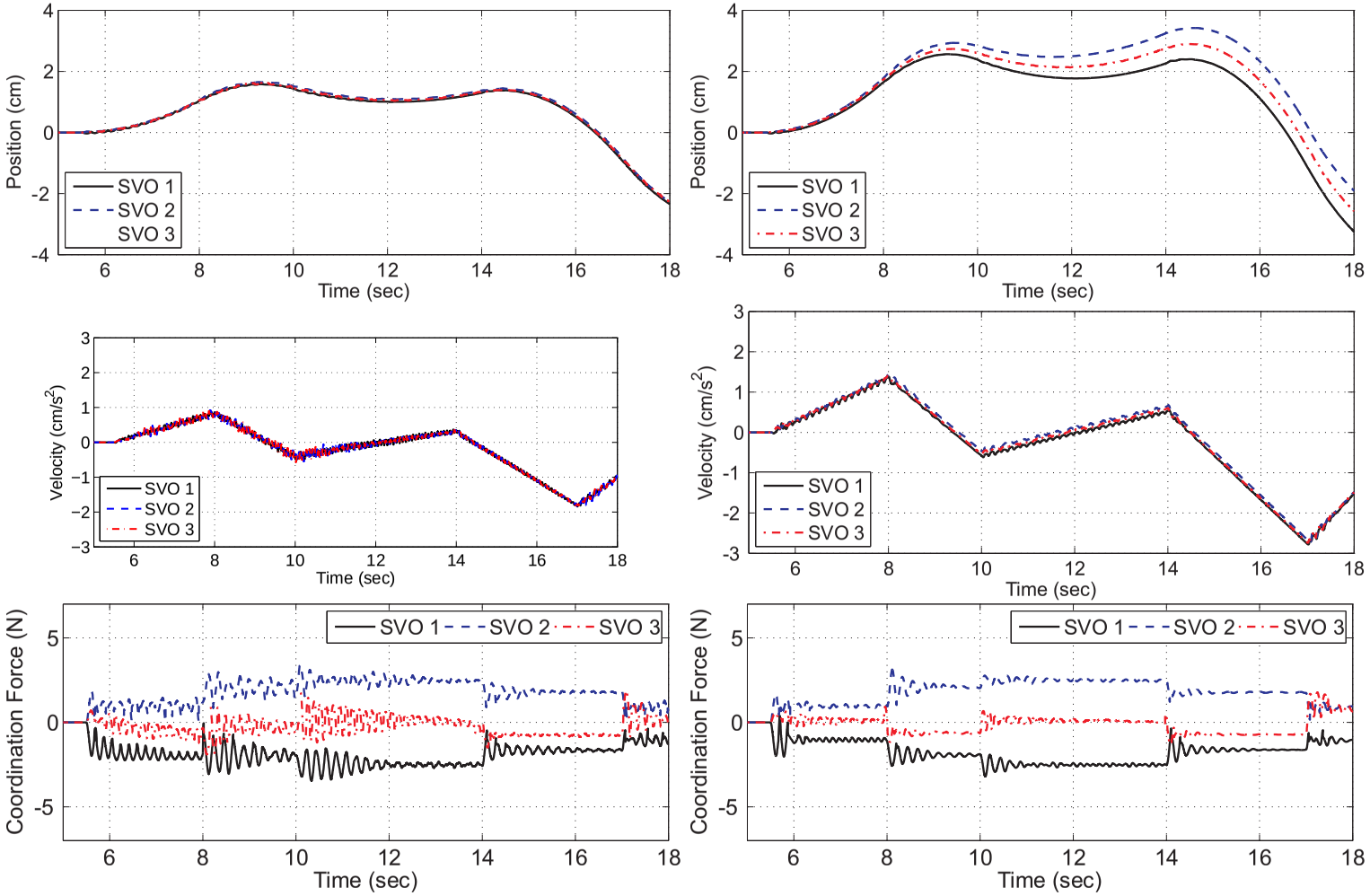

(a) *Node scheme I.* (b) *Node scheme II.*

Figure 4.14: Three-users haptic cooperation with controlled and unbalanced external applied forces on the SVO copies - The copies are interconnected via wave-based communication channels under constant network delay $T_d = 50$ ms.

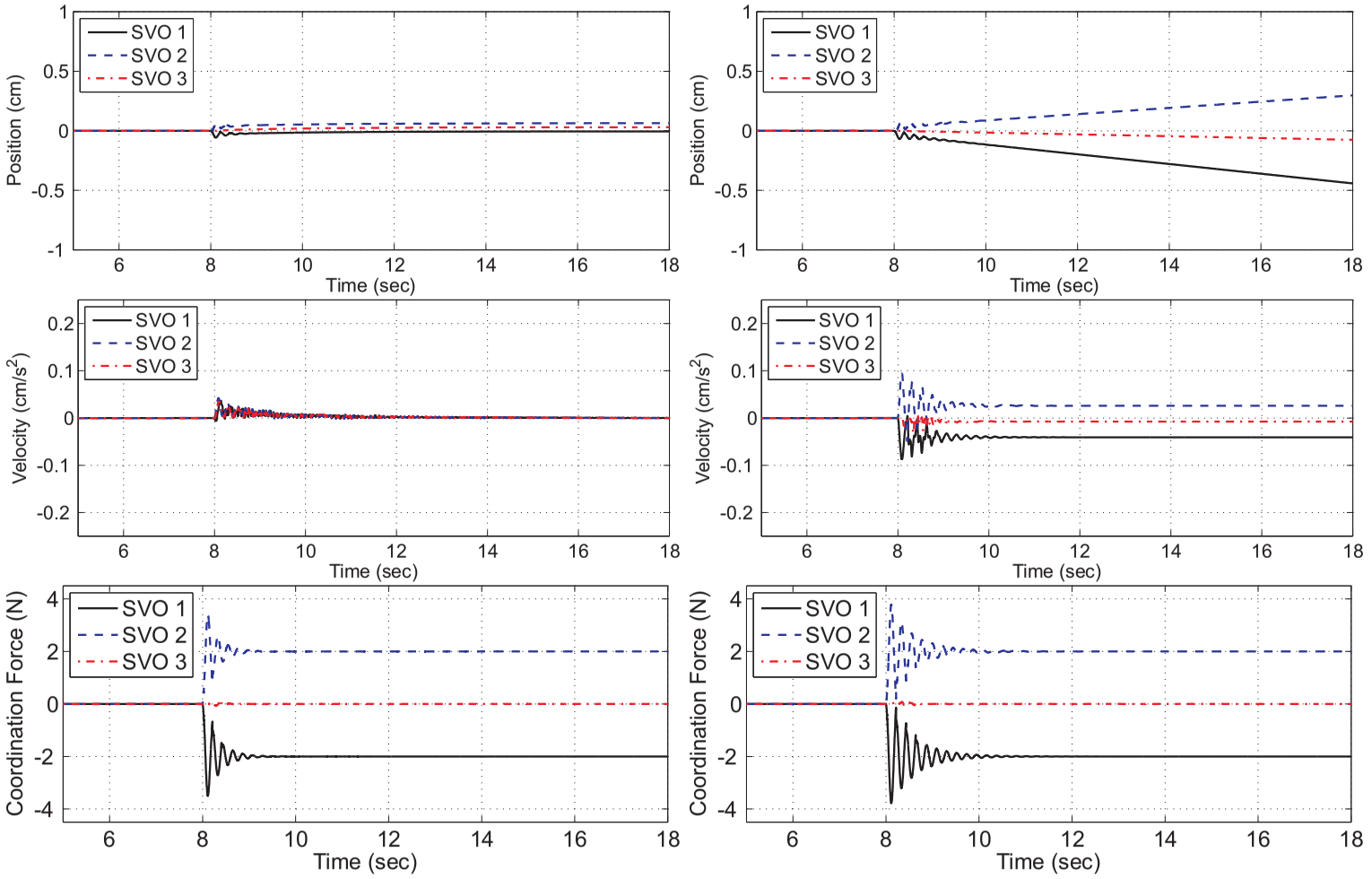

(a) *Node scheme I.* (b) *Node scheme II.*

Figure 4.15: Three-users haptic cooperation with controlled and balanced external applied forces on the SVO copies - The copies are interconnected via wave-based communication channels under varying network delay 20 ms $\leq T_d(k) \leq$ 70 ms.

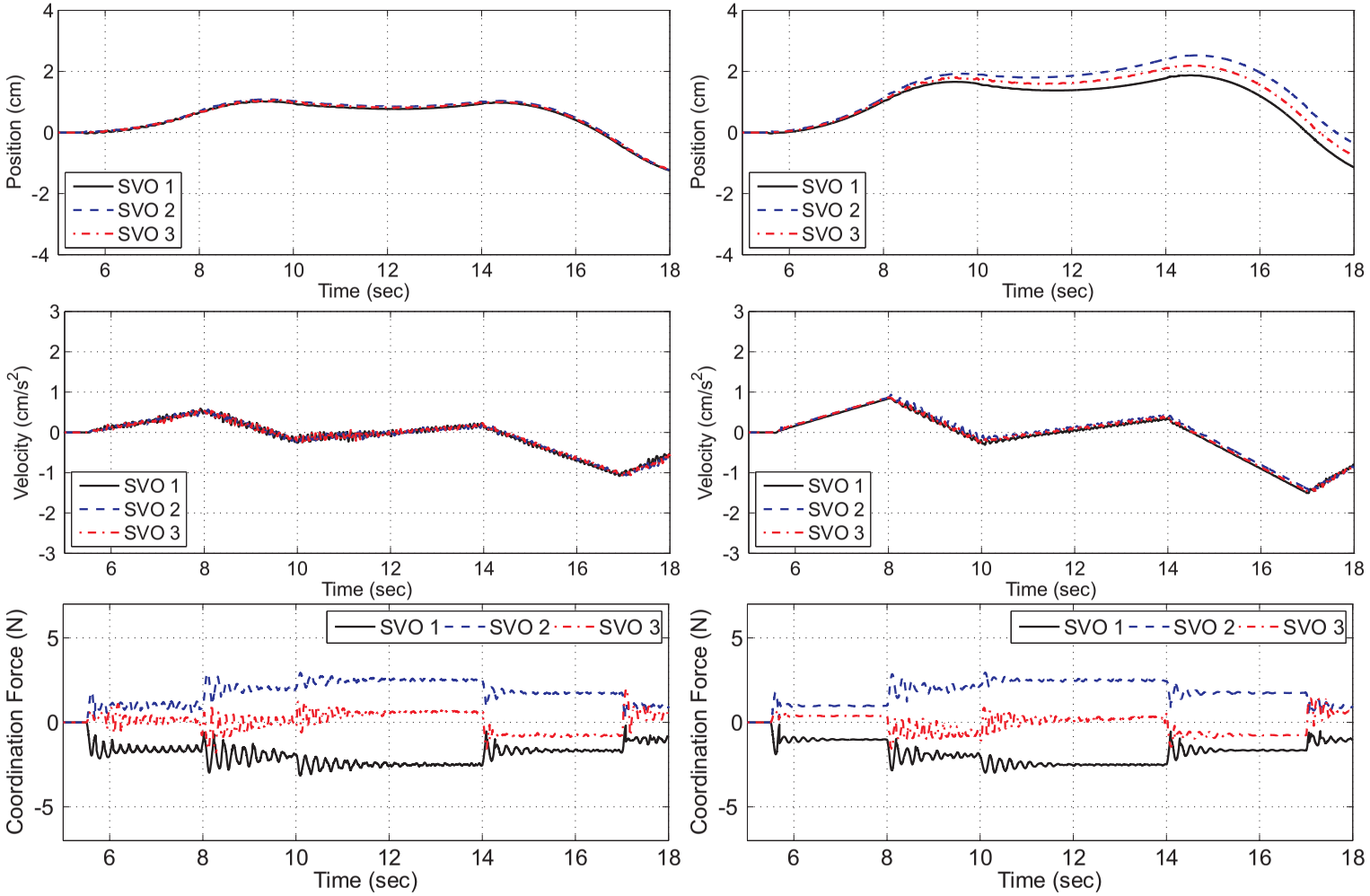

(a) *Node scheme I.* (b) *Node scheme II.*

Figure 4.16: Three-users haptic cooperation with controlled and unbalanced external applied forces on the SVO copies - The copies are interconnected via wave-based communication channels under varying network delay 20 ms $\leq T_d(k) \leq$ 70 ms.

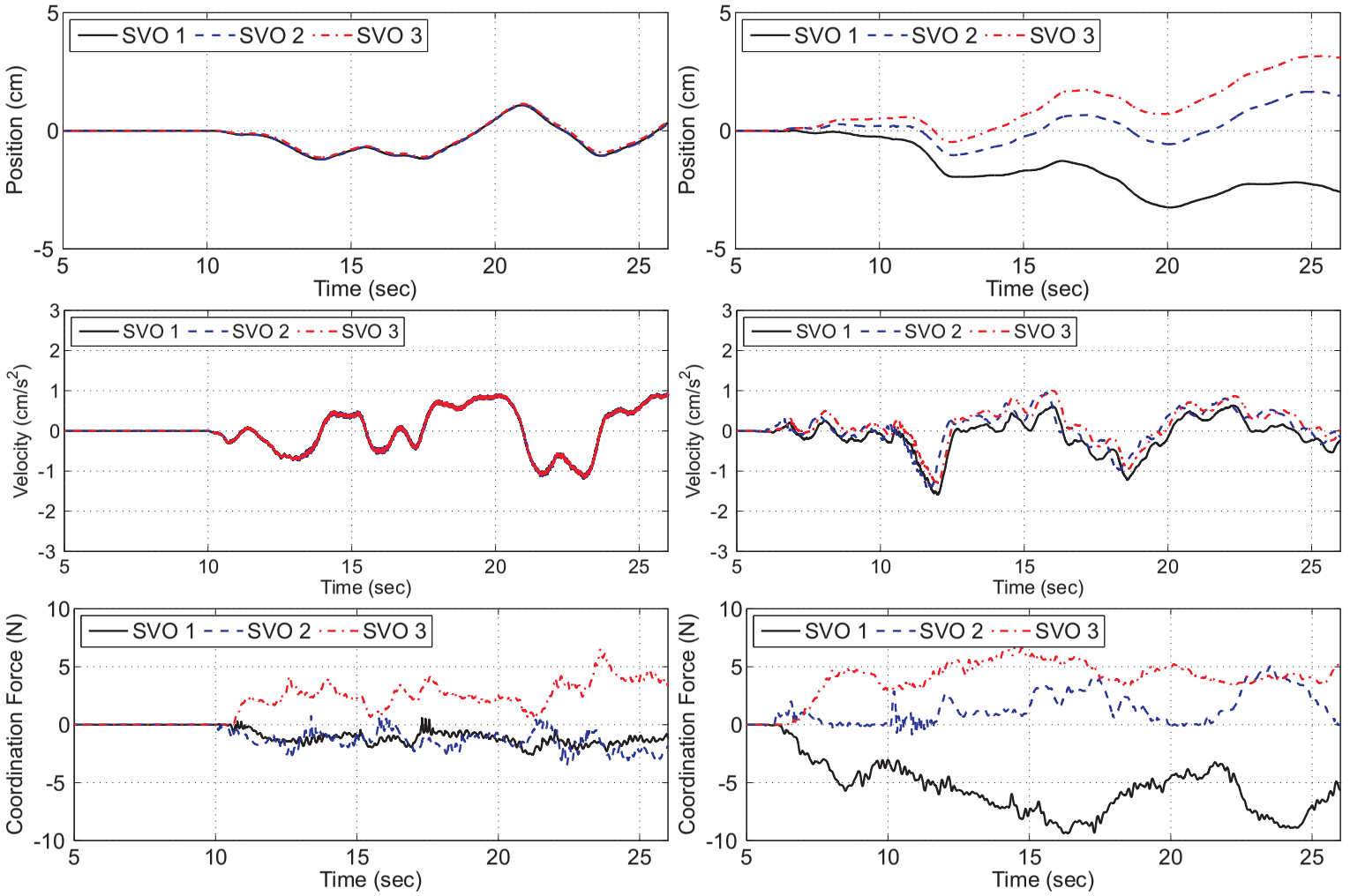

(a) *Node scheme I.* (b) *Node scheme II.*

Figure 4.17: User-in-the-loop - Three users haptic cooperation over the wave-based communication architecture via *node schemes I* and *II*, and under constant network delay $T_d = 50$ ms.

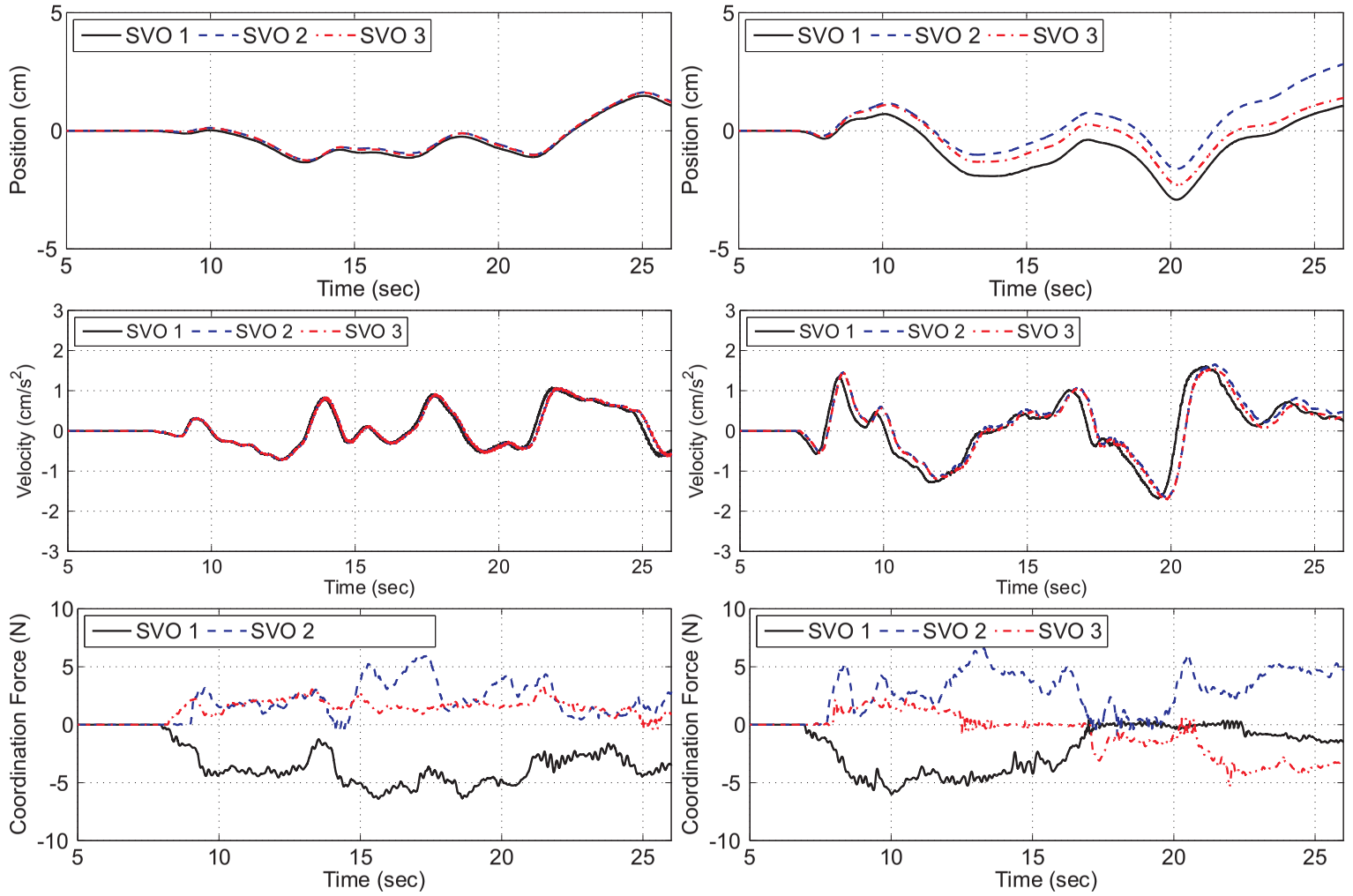

(a) *Node scheme I.* (b) *Node scheme II.*

Figure 4.18: User-in-the-loop - Three users haptic cooperation over the wave-based communication architecture via *node schemes I* and *II*, and under varying network delay 20 ms $\leq T_d(k) \leq$ 70 ms.

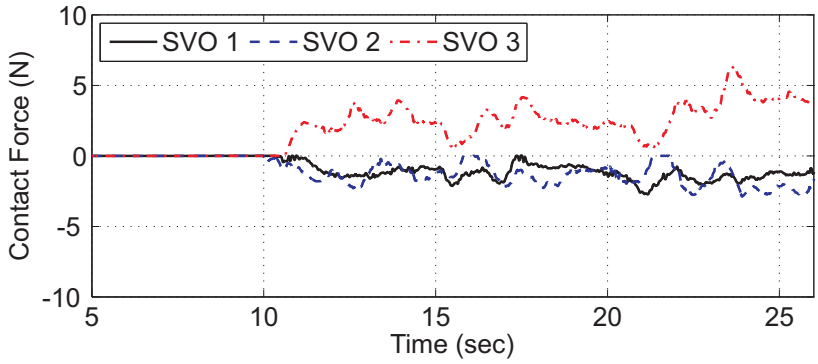

(a) *Node scheme I.*

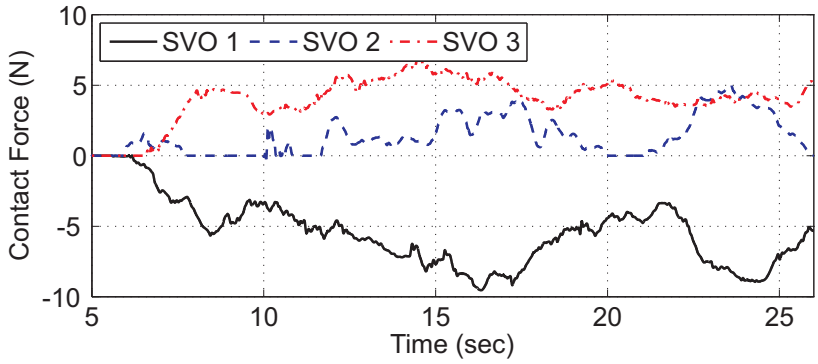

(b) *Node scheme II.*

Figure 4.19: Contact forces between users' avatars and the SVO copies - constant network delay $T_d = 50$ ms.

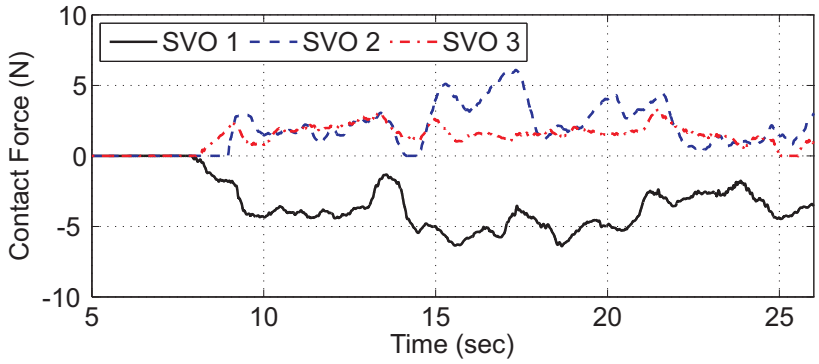

(a) *Node scheme I.*

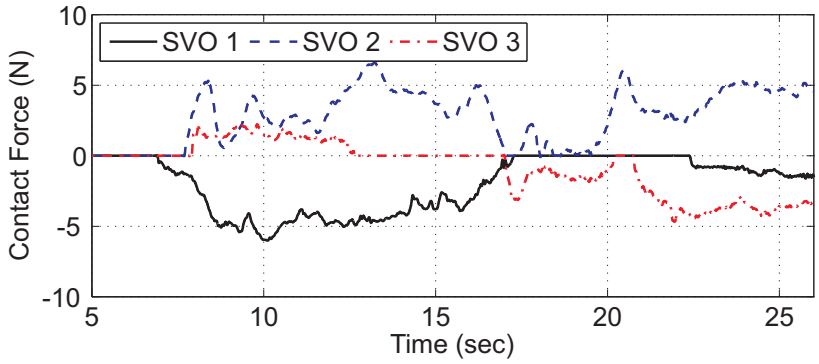

(b) *Node scheme II.*

Figure 4.20: Contact forces between users' avatars and the SVO copies - varying network delay of 20 ms $\leq T_d(k) \leq$ 70 ms.

Chapter 5

Passive SVO for haptic cooperation with varying number of users

The n-port passive SVO, proposed in previous chapter, in closed-loop with passive human users and haptic devices [38] guarantees the stability of the distributed haptic cooperation. However, passivity may not be maintained when the cooperating peers leave or join the network. This chapter studies the passivity maintenance of our proposed n-port passive SVO when the number of cooperating users varies.

5.1 Introduction

At leaving/joining instances, energy may be discharged from or injected into the rest of the closed-loop system via temporary open ports and thus, compromising the passivity. In fact, the passivity could be violated if the extracted energy through the open ports is large enough to exceed the stored energy in the remaining system. In this chapter, we examine the passivity maintenance of our proposed SVO for varying number of SVO copies. Furthermore, the change in the number of SVO copies causes a change in the dynamics of the remaining copies due to variations of the SVO mass.

We introduce an algorithm to address this issue. In particular, the energy jumps attributed to each SVO copy (being passively simulated via the numerical algorithm in [97]) is modified in order to account for the energy variation at leaving/joining instances. Sections 5.2 and 5.3 respectively examine the passivity maintenance of the proposed scheme in Chapter 4 for leaving and joining peers scenarios. An energy-consistency algorithm is then introduced in Section 5.4 that modifies the original energy jump formula for the discrete-time port-Hamiltonian system such that, the system would mimic its continuous-time counterpart with time-variant parameters of the energy storing elements (such as mass or stiffness). Simulations and experimental validations are provided subsequently in Sections 5.4.1, 5.4.2 and 5.5.

5.2 Leaving peer scenario

Consider the n-port passive SVO introduced in previous chapter with n copies distributed across a network with varying time-delay. Suppose T_d^{nj} be the communication time delay from side n to side j. If user n leaves the cooperation, it takes T_d^{nj} seconds for neighbouring peers ($j \in \mathcal{N}_n$) to notice its absence. During this transition time, energy may be extracted from or injected into the remaining system through temporary enabled n_n open ports that were once connected to the n-th peer. Note, the last SVO index in the cooperation is assigned to the leaving copy in this section. The overall passivity of the SVO may be violated if the extracted energy via the temporary open ports is large enough to exceed the stored energy in the remaining communication network. It is worth mentioning that pre- and post-transition phases include two passive systems with n and $n-1$ SVO copies respectively. Hence, our main objective in this section is to examine the passivity of the communication channel during the transition phase.

Let $\underline{k}$ be the time instant when peer n leaves ($T_L = \underline{k}T$). The number of ports at pre- and post- transition phases are n and $n-1$ respectively. During the transition phase, there are n_n open ports that temporarily change the number of ports of the system to $n-1+n_n$ ports. When the transition phase commences, all the communication links connected to the leaving peer n are dropped (see Figure 5.1).

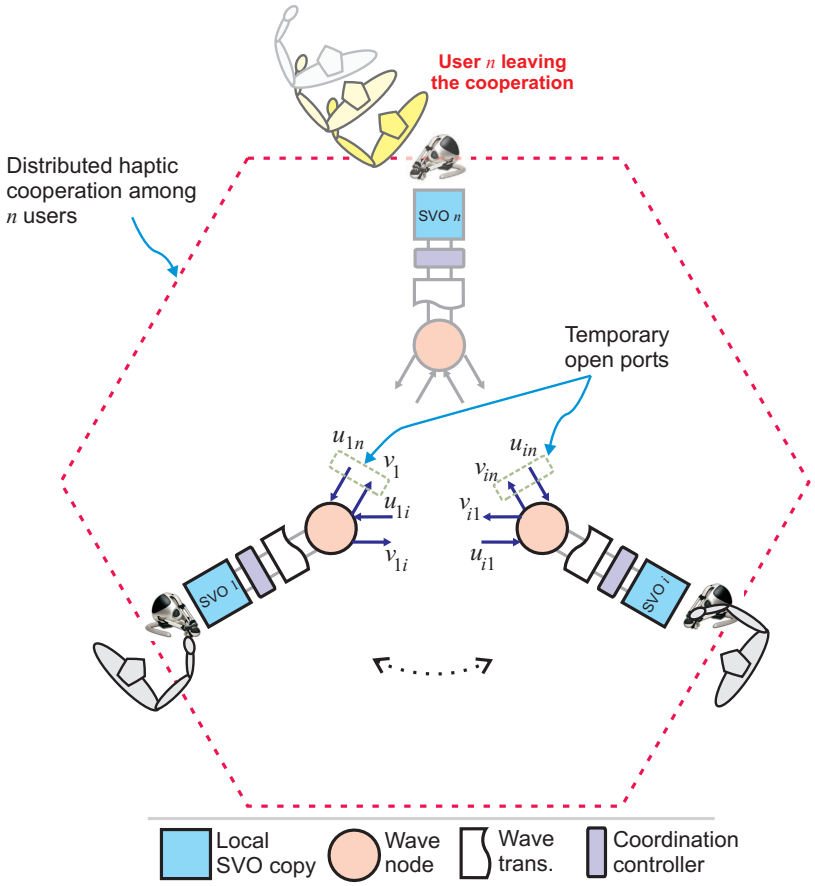

Figure 5.1: Leaving peer scenario - user n leaves the cooperation with n distributed peers.

Thus, the energy flow due to the temporary open port $j \in \mathcal{N}_n$ during the transition is:

$$E_{op_j}(\underline{k}+1 \to \underline{k}+d_{nj}(k)) = \frac{T}{2}\sum_{k=\underline{k}+1}^{\underline{k}+d_{nj}(k)} \Big(u_{jn}^2(k) - v_{jn}^2(k)\Big), \qquad \forall j \in \mathcal{N}_n. \tag{5.1}$$

The last term in Equation (5.1), v_{jn}^2, denotes the outgoing energy quantum from node j which is being dumped, since the temporary open ports are no longer in closed-loop with the rest of the system. Besides, the incoming energy quantum, u_{jn}^2, is a positive term which only results to storing more energy into the remaining communication network. Therefore, it can be concluded that no energy is extracted from the system and the passivity of the SVO is preserved when users leave the cooperation.

5.3 Joining peer scenario

Consider at time instant $\underline{k}$, peer $n+1$ joins the cooperation with n distributed SVO copies. As soon as the arrival of peer $n+1$ is confirmed by the copies residing at its neighbourhood, the number of n_{n+1} wave-based communication channels are established (see Figure 5.2). The *joining peer* scenario is a natural transition of a passive SVO system with n copies to another passive SVO system with $n+1$ copies. The transition occurs instantly without any extraction of energy and therefore, the system maintains its passivity. Let $E_{estab_{n+1}}$ denote the energy of all the established communication channels at peer $n+1$'s neighbourhood. Knowing the fact in Equation (4.18), Equation (5.2) confirms that this energy is always positive and thus, such wave-based link establishment maintains passivity by storing energy during the transition phase.

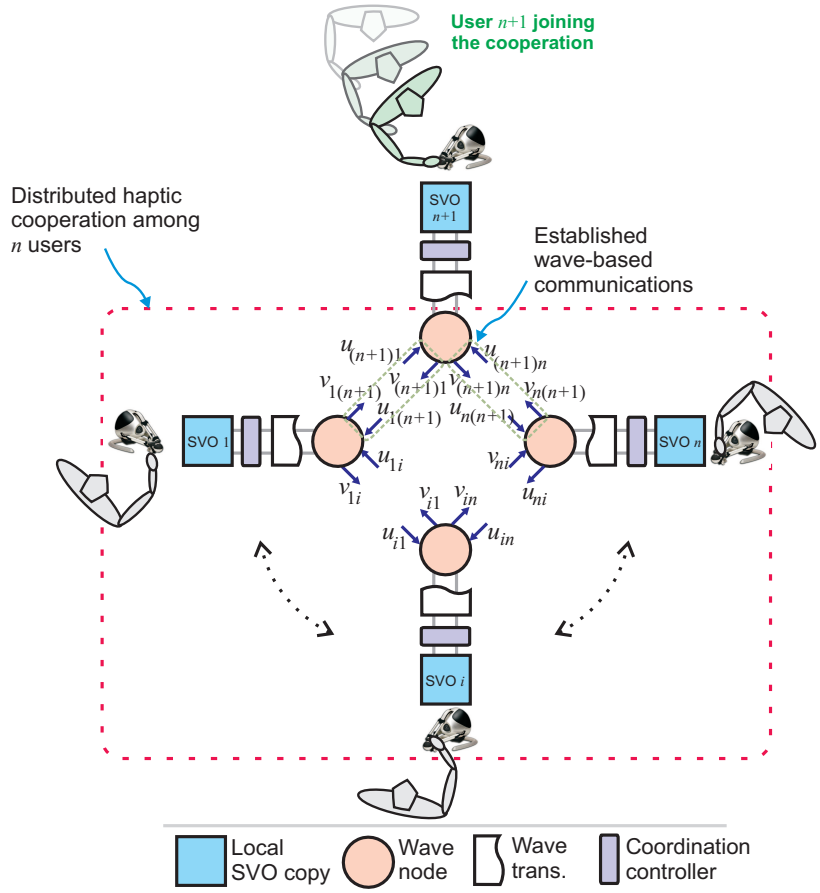

Figure 5.2: Joining peer scenario - user $n+1$ joins the cooperation with n distributed users.

$$E_{estab_{n+1}}(\underline{k}+1 \to \bar{k}) = \frac{T}{2} \sum_{j \in \mathcal{N}_{n+1}} \sum_{k=\underline{k}+1}^{\bar{k}} \left(v_{(n+1)j}^2(k) - u_{(n+1)j}^2(k) + v_{j(n+1)}^2(k) - u_{j(n+1)}^2(k) \right) \geq 0 \tag{5.2}$$

5.4 Enforcement of the energy-consistency algorithm

By definition, discretized port-Hamiltonian systems should mimic the energetic evolution of their continuous-time counterparts. In both of the scenarios mentioned in

Sections 5.2 and 5.3, the change in the number of SVO copies causes a change in the dynamics of the remaining copies. In fact, the value of the local SVO mass depends on the number of cooperating peers. For a single mass at site i (see Fig. 4.5), the energy jump formula in Equation (4.20) is expressed as:

$$\Delta H_i(k) = T\Big(f_{C_i}(k)\dot{x}_{C_i}(k) - f_{T_i}(k)\dot{x}_{T_i}(k) - b\big(\frac{p_i(k)}{m}\big)^2\Big) \tag{5.3}$$

in which, $p_i = m_i\dot{x}_i$ is the momentum of the mass i and, $\dot{x}_{C_i} = \dot{x}_i = \frac{p_i}{m_i}$. However, Equation (5.3) is only valid for non-varying parameters (in this case, non-varying mass m). In fact, the partial derivative of the mass should be taken into account.

Let the initial mass of the SVO copy at site i be $\underline{m}_i = m_i(\underline{k})$. Consider, right after time instant $\underline{k}$, the value of the mass changes to $\bar{m}_i = m_i(\underline{k}+1)$. With $H_i(k) = \frac{p_i(k)^2}{2m_i(k)} = \frac{1}{2}m_i(k)\dot{x}_i(k)^2$ being the energy of the mass i at time instant k, the time difference of the energy at time instant $\underline{k}$ is:

$$\frac{\Delta H_i(\underline{k})}{T} = \frac{1}{2}\frac{\overbrace{m_i(\underline{k}+1)}^{\overline{m}_i} - \overbrace{m_i(\underline{k})}^{\underline{m}_i}}{T}\Big(\frac{p_i(\underline{k})}{m_i(\underline{k})}\Big)^2 - m_i(\underline{k})\big(\frac{\frac{p_i(\underline{k})}{m_i(\underline{k})} - \frac{p_i(\underline{k}-1)}{m_i(\underline{k}-1)}}{T}\big)\frac{p_i(\underline{k})}{m_i(\underline{k})} \tag{5.4}$$

The last term in Equation (5.4) stands for the energy flow corresponding to the energy storing elements of the system (i.e, mass). Therefore, in analogy to Equation (A.92), Equation (5.4) turns to:

$$\Delta H_i(\underline{k}) = \underbrace{\frac{\overline{m}_i - \underline{m}_i}{2}\Big(\frac{p_i(\underline{k})}{m_i(\underline{k})}\Big)^2}_{\Delta KE_i(\underline{k})} + T\Big(f_{C_i}(\underline{k})\dot{x}_{C_i}(\underline{k}) - f_{T_i}(\underline{k})\dot{x}_i(\underline{k}) - b\big(\frac{p_i(\underline{k})}{m_i(\underline{k})}\big)^2\Big) \tag{5.5}$$

Unlike Equation (5.3), the above equation encapsulates the variation of the kinematic energy as well. In fact, instead of Equation (5.3), Equation (5.5) should be employed only for one time step (i.e, during the transition step) to enforce the

energy-consistency in order to mimic the behaviour of the system's continuous-time counterpart. Next, the Equation 5.5 is discussed in details for both joining and leaving instances and switching algorithms are presented consequently.

5.4.1 Leaving instant

Consider a VO with mass M being equally distributed among n peer sides. When user n leaves, $\frac{M}{n}$ and $\frac{M}{n-1}$ are respectively the mass of the local SVOs before and after time instant $\underline{k} + d_{nj}(k)$. Practically, it is impossible to determine that the empty packets detected at the receiver side are due to increasing-delay/packet-loss or absence of the remote peers. Let $T_d^{max} = d_{max}T$ be the maximum amount of delay in the network[1]. We assume "$\underline{k} + d_{max} + 1$" is the time instant at which the absence of the leaving SVO n can be confirmed by its neighbours. Therefore, the momentum of mass $i \in \{1, \ldots, n-1\}$ turns to:

$$p_i(k) = \frac{M}{n-1}\dot{x}_i(k) \quad \text{for} \quad k > \underline{k} + d_{max} \tag{5.6}$$

Hence, for SVO copy i, the first term of Equation (5.5) turns to:

$$\Delta KE_i^L(k) = \frac{M}{2n(n-1)}\dot{x}_i^2(k). \tag{5.7}$$

in which, superscript L denotes the leaving peer scenario. Hence, with $b = 0$, for leaving peer scenario, Equation (5.3) should be modified as:

$$\Delta H_i(k) = T\Big(f_{C_i}(k)\dot{x}_{C_i}(k) - f_{T_i}(k)\dot{x}_i(k)\Big) + \Delta KE_i^L(k). \tag{5.8}$$

[1]In practice, the value of the maximum delay can be obtained via statistically examining the data transition traffic of the network.

Note that Equation (5.8) should only be enabled for one time instant, i.e. $\underline{k}+d_{nj}(k)+d_{max}+1$, to impose the energy change on the overall stored energy in the system. For the consequent steps, Equation (5.3) must be plugged back into the algorithm with the updated value for the mass as $\frac{M}{n-1}$. For the leaving peer scenario, the enforcement of the proposed energy-consistency algorithm is presented within a pseudo-code in Algorithm. 1.

if *leaving peer* $\equiv$ *true* **then**
- $\diamond$ use Equation (5.7) to calculate the kinetic energy jump for the remaining peers at the leaving instant;
- $\diamond$ enable the modified energy jump formula in Equation (5.7) when the absence of peer n is confirmed by its neighbours;
- $\diamond$ for the consequent steps, plug back the original energy jump formula in the algorithm from Equation (5.3), calculated based on the new value for mass, i.e, $\frac{M}{n-1}$;

end

Algorithm 1: Energy-consistency enforcement for leaving peer scenario.

Application of the proposed algorithm is presented in the following example.

Example 5.1. Consider an autonomous undamped mass-spring system[2] including a spring with stiffness of $K = 1000$ N/m. Let mass $\underline{m} = 0.1$ Kg define the initial mass of the system whereas, $\bar{m} = 0.4$ Kg represents the new value of the mass updated at time instant $t = 0.108$ s. Therefore, the energetic levels of the autonomous mass-spring system in continuous-time with the energy function in Equation (5.9) is demonstrated in Figure 5.3.

$$\mathtt{H}(t) = \frac{1}{2}m\dot{x}(t)^2 + \frac{1}{2}Kx(t)^2, \qquad m = \{\underline{m}, \bar{m}\}. \tag{5.9}$$

[2]In order to provide the marginally stable condition, the autonomous undamped mass-spring system is treated as the benchmark in this example.

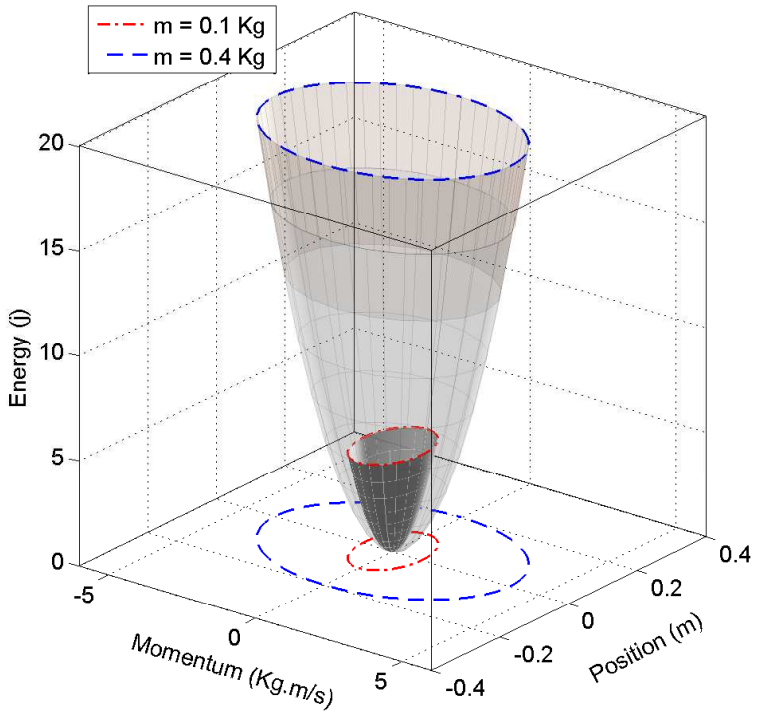

Figure 5.3: Energetic levels of an autonomous mass-spring system with changing mass in continuous-time.

The energy levels of the mass-spring system corresponding to values $\underline{m} = 0.1$ Kg and $\bar{m} = 0.4$ Kg are projected onto the phase plane (i.e, the momentum-position plane) with dashed-dotted and dashed lines respectively. These ellipses are basically the characteristic geodesics of the continuous-time system that the discretized port-Hamiltonian mass-spring must mimic. In fact, these geodesics correspond to the set of all iso-energetic states whose values depend on the initial conditions of the system.

Given the variation of the mass, Figure 5.4 compares the trajectories of the continuous-time autonomous mass-spring system with its discretized port-Hamiltonian counterparts with and without the proposed algorithm.

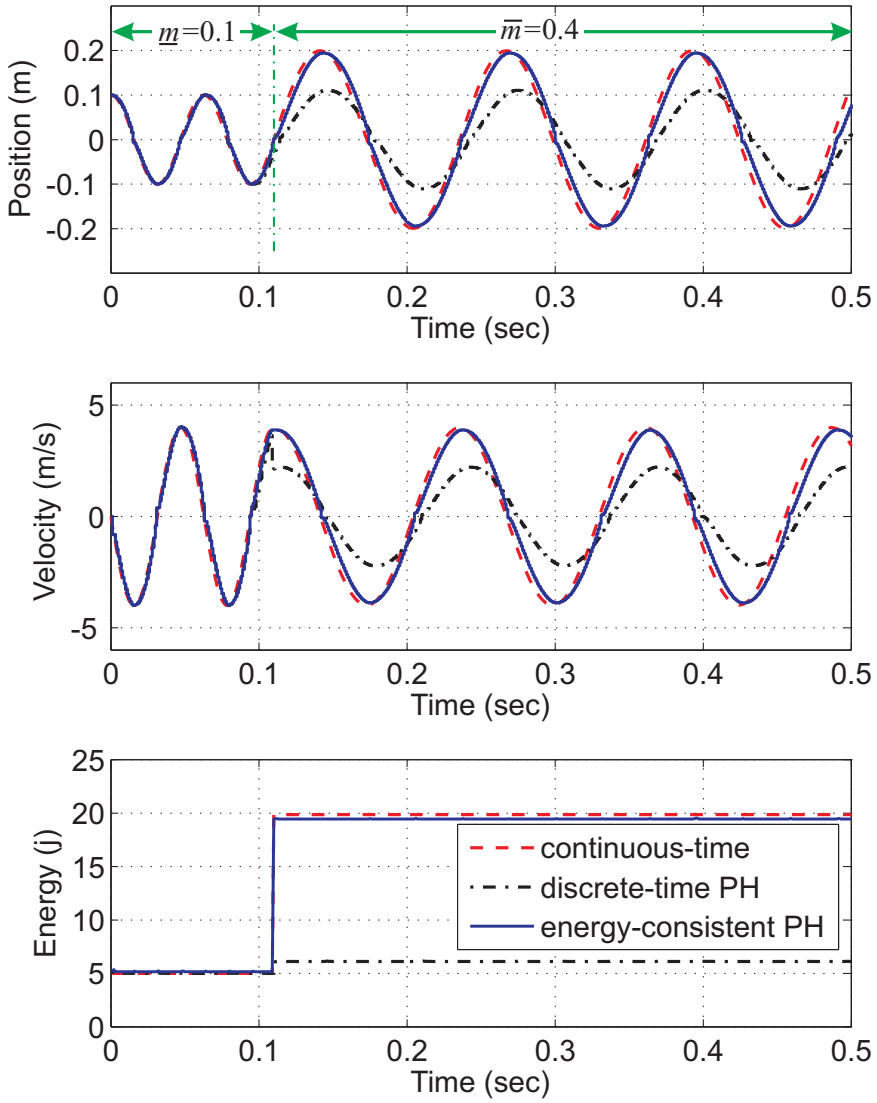

Figure 5.4: Position/momentum/energy evolution of an undamped mass-spring system with varying mass simulated in (i) continuous-time (dotted-line); (ii) discrete-time using port-Hamiltonian formulation (dashed-dotted); and (iii) discrete-time port-Hamiltonian with enforcing the proposed energy-consistency algorithm (solid line). The value of the mass changes as from 0.1 to 0.4 Kg at $t = 0.108$ s.

Let the mass be moved to the initial position, $q_0 = 0.2$ m. Hence, the energy of the system only comprises the potential energy stored in the spring, that is, $H_{\underline{m}}(0) = 5$ j. With zero initial velocity, when released, the potential energy starts to converting to kinetic energy and thus, resulting to the motion of the mass. Since the system is undamped, the amplitude of the oscillation remains constant and the mass-spring

system maintains its marginal stability. However, as the value of the mass changes to $\bar{m} = 0.4$ Kg, the system moves to a new level of energy (i.e, $H_{\bar{m}}(t = 0.108) = 20$ j), resulting to a different oscillation amplitude.

The red dashed-line in Figure 5.4 represents the continuous-time evolution of the mass. The black dashed-dotted line depicts the discretized port-Hamiltonian mass-spring using the unmodified port-Hamiltonian energy jump formula, Equation (5.3). Note, calculation of the energy jumps is only based on the internal dissipation and the energy exchanged via the external power ports. This formula, however, ignores the variation in the dynamics of the energy storing elements in the system (i.e, stiffness of the spring and the mass value). Hence, as reported in Figure 5.4, the discretized port-Hamiltonian system does not characterize the expected continuous-time energy behaviour. Implementation of the proposed algorithm enforces the system to closely follow the energetic evolution of the continuous-time system. One should note that as long as the discrete-time evolution of the mass-spring system mimics its continuous-time counterpart, the passivity is preserved even when the value of the mass changes. In fact, variation of the mass value is a passive action as discussed in Appendix A.8.

5.4.2 Joining instant

In case of "joining peer" scenario, the mass of the SVOs before and after the joining instant are $\frac{M}{n}$ and $\frac{M}{n+1}$ respectively. Thus, when SVO copy $n+1$ joins the network, the kinetic energy jump for SVO $i \in \{1, \ldots, n+1\}$ is:

$$\Delta KE_i^J(k) = \frac{1}{2}\big(\frac{M}{n} - \frac{M}{n+1}\big)\dot{x}_i^2(k) = -\frac{M}{2n(n+1)}\dot{x}_i^2(k). \tag{5.10}$$

Similar to the previous subsection, Equation (5.11) is then employed to measure the energy jump only at the joining peer instant as:

$$\Delta H_i(k) = T\Big(f_{C_i}(k)\dot{x}_{C_i}(k) - f_{T_i}(k)\dot{x}(k)\Big) + \Delta KE_i^J(k) \tag{5.11}$$

In the following steps, Equation (5.3) is plugged back into the algorithm with the new value for mass, $\frac{M}{n+1}$. Note the algorithm for the joining peer scenario is similar to Algorithm 1 except, Equation (5.10) is used to compute the energy jumps and, the new value for the mass $\frac{M}{n+1}$ should be used in Equation (5.11) after the joining instant. Next, we will present experimental validation of the proposed scheme when users leave/join the cooperation.

5.5 Experiments with varying number of peers

In this set of experiments for both leaving and joining scenarios, experiments are carried out on the same set-up in previous chapters for:

- leaving agent scenario in Fig. 5.5a in which, experiment starts with all three users in the VE. One of the peers leaves the cooperation while other two manipulating the shared virtual cube back and fort along the closure. In Fig. 5.5b, the cooperation switches to a single-user setting as the second peer leaves too;

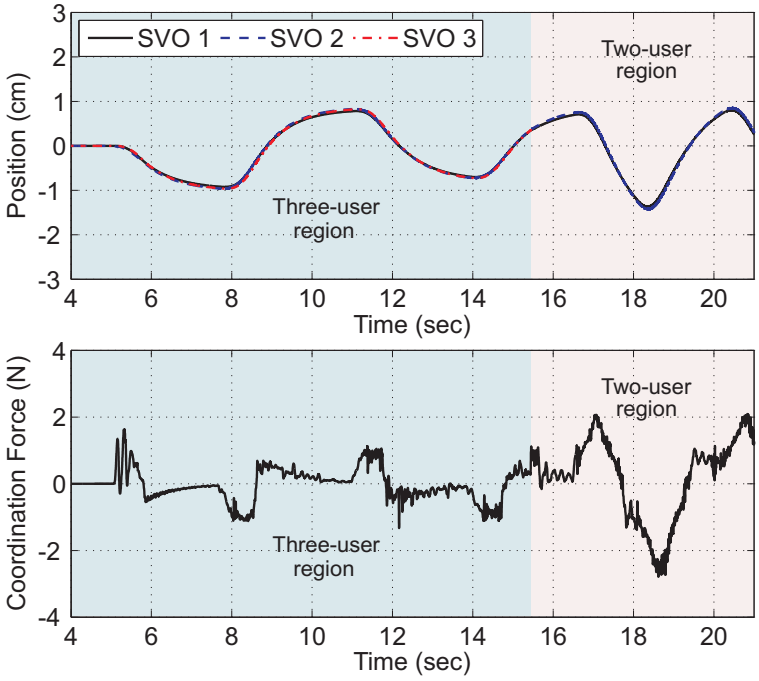

(a) Third peer leaves the cooperation.

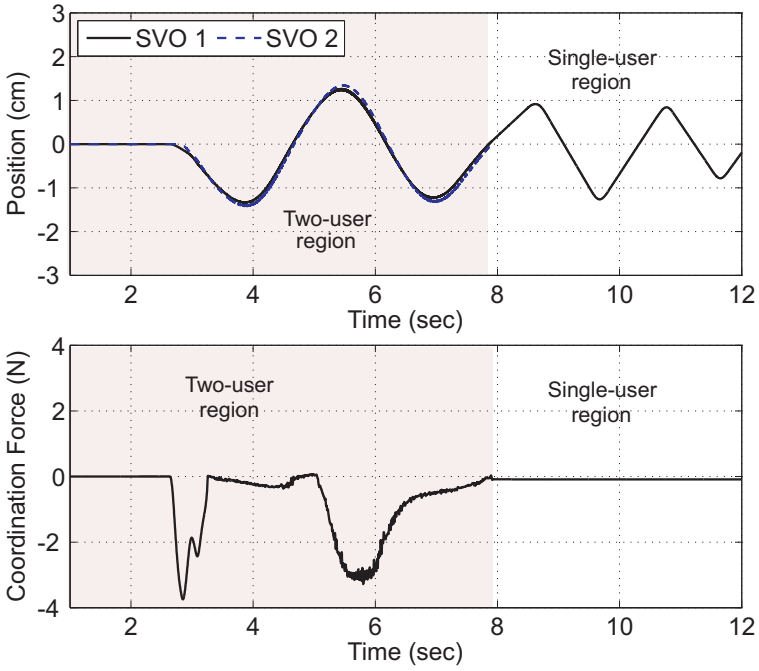

(b) Second peer leaves the cooperation.

Figure 5.5: Leaving peer scenario when users leave the cooperation over a network with varying communication delay 20 ms $\leq T_d(k) \leq$ 70 ms.

- joining peer scenario for which, experiment starts with only one user existing

in the VE. The second and the third peers join the cooperation one after the other. Figure 5.6 demonstrates the position of the SVO copies for this scenario.

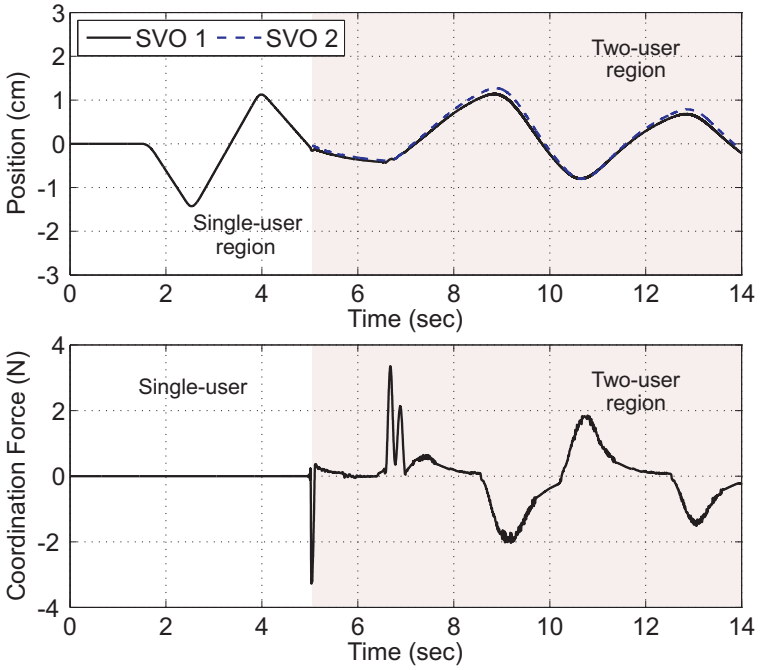

(a) Second peer joins the cooperation.

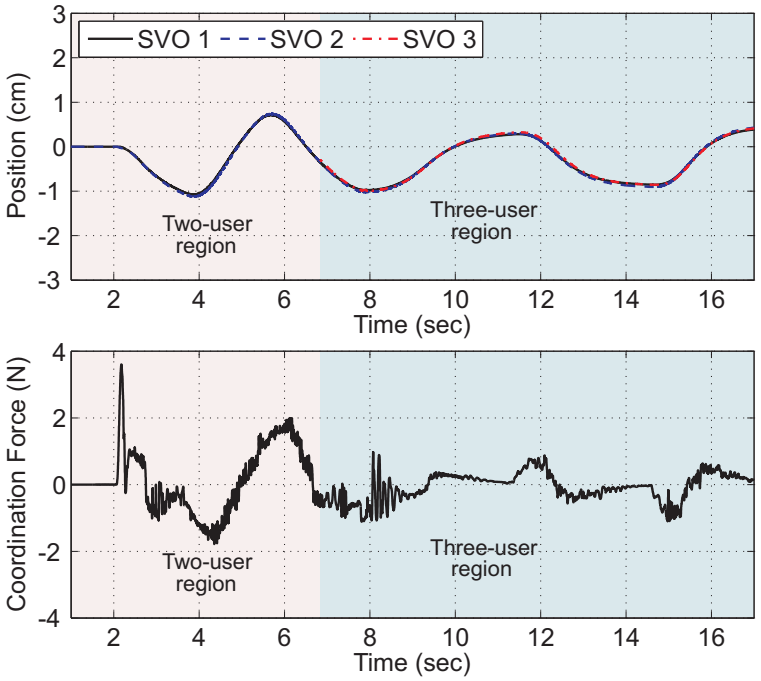

(b) Third peer joins the cooperation.

Figure 5.6: Joining peer scenario when users joins the cooperation over a network with varying communication delay 20 ms $\leq T_d(k) \leq$ 70 ms.

In transition instances when users join/leave the cooperation, the change in the slope of the position trajectory is due to the variation in the mass of the local SVO copies. In Fig. 5.6a, the system transits from the single-user case to the two-users cooperation and from that moment on, the VO is distributed among two peers. The establishment of the coordination controller results in decelerating motion of the SVO copies as shown in the two/three -users regions. Since the coordination control forces are computed based on the decoded wave information arriving from the communication channel, the dissipation of energy in the communication channel (due to increasing delay or data-loss) has a direct effect on dampening the motion of the SVO copies. Since, we consider no local damping on the dynamics of SVO copies, the sluggish motion in three/two -users regions can be solely attributed to the imperfections of the transmission lines.

5.6 Summary

The passive SVO framework proposed in Chapter 4 decouples the design of the coordinating controllers from the network topology and communication line issues. The proposed scheme thus allows for selecting the coordination gains independent of the number of cooperating peers. However, passivity may not be maintained when the cooperating peers leave or join the network. At leaving/joining instances, energy may be discharged from or injected into the rest of the closed-loop system via temporary open ports and therefore, compromises the overall passivity. In this chapter, it was confirmed that the passivity of the proposed SVO is maintained for varying number of cooperating peers. An energy-consistency algorithm was introduced that modified the port-Hamiltonian formulation to account for the kinetic energy variations of the SVO copies (caused by the change in the number of participating peers) in

discrete-time. The proposed paradigm for distributed SVO: (i) guarantees the passivity of the SVO when peers leave/join the cooperation; (ii) allows for selecting the coordination gains independent of the number of cooperating users; (iii) takes into account the variations in the dynamics of the SVO copies by introducing a switching energy-consistency algorithm. The proposed algorithm modifies the original energy jump formula for discrete-time port-Hamiltonian system such that, the system would mimic its continuous-time counterpart with time-variant parameters of the energy storing elements (e.g, mass or stiffness). Experiments in which three users take turn in leaving or joining the cooperation over a network with varying delay are carried out to validate the theoretical results. Future work can be set on extending the proposed paradigm to networks with transmission rate slower than the rate of the local haptic servo-loop.

Chapter 6

Conclusions and future work

6.1 Concluding Remarks

This thesis explained challenges associated with distributed haptic cooperation systems with varying number of participants. At the architecture level, we suggested a new coordination protocol, i.e average-position (AP) scheme, that governs the coupling among distributed shared virtual object (SVO) copies. Over networks with limited bandwidth and constant communication delays, the suggested AP paradigm upper bounds the effective coordination gain of the SVO and thus, increases the stability margins of distributed multi-user haptic cooperation compared to conventional PD coordination scheme. The proposed AP protocol was used throughout the thesis as a benchmark and motivation to achieve a scalable haptic cooperation system.

Seeking for passive SVO, the AP paradigm was then implemented on passive wave-based communication channels with varying delays and packe-losses. This resulted in a passive framework for the design of the shared virtual object (SVO) ascertaining the stability of the distributed haptic cooperation system independent of the number of participating peers. By constructing a passive SVO in closed-loop with n passive

human users and haptic devices, the stability of the distributed haptic cooperation system was guaranteed.

The discrete-time n-port passivity of the SVO with n copies was assured by interconnecting the following passive subsystems: (i) local SVO copies; (ii) coordinating controllers; and (iii) communication network architecture. The dynamics of the SVO local copies and their corresponding coordination controllers were modelled in port-Hamiltonian formulation that guarantees passive simulation in discrete-time. Wave nodes as passive power distributors were implemented on a multilateral wave-based communication architecture. The node scheme introduced in [44], referred to as *node scheme I* in this thesis, was employed to construct an n-port passive wave-based network architecture over an undirected network topology with unreliable data transmission line. Both energetic and steady-state analysis were conducted to compare the performance of the proposed network paradigm with a network architecture built based on the wave node scheme introduced in [54], referred as *node scheme II*. The analysis predicted that:

- our proposed architecture is lossless when subjected to perfect communications with no time delays and, offers less dissipation comparing to the network architectures built based on *node scheme II*;
- the multilateral communications built with *node scheme II* result in unbounded drift in steady-state. Therefore, they are not suitable for practical applications when cooperating operators are in sustained contact with the VO.

Passivity maybe compromised when the number of cooperating participants changes when users join/leave the cooperation. Accordingly, the number of the distributed SVO copies changes that results in a change in the SVOs' dynamics. The proposed passive framework decoupled the design of the coordinating controllers from the communication network topology and thereby, allowing for the selection of coordination

gains independent of the number of cooperating users. The passivity maintenance of the proposed scheme was verified when the number of users varies. Finally, a switching energy-consistency algorithm was proposed to account for the kinetic energy variations of the SVO copies. The proposed design method for distributed SVOs:

(i) guaranteed the passivity of the SVO when peers leave/join the cooperation;

(ii) allowed for selecting the coordination gains independent of the number of cooperating users;

(iii) took into account the variations in the dynamics of the SVO copies.

Experiments in which, at runtime, three users took turn in leaving or joining the cooperation over a network with varying delay are carried out to validated the theoretical results.

6.2 Future work

The following future works are suggested to extend and improve the proposed passive architecture:

- Study the performance of the proposed AP paradigm in virtual environments relevant to applications like multi-user haptic computer games for tele-rehabilitation and/or for education. In these applications, the haptic tasks will be defined in collaboration with therapists and/or educators to help the cooperating users achieve specific therapeutic and/or educational goals.

- Application of the proposed passive SVO scheme to more realistic scenarios such as cooperative virtual surgery training. In fact, simulation of more complex VEs demands heavier numerical computations resulting in slower VE updates.

Combination of high-rate haptic devices with low-frequency simulation of the VE draws a multi-rate framework that demands proper control strategies.

- Extension the results for SVO with coupled multi degrees of freedom dynamics since all the analyses and experiments in this thesis were restricted to one degree of freedom (DOF) or three DOF point interactions.

- Mitigation of the position drift attributed to the transmission of velocity data across the wave communications by: transferring wave integrals as suggested in [104] or, employing predictors.

- Improvement of the system performance by removing the local PD type coordinating controllers and utilizing the proposed wave-based communication architecture as an n-port passive wave controller.

- The stability of the haptic cooperation system can be investigated by incorporating the absolute stability (Llewellyn's) criterion framework [6, 35]. Indeed, passivity of the human operators plays a key role for such technique.

- Extension to the case where SVO copies are interconnected over networks with transmission rate slower than the rate of the local haptic servo-loop.

Appendix A

A.1 Multi-rate state-space representation of the average-position (AP) scheme for three users

This appendix presents the detailed matrices needed to derive the stability region for the proposed averaged-position (AP) distributed control architecture. The dimensions of the state, the input, and the output vectors are as follows:

$n_x = 12$	number of states of continuous-time system
$n_{cu} = 6$	number of fast inputs of continuous-time system
$n_{1cu} = 2$	number of fast inputs of continuous-time system at the Peer 1 side
$n_{2cu} = 2$	number of fast inputs of continuous-time system at the Peer 2 side
$n_{3cu} = 2$	number of fast inputs of continuous-time system at the Peer 3 side
$n_{nu} = 3$	number of slow inputs of continuous-time system
$n_{1nu} = 1$	number of slow inputs of continuous-time system at the Peer 1 side
$n_{2nu} = 2$	number of slow inputs of continuous-time system at the Peer 2 side
$n_{3cu} = 2$	number of fast inputs of continuous-time system at the Peer 3 side
$n_u = n_{cu} + n_{nu} = 9$	number of inputs of continuous-time system
$n_{cy} = 12$	number of fast outputs of continuous-time system
$n_{1cy} = 4$	number of fast outputs of continuous-time system at the Peer 1 side
$n_{2cy} = 4$	number of fast outputs of continuous-time system at the Peer 2 side
$n_{3cy} = 4$	number of fast outputs of continuous-time system at the Peer 3 side
$n_{ny} = 6$	number of slow outputs of continuous-time system
$n_{1ny} = 2$	number of slow outputs of continuous-time system at the Peer 1 side
$n_{2ny} = 2$	number of slow outputs of continuous-time system at the Peer 2 side
$n_{3ny} = 2$	number of slow outputs of continuous-time system at the Peer 3 side
$n_y = n_{cy} + n_{ny} = 18$	number of outputs of continuous-time system

A.1.1 Open-loop continuous time state-space representation for three users haptic cooperation using AP scheme

The continuous-time state-space representation of the open-loop three-users networked haptic cooperation is obtained from the dynamics of the users, haptic interfaces, and SVO copies. The system inputs and outputs are grouped into the fast and slow sub-vectors, denoted by c and n indices respectively. The system inputs comprise the contact forces, updated at the fast haptic rate (Equation (3.9)), and the SVO coordination forces, including both fast and slow updated components (Equation (3.10)):

$$\mathbf{u}^T = (\mathbf{u}_c^T \quad \mathbf{u}_n^T)^T \tag{A.1}$$

where:

$$\mathbf{u}_c^T = (F_{C_1} \quad F_{T_{1_c}} \quad F_{C_2} \quad F_{T_{2_c}} \quad F_{C_3} \quad F_{T_{3_c}})^T \tag{A.2}$$

$$\mathbf{u}_n^T = (F_{T_{1_n}} \quad F_{T_{2_n}} \quad F_{T_{3_n}})^T \tag{A.3}$$

$$F_{T_{i_c}} \;=\; K_T x_{O_i} + B_T \dot{x}_{O_i} \tag{A.4}$$

and,

$$F_{T_{i_n}} \;=\; -K_T x_{O_{i_d}} - B_T \dot{x}_{O_{i_d}} \tag{A.5}$$

The state vector comprises the states of all haptic interfaces and SVO copies:

$$\mathbf{x}^T = (\mathbf{x}_{peer1} \quad \mathbf{x}_{peer2} \quad \mathbf{x}_{peer3})^T \tag{A.6}$$

where:

$$\mathbf{x}_{peeri}^{T} = (x_{HD_i} \quad \dot{x}_{HD_i} \quad x_{O_i} \quad \dot{x}_{O_i})^T; \quad i = 1, 2, 3. \tag{A.7}$$

The output vector is:

$$\mathbf{y}^T = ({\mathbf{y}_c}^T \quad {\mathbf{y}_n}^T)^T, \tag{A.8}$$

where:

$${\mathbf{y}_c}^T = \mathbf{x}^T, \tag{A.9}$$

$$\mathbf{y}_n^T = (\mathbf{y}_{peer1_n} \quad \mathbf{y}_{peer2_n} \quad \mathbf{y}_{peer3_n})^T \tag{A.10}$$

and

$$\mathbf{y}_{peeri_n}^T = (x_{O_{i_d}} \quad \dot{x}_{O_{i_d}})^T; \quad i = 1, 2, 3. \tag{A.11}$$

The dynamics of the haptic cooperation among three peers for traditional distributed control are:

- for the peer haptic devices:

$$m_{HDi}\ddot{x}_{HDi} + b_{HDi}\dot{x}_{HDi} = F_{hi} - F_{Ci}; \quad i = 1, 2, 3 \tag{A.12}$$

$$\begin{pmatrix} \dot{x}_{HDi} \\ \ddot{x}_{HDi} \end{pmatrix} = \begin{bmatrix} 0 & 1 \\ 0 & -b_{HDi}/m_{HDi} \end{bmatrix} \begin{pmatrix} x_{HDi} \\ \dot{x}_{HDi} \end{pmatrix} + \begin{bmatrix} 0 \\ -1/m_{HDi} \end{bmatrix} \begin{pmatrix} F_{Ci} \end{pmatrix} \tag{A.13}$$

- for the copies of the shared virtual object:

$$m_{Oi}\ddot{x}_{Oi} + b_{Oi}\dot{x}_{Oi} = F_{Ci} - F_{Ti}; \quad i = 1, 2, 3 \tag{A.14}$$

in which:

$$F_{Ci} = K_{Ci}(x_{HDi} - x_{Oi}) + B_{Ci}(\dot{x}_{HDi} - \dot{x}_{Oi}) \tag{A.15}$$

$$\begin{aligned} F_{Ti} &= K_T(x_{Oi} - x_{Oi_d}) + B_T(\dot{x}_{Oi} - \dot{x}_{Oi_d}) \\ &= K_T x_{Oi} + B_T \dot{x}_{Oi} + (-K_T x_{Oi_d} - B_T \dot{x}_{Oi_d}) \\ &= K_T x_{Oi} + B_T \dot{x}_{Oi} + \left(-K_T \frac{\sum_{j=1, j\neq i}^{3} x_{Oj_n}}{2} - B_T \frac{\sum_{j=1, j\neq i}^{3} \dot{x}_{Oj_n}}{2} \right) \\ &= F_{Ti_c} + F_{Ti_n} \end{aligned} \tag{A.16}$$

$$\begin{pmatrix} \dot{x}_{Oi} \\ \ddot{x}_{Oi} \end{pmatrix} = \begin{bmatrix} 0 & 1 \\ 0 & -b_{Oi}/m_{Oi} \end{bmatrix} \begin{pmatrix} x_{Oi} \\ \dot{x}_{Oi} \end{pmatrix} + \begin{bmatrix} 0 & 0 & 0 \\ 1/m_{Oi} & -1/m_{Oi} & -1/m_{Oi} \end{bmatrix} \begin{pmatrix} F_{Ci} \\ F_{Ti_c} \\ F_{Ti_n} \end{pmatrix} \tag{A.17}$$

By grouping theses equations on the Peer i site:

$$
\begin{aligned}
\dot{\mathbf{x}}_{1_{4\times1}} &= \begin{pmatrix} \dot{x}_{HDi} \\ \ddot{x}_{HDi} \\ \dot{x}_{Oi} \\ \ddot{x}_{Oi} \end{pmatrix} \\
&= \begin{bmatrix} 0 & 1 & 0 & 0 \\ 0 & -b_{HDi}/m_{HDi} & 0 & 0 \\ 0 & 0 & 0 & 1 \\ 0 & 0 & 0 & -b_{Oi}/m_{Oi} \end{bmatrix} \begin{pmatrix} x_{HDi} \\ \dot{x}_{HDi} \\ x_{Oi} \\ \dot{x}_{Oi} \end{pmatrix} \\
&+ \begin{bmatrix} 0 & 0 & 0 \\ -1/m_{HDi} & 0 & 0 \\ 0 & 0 & 0 \\ 1/m_{Oi} & -1/m_{Oi} & -1/m_{Oi} \end{bmatrix} \begin{pmatrix} F_{Ci} \\ F_{Ti_c} \\ F_{Ti_n} \end{pmatrix} \\
&= \mathbf{A}_{i_{4\times4}} \mathbf{x}_{i_{4\times1}} + \begin{bmatrix} \mathbf{B}_{i_{c_{4\times2}}} & \mathbf{B}_{i_{n_{4\times1}}} \end{bmatrix}_{4\times3} \begin{pmatrix} \mathbf{u}_{i_{c_{2\times1}}} \\ \mathbf{u}_{i_{n_{1\times1}}} \end{pmatrix}_{3\times1}
\end{aligned} \tag{A.18}
$$

where:

$$
\mathbf{B}_{i_{c_{4\times2}}} = \begin{bmatrix} 0 & 0 \\ -1/m_{HDi} & 0 \\ 0 & 0 \\ 1/m_{Oi} & -1/m_{Oi} \end{bmatrix} \quad \text{and} \quad \mathbf{B}_{i_{n_{4\times1}}} = \begin{bmatrix} 0 \\ 0 \\ 0 \\ -1/m_{Oi} \end{bmatrix} \tag{A.19}
$$

and:

$$\begin{pmatrix} \mathbf{u}_{i_{c_{2\times1}}} \\ \mathbf{u}_{i_{n_{1\times1}}} \end{pmatrix}_{3\times1} = \begin{pmatrix} F_{Ci} \\ F_{Ti_c} \\ F_{Ti_n} \end{pmatrix} = \begin{bmatrix} \mathbf{F}_{i_{c_{2\times4}}} & 0_{2\times2} \\ 0_{1\times4} & \mathbf{F}_{i_{n_{1\times2}}} \end{bmatrix}_{3\times6} \begin{pmatrix} \mathbf{y}_{i_{c_{4\times1}}} \\ \mathbf{y}_{i_{n_{2\times1}}} \end{pmatrix}_{6\times1} \tag{A.20}$$

where:

$$\begin{aligned} \mathbf{F}_{i_{c_{2\times4}}} &= \begin{bmatrix} K_{C_i} & B_{C_i} & -K_{C_i} & -B_{C_i} \\ 0 & 0 & K_T & B_T \end{bmatrix}_{2\times4} \\ \mathbf{F}_{i_{n_{1\times2}}} &= \begin{bmatrix} -K_T & -B_T \end{bmatrix}_{1\times2} \end{aligned} \tag{A.21}$$

and:

$$\begin{aligned} \mathbf{y}_{i_{c_{n_{icy}\times1}}} = \mathbf{y}_{i_{c_{4\times1}}} &= \begin{pmatrix} x_{HDi} \\ \dot{x}_{HDi} \\ x_{Oi} \\ \dot{x}_{Oi} \end{pmatrix} \\ \mathbf{y}_{i_{n_{n_{iny}\times1}}} = \mathbf{y}_{i_{n_{2\times1}}} &= \begin{pmatrix} x_{Oi_d} \\ \dot{x}_{Oi_d} \end{pmatrix} \end{aligned} \tag{A.22}$$

The state equation is:

$$\begin{aligned}
\dot{\mathbf{x}}_{n_x\times 1} &= \mathbf{A}_{n_x\times n_x}\mathbf{x}_{n_x\times 1} + \mathbf{B}_{n_x\times n_u}\mathbf{u}_{n_u\times 1} \\
&= \mathbf{A}_{n_x\times n_x}\mathbf{x}_{n_x\times 1} \\
&+ \begin{bmatrix} \mathbf{B}_{c_{n_x\times n_{1cu}}} & \mathbf{B}_{c_{n_x\times n_{2cu}}} & \mathbf{B}_{c_{n_x\times n_{3cu}}} & \mathbf{B}_{n_{n_x\times n_{1nu}}} & \mathbf{B}_{n_{n_x\times n_{2nu}}} & \mathbf{B}_{n_{n_x\times n_{3nu}}} \end{bmatrix} \begin{pmatrix} \mathbf{u}_{1_{c_{n_{1cu}\times 1}}} \\ \mathbf{u}_{2_{c_{n_{2cu}\times 1}}} \\ \mathbf{u}_{3_{c_{n_{3cu}\times 1}}} \\ \mathbf{u}_{1_{n_{n_{1nu}\times 1}}} \\ \mathbf{u}_{2_{n_{n_{2nu}\times 1}}} \\ \mathbf{u}_{3_{n_{n_{3nu}\times 1}}} \end{pmatrix}
\end{aligned} \tag{A.23}$$

in which:

$$\begin{aligned}
\dot{\mathbf{x}}_{12\times 1} &= \mathbf{A}_{12\times 12}\mathbf{x}_{12\times 1} \\
&+ \begin{bmatrix} \mathbf{B}_{c_{12\times 2}} & \mathbf{B}_{c_{12\times 2}} & \mathbf{B}_{c_{12\times 2}} & \mathbf{B}_{n_{12\times 1}} & \mathbf{B}_{n_{12\times 1}} & \mathbf{B}_{n_{12\times 1}} \end{bmatrix} \begin{pmatrix} \mathbf{u}_{1_{c_{2\times 1}}} \\ \mathbf{u}_{2_{c_{2\times 1}}} \\ \mathbf{u}_{3_{c_{2\times 1}}} \\ \mathbf{u}_{1_{n_{1\times 1}}} \\ \mathbf{u}_{2_{n_{1\times 1}}} \\ \mathbf{u}_{3_{n_{1\times 1}}} \end{pmatrix}
\end{aligned} \tag{A.24}$$

$$\begin{pmatrix} \dot{\mathbf{x}}_{1_{4\times1}} \\ \dot{\mathbf{x}}_{2_{4\times1}} \\ \dot{\mathbf{x}}_{3_{4\times1}} \end{pmatrix} = \begin{bmatrix} \mathbf{A}_{1_{4\times4}} & 0_{4\times4} & 0_{4\times4} \\ 0_{4\times4} & \mathbf{A}_{2_{4\times4}} & 0_{4\times4} \\ 0_{4\times4} & 0_{4\times4} & \mathbf{A}_{3_{4\times4}} \end{bmatrix}_{12\times12} \begin{pmatrix} \mathbf{x}_{1_{4\times1}} \\ \mathbf{x}_{2_{4\times1}} \\ \mathbf{x}_{3_{4\times1}} \end{pmatrix}$$

$$+ \begin{bmatrix} \mathbf{B}_{1_{c_{4\times2}}} & 0_{4\times2} & 0_{4\times2} & \mathbf{B}_{1_{n_{4\times1}}} & 0_{4\times1} & 0_{4\times1} \\ 0_{4\times2} & \mathbf{B}_{2_{c_{4\times2}}} & 0_{4\times2} & 0_{4\times1} & \mathbf{B}_{2_{n_{4\times1}}} & 0_{4\times1} \\ 0_{4\times2} & 0_{4\times2} & \mathbf{B}_{3_{c_{4\times2}}} & 0_{4\times1} & 0_{4\times1} & \mathbf{B}_{3_{n_{4\times1}}} \end{bmatrix}_{12\times9} \begin{pmatrix} \mathbf{u}_{1_{c_{2\times1}}} \\ \mathbf{u}_{2_{c_{2\times1}}} \\ \mathbf{u}_{3_{c_{2\times1}}} \\ \mathbf{u}_{1_{n_{1\times1}}} \\ \mathbf{u}_{2_{n_{1\times1}}} \\ \mathbf{u}_{3_{n_{1\times1}}} \end{pmatrix} \tag{A.25}$$

where:

$$\mathbf{u}_{i_{c_{n_{icu}\times1}}} = \mathbf{u}_{i_{c_{2\times1}}} = \begin{bmatrix} F_{Ci} \\ F_{Ti_c} \end{bmatrix}; \quad i = 1, 2, 3. \tag{A.26}$$

and:

$$\mathbf{u}_{i_{n_{n_{inu}\times1}}} = \mathbf{u}_{i_{n_{1\times1}}} = \begin{bmatrix} F_{Ti_n} \end{bmatrix}; \quad i = 1, 2, 3. \tag{A.27}$$

Thus:

$$\begin{pmatrix} \dot{x}_{HD1} \\ \ddot{x}_{HD1} \\ \dot{x}_{O1} \\ \ddot{x}_{O1} \\ \dot{x}_{HD2} \\ \ddot{x}_{HD2} \\ \dot{x}_{O2} \\ \ddot{x}_{O2} \\ \dot{x}_{HD3} \\ \ddot{x}_{HD3} \\ \dot{x}_{O3} \\ \ddot{x}_{O3} \end{pmatrix} = \begin{bmatrix} \mathbf{A}_{1_{4\times4}} & 0_{4\times4} & 0_{4\times4} \\ 0_{4\times4} & \mathbf{A}_{2_{4\times4}} & 0_{4\times4} \\ 0_{4\times4} & 0_{4\times4} & \mathbf{A}_{3_{4\times4}} \end{bmatrix}_{12\times12} \begin{pmatrix} x_{HD1} \\ \dot{x}_{HD1} \\ x_{O1} \\ \dot{x}_{O1} \\ x_{HD2} \\ \dot{x}_{HD2} \\ x_{O2} \\ \dot{x}_{O2} \\ x_{HD3} \\ \dot{x}_{HD3} \\ x_{O3} \\ \dot{x}_{O3} \end{pmatrix}_{12\times1}$$

$$+ \begin{bmatrix} \mathbf{B}_{1_{c_{4\times2}}} & 0_{4\times2} & 0_{4\times2} & \mathbf{B}_{1_{n_{4\times1}}} & 0_{4\times1} & 0_{4\times1} \\ 0_{4\times2} & \mathbf{B}_{2_{c_{4\times2}}} & 0_{4\times2} & 0_{4\times1} & \mathbf{B}_{2_{n_{4\times1}}} & 0_{4\times1} \\ 0_{4\times2} & 0_{4\times2} & \mathbf{B}_{3_{c_{4\times2}}} & 0_{4\times1} & 0_{4\times1} & \mathbf{B}_{3_{n_{4\times1}}} \end{bmatrix}_{12\times9} \begin{pmatrix} F_{C1} \\ F_{T1_c} \\ F_{C2} \\ F_{T2_c} \\ F_{C3} \\ F_{T3_c} \\ F_{T1_n} \\ F_{T2_n} \\ F_{T3_n} \end{pmatrix}_{9\times1} \tag{A.28}$$

The output equations are:

$$\mathbf{y}_{n_y \times 1} = \begin{pmatrix} \mathbf{y}_{1_{c_{n_{1cy} \times 1}}} \\ \mathbf{y}_{2_{c_{n_{2cy} \times 1}}} \\ \mathbf{y}_{3_{c_{n_{3cy} \times 1}}} \\ \mathbf{y}_{1_{n_{n_{1ny} \times 1}}} \\ \mathbf{y}_{2_{n_{n_{2ny} \times 1}}} \\ \mathbf{y}_{3_{n_{n_{3ny} \times 1}}} \end{pmatrix} = \mathbf{C}_{n_y \times n_x} \mathbf{x}_{n_x \times 1} = \begin{bmatrix} \mathbf{C}_{1_{c_{n_{1cy} \times n_x}}} \\ \mathbf{C}_{2_{c_{n_{2cy} \times n_x}}} \\ \mathbf{C}_{3_{c_{n_{3cy} \times n_x}}} \\ \mathbf{C}_{1_{n_{n_{1ny} \times n_x}}} \\ \mathbf{C}_{2_{n_{n_{2ny} \times n_x}}} \\ \mathbf{C}_{3_{n_{n_{3ny} \times n_x}}} \end{bmatrix} = \mathbf{x}_{n_x \times 1} \tag{A.29}$$

$$\mathbf{y}_{18 \times 1} = \begin{pmatrix} \mathbf{y}_{1_{c_{4 \times 1}}} \\ \mathbf{y}_{2_{c_{4 \times 1}}} \\ \mathbf{y}_{3_{c_{4 \times 1}}} \\ \mathbf{y}_{1_{n_{2 \times 1}}} \\ \mathbf{y}_{2_{n_{2 \times 1}}} \\ \mathbf{y}_{3_{n_{2 \times 1}}} \end{pmatrix} = \mathbf{C}_{18 \times 12} \mathbf{x}_{12 \times 1} = \begin{bmatrix} \mathbf{C}_{1_{c_{4 \times 12}}} \\ \mathbf{C}_{2_{c_{4 \times 12}}} \\ \mathbf{C}_{3_{c_{4 \times 12}}} \\ \mathbf{C}_{1_{n_{2 \times 12}}} \\ \mathbf{C}_{2_{n_{2 \times 12}}} \\ \mathbf{C}_{3_{n_{2 \times 12}}} \end{bmatrix} = \mathbf{x}_{12 \times 1} \tag{A.30}$$

$$\begin{pmatrix} \mathbf{x}_{12\times1} \\ x_{O1_{d_n}} \\ \dot{x}_{O1_{d_n}} \\ x_{O2_{d_n}} \\ \dot{x}_{O2_{d_n}} \\ x_{O3_{d_n}} \\ \dot{x}_{O3_{d_n}} \end{pmatrix}_{18\times1} = \begin{bmatrix} & & & \mathbf{I}_{12\times12} & & \\ 0_{2\times2} & 0_{2\times2} & 0_{2\times2} & \frac{1}{2}\mathbf{I}_{2\times2} & 0_{2\times2} & \frac{1}{2}\mathbf{I}_{2\times2} \\ 0_{2\times2} & \frac{1}{2}\mathbf{I}_{2\times2} & 0_{2\times2} & 0_{2\times2} & 0_{2\times2} & \frac{1}{2}\mathbf{I}_{2\times2} \\ 0_{2\times2} & \frac{1}{2}\mathbf{I}_{2\times2} & 0_{2\times2} & \frac{1}{2}\mathbf{I}_{2\times2} & 0_{2\times2} & 0_{2\times2} \end{bmatrix} \begin{pmatrix} x_{HD1} \\ \dot{x}_{HD1} \\ x_{O1} \\ \dot{x}_{O1} \\ x_{HD2} \\ \dot{x}_{HD2} \\ x_{O2} \\ \dot{x}_{O2} \\ x_{HD3} \\ \dot{x}_{HD3} \\ x_{O3} \\ \dot{x}_{O3} \end{pmatrix}_{12\times1} \tag{A.31}$$

where:

$$\mathbf{y}_{i_{c_{n_{icy}\times1}}} = \mathbf{y}_{i_{c_{4\times1}}} = \mathbf{C}_{i_{c_{n_{icy}\times n_x}}} \mathbf{x}_{n_{x}\times1} = \mathbf{C}_{i_{c_{4\times12}}} \mathbf{x}_{12\times1}; \quad i = 1, 2, 3 \tag{A.32}$$

and:

$$\mathbf{y}_{i_{n_{n_{iny}\times1}}} = \mathbf{y}_{i_{n_{2\times1}}} = \begin{pmatrix} x_{Oi_{d_n}} \\ \dot{x}_{Oi_{d_n}} \end{pmatrix}; \quad i = 1, 2, 3 \tag{A.33}$$

$$\begin{pmatrix} \mathbf{C}_{1_{c_{n_{1cy}\times n_x}}} \\ \mathbf{C}_{2_{c_{n_{2cy}\times n_x}}} \\ \mathbf{C}_{3_{c_{n_{3cy}\times n_x}}} \end{pmatrix} = \begin{pmatrix} \mathbf{C}_{1_{c_{4\times12}}} \\ \mathbf{C}_{2_{c_{4\times12}}} \\ \mathbf{C}_{3_{c_{4\times12}}} \end{pmatrix} = \mathbf{I}_{12\times12} \tag{A.34}$$

$$\begin{aligned}
\mathbf{C}_{1_{n_{n_{1ny}\times n_x}}} &= \mathbf{C}_{1_{n_{2\times 12}}} = \begin{bmatrix} 0_{2\times 2} & 0_{2\times 2} & 0_{2\times 2} & \frac{1}{2}\mathbf{I}_{2\times 2} & 0_{2\times 2} & \frac{1}{2}\mathbf{I}_{2\times 2} \end{bmatrix} \\
\mathbf{C}_{2_{n_{n_{2ny}\times n_x}}} &= \mathbf{C}_{1_{n_{2\times 12}}} = \begin{bmatrix} 0_{2\times 2} & \frac{1}{2}\mathbf{I}_{2\times 2} & 0_{2\times 2} & 0_{2\times 2} & 0_{2\times 2} & \frac{1}{2}\mathbf{I}_{2\times 2} \end{bmatrix} \\
\mathbf{C}_{3_{n_{n_{3ny}\times n_x}}} &= \mathbf{C}_{1_{n_{2\times 12}}} = \begin{bmatrix} 0_{2\times 2} & \frac{1}{2}\mathbf{I}_{2\times 2} & 0_{2\times 2} & \frac{1}{2}\mathbf{I}_{2\times 2} & 0_{2\times 2} & 0_{2\times 2} \end{bmatrix}
\end{aligned} \tag{A.35}$$

and finally, the feedback equation is:

$$\mathbf{u}_{n_u\times 1} = \mathbf{F}_{n_u\times n_y}\mathbf{y}_{n_y\times 1} \tag{A.36}$$

$$\begin{pmatrix} \mathbf{u}_{1_{c_{n_{1cu}\times 1}}} \\ \mathbf{u}_{2_{c_{n_{2cu}\times 1}}} \\ \mathbf{u}_{3_{c_{n_{3cu}\times 1}}} \\ \mathbf{u}_{1_{n_{n_{1nu}\times 1}}} \\ \mathbf{u}_{2_{n_{n_{2nu}\times 1}}} \\ \mathbf{u}_{3_{n_{n_{3nu}\times 1}}} \end{pmatrix} =$$

$$\begin{bmatrix} \mathbf{F}_{1_{c_{n_{1cu}\times n_{1cy}}}} & 0_{2\times 4} & 0_{2\times 4} & 0_{2\times 2} & 0_{2\times 2} & 0_{2\times 2} \\ 0_{2\times 4} & \mathbf{F}_{2_{c_{n_{2cu}\times n_{2cy}}}} & 0_{2\times 4} & 0_{2\times 2} & 0_{2\times 2} & 0_{2\times 2} \\ 0_{2\times 4} & 0_{2\times 4} & \mathbf{F}_{3_{c_{n_{3cu}\times n_{3cy}}}} & 0_{2\times 2} & 0_{2\times 2} & 0_{2\times 2} \\ 0_{1\times 4} & 0_{1\times 4} & 0_{1\times 4} & \mathbf{F}_{1_{n_{n_{1nu}\times n_{1ny}}}} & 0_{1\times 2} & 0_{1\times 2} \\ 0_{1\times 4} & 0_{1\times 4} & 0_{1\times 4} & 0_{1\times 2} & \mathbf{F}_{2_{n_{n_{2nu}\times n_{2ny}}}} & 0_{1\times 2} \\ 0_{1\times 4} & 0_{1\times 4} & 0_{1\times 4} & 0_{1\times 2} & 0_{1\times 2} & \mathbf{F}_{3_{n_{n_{3nu}\times n_{3ny}}}} \end{bmatrix}$$

$$\cdot \begin{pmatrix} \mathbf{y}_{1_{c_{n_{1cy}\times 1}}} \\ \mathbf{y}_{2_{c_{n_{2cy}\times 1}}} \\ \mathbf{y}_{3_{c_{n_{3cy}\times 1}}} \\ \mathbf{y}_{1_{n_{n_{1ny}\times 1}}} \\ \mathbf{y}_{2_{n_{n_{2ny}\times 1}}} \\ \mathbf{y}_{3_{n_{n_{3ny}\times 1}}} \end{pmatrix} \tag{A.37}$$

$$\mathbf{u}_{9\times 1} = \mathbf{F}_{9\times 18}\mathbf{y}_{18\times 1} \tag{A.38}$$

$$
\begin{pmatrix}
\mathbf{u}_{1_{c_{2\times1}}} \\
\mathbf{u}_{2_{c_{2\times1}}} \\
\mathbf{u}_{3_{c_{2\times1}}} \\
\mathbf{u}_{1_{n_{1\times1}}} \\
\mathbf{u}_{2_{n_{1\times1}}} \\
\mathbf{u}_{3_{n_{1\times1}}}
\end{pmatrix} =
$$

$$
\begin{bmatrix}
\mathbf{F}_{1_{c_{2\times4}}} & 0_{2\times4} & 0_{2\times4} & 0_{2\times2} & 0_{2\times2} & 0_{2\times2} \\
0_{2\times4} & \mathbf{F}_{2_{c_{2\times4}}} & 0_{2\times4} & 0_{2\times2} & 0_{2\times2} & 0_{2\times2} \\
0_{2\times4} & 0_{2\times4} & \mathbf{F}_{3_{c_{2\times4}}} & 0_{2\times2} & 0_{2\times2} & 0_{2\times2} \\
0_{1\times4} & 0_{1\times4} & 0_{1\times4} & \mathbf{F}_{1_{n_{1\times2}}} & 0_{1\times2} & 0_{1\times2} \\
0_{1\times4} & 0_{1\times4} & 0_{1\times4} & 0_{1\times2} & \mathbf{F}_{2_{n_{1\times2}}} & 0_{1\times2} \\
0_{1\times4} & 0_{1\times4} & 0_{1\times4} & 0_{1\times2} & 0_{1\times2} & \mathbf{F}_{3_{n_{1\times2}}}
\end{bmatrix}
\cdot
\begin{pmatrix}
\mathbf{y}_{1_{c_{4\times1}}} \\
\mathbf{y}_{2_{c_{4\times1}}} \\
\mathbf{y}_{3_{c_{4\times1}}} \\
\mathbf{y}_{1_{n_{2\times1}}} \\
\mathbf{y}_{2_{n_{2\times1}}} \\
\mathbf{y}_{3_{n_{2\times1}}}
\end{pmatrix}
\tag{A.39}
$$

Hence, the continuous-time state-space model of open-loop three-user networked haptic cooperation with AP coordination is:

$$
\begin{aligned}
\dot{\mathbf{x}}_{12\times1} &= \mathbf{A}_{12\times12}\mathbf{x}_{12\times1} + \mathbf{B}_{12\times9}\mathbf{u}_{9\times1} \\
\mathbf{y}_{18\times1} &= \mathbf{C}_{18\times12}\mathbf{x}_{12\times1}
\end{aligned}
\tag{A.40}
$$

A.1.2 Discrete-time state-space representation for three users haptic cooperation using AP scheme

Following the approach [8], the continuous state space representation of the AP control system can be discretized with state vector that expanded according to the multiple sampling rates (the network sampling interval is an integer multiple of the sampling interval of the peers' force control loops). Besides, the force feedback and network update sampling times are synchronized. Thus, the discrete-time state-space representation of the open-loop system can be written as:

$$\begin{aligned} \mathbf{x}_{D_{96\times1}}[k+1] &= \mathbf{A}_{D_{96\times96}}\ \mathbf{x}_{D_{96\times1}}[k] + \mathbf{B}_{D_{96\times51}}\ \mathbf{u}_{D_{51\times1}}[k] \\ \mathbf{y}_{D_{102\times1}}[k] &= \hat{\mathbf{C}}_{D_{102\times96}}\ \mathbf{x}_{D_{96\times1}}[k] + \hat{\mathbf{D}}_{D_{102\times51}}\ \mathbf{u}_{D_{51\times1}}[k] \end{aligned} \tag{A.41}$$

where k is the k-th network update interval and more details about the derivations of the system matrices A_D, B_D, $\hat{C}_D$ and $\hat{D}_D$ can be found in [28]. Furthermore, by augmenting the state vector with the delayed inputs [28], computational and communication delays will be incorporated into the discrete-time open-loop model. In the following sections, the following values apply to three users haptic cooperation:

$p = 2$	number of sample times in the system (T_c and T_n in this case)
$T_c = \frac{1}{1000}$	control sampling rate
$T_n = \frac{8}{1000}$	network sampling rate
$T_0 = \frac{8}{1000}$	smallest sampling rate integer multiple of all sampling rates in the system
$N_c = \frac{T_0}{T_c} = \frac{\frac{8}{1000}}{\frac{1}{1000}} = 8$	number of control sampling periods in T_0
$N_n = \frac{T_0}{T_n} = \frac{\frac{8}{1000}}{\frac{8}{1000}} = 1$	number of network sampling periods in T_0
$\bar{N} = N_c + N_n = 8 + 1 = 9$	sum of all N-s
$\tau_0 = \frac{1}{1000}$	base sampling rate, i.e., largest sampling rate that fits an integer number of times in all system sampling rates
$l_c = \frac{T_c}{\tau_0} = \frac{\frac{1}{1000}}{\frac{1}{1000}} = 1$	number of fundamental sampling periods in T_c
$l_n = \frac{T_n}{\tau_0} = \frac{\frac{8}{1000}}{\frac{8}{1024}} = 8$	number of fundamental sampling periods in T_n
$N_0 = 8$	the least common multiple of N_c and N_n

With the multiple sampling rates existing in the control system, the state vector

for the discrete-time system is expanded as:

$$\begin{aligned}
\mathbf{x}_{D_{N_0 \cdot n_x \times 1}}[k] &= \mathbf{x}_{D_{8 \cdot 12 \times 1}}[k] = \mathbf{x}_{D_{96 \times 1}}[k] \\
&= \begin{pmatrix} \mathbf{x}_{n_x \times 1}\left((k-1)\,T_0 + \tau_0\right) \\ \mathbf{x}_{n_x \times 1}\left((k-1)\,T_0 + 2\tau_0\right) \\ \vdots \\ \mathbf{x}_{n_x \times 1}\left((k-1)\,T_0 + (N_0-1)\,\tau_0\right) \\ \mathbf{x}_{n_x \times 1}\left(kT_0\right) \end{pmatrix} = \begin{pmatrix} \mathbf{x}_{12 \times 1}\left((k-1)\,T_0 + \tau_0\right) \\ \mathbf{x}_{12 \times 1}\left((k-1)\,T_0 + 2\tau_0\right) \\ \vdots \\ \mathbf{x}_{12 \times 1}\left((k-1)\,T_0 + 7\tau_0\right) \\ \mathbf{x}_{12 \times 1}\left(kT_0\right) \end{pmatrix} \\
&= \begin{pmatrix} \mathbf{x}_{n_x \times 1}\left(kT_0 - (N_0-1)\,\tau_0\right) \\ \mathbf{x}_{n_x \times 1}\left(kT_0 - (N_0-2)\,\tau_0\right) \\ \vdots \\ \mathbf{x}_{n_x \times 1}\left(kT_0 - \tau_0\right) \\ \mathbf{x}_{n_x \times 1}\left(kT_0\right) \end{pmatrix} = \begin{pmatrix} \mathbf{x}_{12 \times 1}\left(kT_0 - 7\tau_0\right) \\ \mathbf{x}_{12 \times 1}\left(kT_0 - 6\tau_0\right) \\ \vdots \\ \mathbf{x}_{12 \times 1}\left(kT_0 - \tau_0\right) \\ \mathbf{x}_{12 \times 1}\left(kT_0\right) \end{pmatrix}
\end{aligned} \tag{A.42}$$

The output vector is expanded as:

$$\begin{aligned}
\mathbf{y}_{D_{(N_c \cdot n_{cy} + N_n \cdot n_{ny}) \times 1}}[k] &= \mathbf{y}_{D_{(8 \cdot 12 + 1 \cdot 6) \times 1}}[k] = \mathbf{y}_{D_{102 \times 1}}[k] = \begin{pmatrix} \mathbf{y}_{D_{c_{N_c \cdot n_{cy} \times 1}}}[k] \\ \mathbf{y}_{D_{n_{N_n \cdot n_{ny} \times 1}}}[k] \end{pmatrix} \\
&= \begin{pmatrix} \mathbf{y}_{D_{c_{8 \cdot 12 \times 1}}}[k] \\ \mathbf{y}_{D_{n_{1 \cdot 6 \times 1}}}[k] \end{pmatrix} = \begin{pmatrix} \mathbf{y}_{D_{c_{96 \times 1}}}[k] \\ \mathbf{y}_{D_{n_{6 \times 1}}}[k] \end{pmatrix}
\end{aligned} \tag{A.43}$$

where:

$$
\begin{aligned}
\mathbf{y}_{D_{c_{N_c \times n_{cy}}}}[k] &= \mathbf{y}_{D_{c_{8\cdot 12\times 1}}}[k] = \mathbf{y}_{D_{c_{96\times 1}}}[k] \\
&= \begin{pmatrix} \mathbf{y}_{D_{c_{n_{cy}\times 1}}}(kT_0) \\ \mathbf{y}_{D_{c_{n_{cy}\times 1}}}(kT_0 + T_c) \\ \vdots \\ \mathbf{y}_{D_{c_{n_{cy}\times 1}}}(kT_0 + (N_c - 1)T_c) \end{pmatrix} = \begin{pmatrix} \mathbf{y}_{D_{c_{12\times 1}}}(kT_0) \\ \mathbf{y}_{D_{c_{12\times 1}}}(kT_0 + T_c) \\ \vdots \\ \mathbf{y}_{c_{12\times 1}}(kT_0 + 7T_c) \end{pmatrix} \\
&= \begin{pmatrix} \mathbf{y}_{D_{1c_{n_{1cy}\times 1}}}(kT_0) \\ \mathbf{y}_{D_{2c_{n_{2cy}\times 1}}}(kT_0) \\ \mathbf{y}_{D_{3c_{n_{3cy}\times 1}}}(kT_0) \\ \mathbf{y}_{D_{1c_{n_{1cy}\times 1}}}(kT_0 + T_c) \\ \mathbf{y}_{D_{2c_{n_{2cy}\times 1}}}(kT_0 + T_c) \\ \mathbf{y}_{D_{3c_{n_{3cy}\times 1}}}(kT_0 + T_c) \\ \vdots \\ \mathbf{y}_{D_{1c_{n_{1cy}\times 1}}}(kT_0 + 7T_c) \\ \mathbf{y}_{D_{2c_{n_{2cy}\times 1}}}(kT_0 + 7T_c) \\ \mathbf{y}_{D_{3c_{n_{3cy}\times 1}}}(kT_0 + 7T_c) \end{pmatrix} = \begin{pmatrix} \mathbf{y}_{D_{1c_{4\times 1}}}(kT_0) \\ \mathbf{y}_{D_{2c_{4\times 1}}}(kT_0) \\ \mathbf{y}_{D_{3c_{4\times 1}}}(kT_0) \\ \mathbf{y}_{D_{1c_{4\times 1}}}(kT_0 + T_c) \\ \mathbf{y}_{D_{2c_{4\times 1}}}(kT_0 + T_c) \\ \mathbf{y}_{D_{3c_{4\times 1}}}(kT_0 + T_c) \\ \vdots \\ \mathbf{y}_{D_{1c_{4\times 1}}}(kT_0 + 7T_c) \\ \mathbf{y}_{D_{2c_{4\times 1}}}(kT_0 + 7T_c) \\ \mathbf{y}_{D_{3c_{4\times 1}}}(kT_0 + 7T_c) \end{pmatrix}
\end{aligned}
\tag{A.44}
$$

$$
\begin{aligned}
\mathbf{y}_{D_{n_{N_n \times n_{ny}}}}[k] &= \mathbf{y}_{D_{n_{1\cdot 6\times 1}}}[k] = \mathbf{y}_{D_{n_{6\times 1}}}[k] \\
&= \begin{pmatrix} \mathbf{y}_{D_{n_{n_{ny}\times 1}}}(kT_0) \\ \mathbf{y}_{D_{n_{n_{ny}\times 1}}}(kT_0 + T_n) \\ \vdots \\ \mathbf{y}_{D_{n_{n_{ny}\times 1}}}(kT_0 + (N_n - 1)\,T_n) \end{pmatrix} = \begin{bmatrix} \mathbf{y}_{D_{n_{6\times 1}}}(kT_0) \end{bmatrix} \\
&= \begin{pmatrix} \mathbf{y}_{D_{1n_{n_{1ny}\times 1}}}(kT_0) \\ \mathbf{y}_{D_{2n_{n_{2ny}\times 1}}}(kT_0) \\ \mathbf{y}_{D_{3n_{n_{3ny}\times 1}}}(kT_0) \\ \mathbf{y}_{D_{1n_{n_{1ny}\times 1}}}(kT_0 + T_n) \\ \mathbf{y}_{D_{2n_{n_{2ny}\times 1}}}(kT_0 + T_n) \\ \mathbf{y}_{D_{3n_{n_{3ny}\times 1}}}(kT_0 + T_n) \\ \vdots \\ \mathbf{y}_{D_{1n_{n_{1ny}\times 1}}}(kT_0 + (N_n - 1)\,T_n) \\ \mathbf{y}_{D_{2n_{n_{2ny}\times 1}}}(kT_0 + (N_n - 1)\,T_n) \\ \mathbf{y}_{D_{3n_{n_{3ny}\times 1}}}(kT_0 + (N_n - 1)\,T_n) \end{pmatrix} = \begin{bmatrix} \mathbf{y}_{1n_{2\times 1}}(kT_0) \\ \mathbf{y}_{2n_{2\times 1}}(kT_0) \\ \mathbf{y}_{3n_{2\times 1}}(kT_0) \end{bmatrix}
\end{aligned}
\tag{A.45}
$$

The input vector is expanded as:

$$
\begin{aligned}
\mathbf{u}_{D_{(N_c\cdot n_{cu}+N_n\cdot n_{nu})\times 1}}[k] &= \mathbf{u}_{D_{(8\cdot 6+1\cdot 3)\times 1}}[k] = \mathbf{u}_{D_{51\times 1}}[k] \\
&= \begin{pmatrix} \mathbf{u}_{D_{c_{N_c\cdot n_{cu}\times 1}}}[k] \\ \mathbf{u}_{D_{n_{N_n\cdot n_{nu}\times 1}}}[k] \end{pmatrix} = \begin{pmatrix} \mathbf{u}_{D_{c_{8\cdot 6\times 1}}}[k] \\ \mathbf{u}_{D_{n_{1\cdot 3\times 1}}}[k] \end{pmatrix} = \begin{pmatrix} \mathbf{u}_{D_{c_{48\times 1}}}[k] \\ \mathbf{u}_{D_{n_{3\times 1}}}[k] \end{pmatrix}
\end{aligned}
\tag{A.46}
$$

where $\mathbf{u}_{D_{c_{N_c \cdot n_{cu} \times 1}}}[k]$ depends on positions and velocities measured locally at the control sampling rate T_c:

$$
\begin{aligned}
\mathbf{u}_{D_{c_{N_c \cdot n_{cu} \times 1}}}[k] &= \mathbf{u}_{D_{c_{8 \cdot 6 \times 1}}}[k] = \mathbf{u}_{D_{c_{48 \times 1}}}[k] = \\
&= \begin{pmatrix} \mathbf{u}_{c_{n_{cu} \times 1}}(kT_0) \\ \vdots \\ \mathbf{u}_{c_{n_{cu} \times 1}}(kT_0 + (N_c - 1)T_c) \end{pmatrix} = \begin{pmatrix} \mathbf{u}_{c_{6 \times 1}}(kT_0) \\ \vdots \\ \mathbf{u}_{c_{6 \times 1}}(kT_0 + 7T_c) \end{pmatrix} \\
&= \begin{pmatrix} \mathbf{u}_{1c_{n_{1cu} \times 1}}(kT_0) \\ \mathbf{u}_{2c_{n_{2cu} \times 1}}(kT_0) \\ \mathbf{u}_{3c_{n_{3cu} \times 1}}(kT_0) \\ \vdots \\ \mathbf{u}_{1c_{n_{1cu} \times 1}}(kT_0 + (N_c - 1)T_c) \\ \mathbf{u}_{2c_{n_{2cu} \times 1}}(kT_0 + (N_c - 1)T_c) \\ \mathbf{u}_{3c_{n_{3cu} \times 1}}(kT_0 + (N_c - 1)T_c) \end{pmatrix} = \begin{pmatrix} \mathbf{u}_{1c_{2 \times 1}}(kT_0) \\ \mathbf{u}_{2c_{2 \times 1}}(kT_0) \\ \mathbf{u}_{3c_{2 \times 1}}(kT_0) \\ \vdots \\ \mathbf{u}_{1c_{2 \times 1}}(kT_0 + 7T_c) \\ \mathbf{u}_{2c_{2 \times 1}}(kT_0 + 7T_c) \\ \mathbf{u}_{3c_{2 \times 1}}(kT_0 + 7T_c) \end{pmatrix}
\end{aligned}
\tag{A.47}
$$

and $\mathbf{u}_{D_{n_{N_n \cdot n_{nu} \times 1}}}[k]$ depends on positions and velocities received from the remote peer at the network sampling rate T_n:

$$\begin{aligned}
\mathbf{u}_{D_{n_{N_n \cdot n_{nu} \times 1}}}[k] &= \mathbf{u}_{D_{n_{1 \cdot 3 \times 1}}}[k] = \mathbf{u}_{D_{n_{3 \times 1}}}[k] = \\
&= \begin{pmatrix} \mathbf{u}_{n_{n_{nu} \times 1}}(kT_0) \\ \vdots \\ \mathbf{u}_{n_{n_{nu} \times 1}}(T_0 + (N_n - 1)T_n) \end{pmatrix} = \left(\mathbf{u}_{n_{3 \times 1}}(kT_0) \right) \\
&= \begin{pmatrix} \mathbf{u}_{1n_{n_{1nu} \times 1}}(kT_0) \\ \mathbf{u}_{2n_{n_{2nu} \times 1}}(kT_0) \\ \mathbf{u}_{3n_{n_{3nu} \times 1}}(kT_0) \\ \vdots \\ \mathbf{u}_{1n_{n_{1nu} \times 1}}(T_0 + (N_n - 1)T_n) \\ \mathbf{u}_{2n_{n_{2nu} \times 1}}(T_0 + (N_n - 1)T_n) \\ \mathbf{u}_{3n_{n_{3nu} \times 1}}(T_0 + (N_n - 1)T_n) \end{pmatrix} = \begin{pmatrix} \mathbf{u}_{1n_{1 \times 1}}(kT_0) \\ \mathbf{u}_{2n_{1 \times 1}}(kT_0) \\ \mathbf{u}_{3n_{1 \times 1}}(kT_0) \end{pmatrix}
\end{aligned} \tag{A.48}$$

Hence, the discrete-time state-space representation of the open-loop system is:

$$\begin{aligned}
\mathbf{x}_D[k+1] &= \mathbf{A}_D \mathbf{x}_D[k] + \mathbf{B}_D \mathbf{u}_D[k] \\
\mathbf{y}_D[k] &= \mathbf{C}_D \left(\mathbf{U}_1 \mathbf{x}_D[k+1] + \mathbf{U}_2 \mathbf{x}_D[k] \right)
\end{aligned} \tag{A.49}$$

The computation of all matrices in Equation (A.49) is detailed in the following.

$$\begin{aligned}\mathbf{A}_{D_{N_0\cdot n_x\times N_0\cdot n_x}} &= \mathbf{A}_{D_{8\cdot 12\times 8\cdot 12}} = \mathbf{A}_{D_{96\times 96}} = \\ &= \begin{bmatrix} \mathbf{0}_{12\times 12} & \cdots & \mathbf{0}_{12\times 12} & \mathbf{A}_{D_1{}_{12\times 12}} \\ \mathbf{0}_{12\times 12} & \cdots & \mathbf{0}_{12\times 12} & \mathbf{A}_{D_2{}_{12\times 12}} \\ \mathbf{0}_{12\times 12} & \cdots & \mathbf{0}_{12\times 12} & \mathbf{A}_{D_3{}_{12\times 12}} \\ \mathbf{0}_{12\times 12} & \cdots & \mathbf{0}_{12\times 12} & \mathbf{A}_{D_4{}_{12\times 12}} \\ \mathbf{0}_{12\times 12} & \cdots & \mathbf{0}_{12\times 12} & \mathbf{A}_{D_5{}_{12\times 12}} \\ \mathbf{0}_{12\times 12} & \cdots & \mathbf{0}_{12\times 12} & \mathbf{A}_{D_6{}_{12\times 12}} \\ \mathbf{0}_{12\times 12} & \cdots & \mathbf{0}_{12\times 12} & \mathbf{A}_{D_7{}_{12\times 12}} \\ \mathbf{0}_{12\times 12} & \cdots & \mathbf{0}_{12\times 12} & \mathbf{A}_{D_8{}_{12\times 12}} \end{bmatrix}_{96\times 96}\end{aligned} \tag{A.50}$$

where:

$$\mathbf{A}_{D_{l}{}_{12\times 12}} = e^{\mathbf{A}_{12\times 12}\cdot l\cdot \tau_0} = e^{\mathbf{A}_{12\times 12}\cdot l\cdot \frac{1}{1000}} \qquad l = 1,\cdots,N_0 = 1,\cdots,8 \tag{A.51}$$

$$\begin{aligned}\mathbf{B}_{D_{N_0\cdot n_x\times(N_c\cdot n_{cu}+N_n\cdot n_{nu})}} &= \begin{bmatrix}\mathbf{B}_{D_{c}{}_{N_0\cdot n_x\times N_c\cdot n_{cu}}} & \mathbf{B}_{D_{n}{}_{N_0\cdot n_x\times N_n\cdot n_{nu}}}\end{bmatrix} \Longleftrightarrow \\ \mathbf{B}_{D_{8\cdot 12\times(8\cdot 6+1\cdot 3)}} &= \begin{bmatrix}\mathbf{B}_{D_{c}{}_{8\cdot 12\times 8\cdot 6}} & \mathbf{B}_{D_{n}{}_{8\cdot 12\times 1\cdot 3}}\end{bmatrix} \Longleftrightarrow \\ \mathbf{B}_{D_{96\times 51}} &= \begin{bmatrix}\mathbf{B}_{D_{c}{}_{96\times 48}} & \mathbf{B}_{D_{n}{}_{96\times 3}}\end{bmatrix}\end{aligned} \tag{A.52}$$

The $\mathbf{B}_{D_{c_{96\times 48}}}$ matrix is an $N_0 \times N_c = 8 \times 8$ block matrix:

$$\begin{aligned}
\mathbf{B}_{D_{c_{N_0 \cdot n_x \times N_c \cdot n_{cu}}}} &= \left[\mathbf{b}_{D_{c,l\mu_{n_x \times n_{cu}}}}\right] = \left[\begin{pmatrix} \mathbf{b}_{D_{1c,l\mu_{n_x \times n_{1cu}}}} & \mathbf{b}_{D_{2c,l\mu_{n_x \times n_{2cu}}}} & \mathbf{b}_{D_{3c,l\mu_{n_x \times n_{3cu}}}} \end{pmatrix}\right] \\
l &= 1, \ldots, N_0;\ \mu = 0, \ldots, N_c - 1 \\
&\Longleftrightarrow \\
\mathbf{B}_{D_{c_{96\times 48}}} &= \left[\mathbf{b}_{D_{c,l\mu_{12\times 6}}}\right] = \left[\begin{pmatrix} \mathbf{b}_{D_{1c,l\mu_{12\times 2}}} & \mathbf{b}_{D_{2c,l\mu_{12\times 2}}} & \mathbf{b}_{D_{3c,l\mu_{12\times 2}}} \end{pmatrix}\right] \\
l &= 1, \ldots, 8;\ \mu = 0, \ldots, 7
\end{aligned} \tag{A.53}$$

with the $l\mu$ block computed via:

$$\mathbf{b}_{D_{ic,l\mu_{n_x\times n_{ic}}}} = \begin{cases} \mathbf{0}_{n_x\times n_{ic}} & l \le l_c\cdot\mu \\ \int_{\mu\cdot l_c\cdot\tau_0}^{l\cdot\tau_0} e^{\mathbf{A}_{n_x\times n_x}(l\cdot\tau_0-\tau)}\mathbf{B}_{ic_{n_x\times n_{ic}}}d\tau & l_c\cdot\mu < l \le l_c\cdot(\mu+1) \\ \int_{\mu\cdot l_c\cdot\tau_0}^{(\mu+1)\cdot l_c\cdot\tau_0} e^{\mathbf{A}_{n_x\times n_x}(l\cdot\tau_0-\tau)}\mathbf{B}_{ic_{n_x\times n_{ic}}}d\tau & l_c\cdot(\mu+1) < l \end{cases}$$

$(i=1,2,3)$

$$\Longleftrightarrow$$

$$\mathbf{b}_{D_{1c,l\mu_{12\times 2}}} = \begin{cases} \mathbf{0}_{12\times 2} & l \le 1\cdot\mu \\ \int_{\mu\cdot 1\cdot\tau_0}^{l\cdot\tau_0} e^{\mathbf{A}_{12\times 12}(l\cdot\tau_0-\tau)}\mathbf{B}_{1c_{12\times 2}}d\tau & 1\cdot\mu < l \le 1\cdot(\mu+1) \\ \int_{\mu\cdot 1\cdot\tau_0}^{(\mu+1)\cdot 1\cdot\tau_0} e^{\mathbf{A}_{12\times 12}(l\cdot\tau_0-\tau)}\mathbf{B}_{1c_{12\times 2}}d\tau & 1\cdot(\mu+1) < l \end{cases}$$

$$\mathbf{b}_{D_{2c,l\mu_{12\times 2}}} = \begin{cases} \mathbf{0}_{12\times 2} & l \le 1\cdot\mu \\ \int_{\mu\cdot 1\cdot\tau_0}^{l\cdot\tau_0} e^{\mathbf{A}_{12\times 12}(l\cdot\tau_0-\tau)}\mathbf{B}_{2c_{12\times 2}}d\tau & 1\cdot\mu < l \le 1\cdot(\mu+1) \\ \int_{\mu\cdot 1\cdot\tau_0}^{(\mu+1)\cdot 1\cdot\tau_0} e^{\mathbf{A}_{12\times 12}(l\cdot\tau_0-\tau)}\mathbf{B}_{2c_{12\times 2}}d\tau & 1\cdot(\mu+1) < l \end{cases}$$

$$\mathbf{b}_{D_{3c,l\mu_{12\times 2}}} = \begin{cases} \mathbf{0}_{12\times 2} & l \le 1\cdot\mu \\ \int_{\mu\cdot 1\cdot\tau_0}^{l\cdot\tau_0} e^{\mathbf{A}_{12\times 12}(l\cdot\tau_0-\tau)}\mathbf{B}_{3c_{12\times 2}}d\tau & 1\cdot\mu < l \le 1\cdot(\mu+1) \\ \int_{\mu\cdot 1\cdot\tau_0}^{(\mu+1)\cdot 1\cdot\tau_0} e^{\mathbf{A}_{12\times 12}(l\cdot\tau_0-\tau)}\mathbf{B}_{3c_{12\times 2}}d\tau & 1\cdot(\mu+1) < l \end{cases}$$

(A.54)

Then:

$$\begin{aligned}
\mathbf{B}_{D_{c_{N_0\cdot n_x\times N_c\cdot n_{cu}=8\cdot 12\times 8\cdot 6=96\times 48}}} &= \begin{bmatrix}
\mathbf{b}_{D_{c,10}{}_{12\times 6}} & \mathbf{0}_{12\times 6} & \cdots & \mathbf{0}_{12\times 6} & \mathbf{0}_{12\times 6} \\
\mathbf{b}_{D_{c,20}{}_{12\times 6}} & \mathbf{b}_{D_{c,21}{}_{12\times 6}} & \cdots & \mathbf{0}_{12\times 6} & \mathbf{0}_{12\times 6} \\
\mathbf{b}_{D_{c,30}{}_{12\times 6}} & \mathbf{b}_{D_{c,31}{}_{12\times 6}} & \cdots & \mathbf{0}_{12\times 6} & \mathbf{0}_{12\times 6} \\
\mathbf{b}_{D_{c,40}{}_{12\times 6}} & \mathbf{b}_{D_{c,41}{}_{12\times 6}} & \cdots & \mathbf{0}_{12\times 6} & \mathbf{0}_{12\times 6} \\
\mathbf{b}_{D_{c,50}{}_{12\times 6}} & \mathbf{b}_{D_{c,51}{}_{12\times 6}} & \cdots & \mathbf{0}_{12\times 6} & \mathbf{0}_{12\times 6} \\
\mathbf{b}_{D_{c,60}{}_{12\times 6}} & \mathbf{b}_{D_{c,61}{}_{12\times 6}} & \cdots & \mathbf{0}_{12\times 6} & \mathbf{0}_{12\times 6} \\
\mathbf{b}_{D_{c,70}{}_{12\times 6}} & \mathbf{b}_{D_{c,71}{}_{12\times 6}} & \cdots & \mathbf{b}_{D_{c,76}{}_{12\times 6}} & \mathbf{0}_{12\times 6} \\
\mathbf{b}_{D_{c,80}{}_{12\times 6}} & \mathbf{b}_{D_{c,81}{}_{12\times 6}} & \cdots & \mathbf{b}_{D_{c,86}{}_{12\times 6}} & \mathbf{b}_{D_{c,87}{}_{12\times 6}}
\end{bmatrix} \\
&= \begin{bmatrix}
\mathbf{b}_{D_{c,0}{}_{96\times 6}} & \mathbf{b}_{D_{c,1}{}_{96\times 6}} & \cdots & \mathbf{b}_{D_{c,6}{}_{96\times 6}} & \mathbf{b}_{D_{c,7}{}_{96\times 6}}
\end{bmatrix}
\end{aligned} \tag{A.55}$$

The $\mathbf{B}_{D_{n_{96\times 3}}}$ matrix is an $N_0 \times N_n = 8 \times 1$ block matrix:

$$\begin{aligned}
\mathbf{B}_{D_{n_{N_0\cdot n_x\times N_n\cdot n_{nu}}}} &= \left[\mathbf{b}_{D_{n,l\mu_{n_x\times n_{nu}}}}\right] = \left[\begin{pmatrix}
\mathbf{b}_{D_{1n,l\mu_{n_x\times n_{1nu}}}} & \mathbf{b}_{D_{2n,l\mu_{n_x\times n_{2nu}}}} & \mathbf{b}_{D_{3n,l\mu_{n_x\times n_{3nu}}}}
\end{pmatrix}\right] \\
l &= 1,\ldots,N_0;\ \mu = 0,\ldots,N_n-1 \\
&\Longleftrightarrow \\
\mathbf{B}_{D_{n_{96\times 3}}} &= \left[\mathbf{b}_{D_{n,l\mu_{12\times 3}}}\right] = \left[\begin{pmatrix}
\mathbf{b}_{D_{1n,l\mu_{12\times 1}}} & \mathbf{b}_{D_{2n,l\mu_{12\times 1}}} & \mathbf{b}_{D_{3n,l\mu_{12\times 1}}}
\end{pmatrix}\right] \\
l &= 1,\ldots,8;\ \mu = 0
\end{aligned} \tag{A.56}$$

with the $l\mu$ block computed via:

$$\mathbf{b}_{D_{in,l\mu_{n_x\times n_{inu}}}} = \begin{cases} \mathbf{0}_{n_x\times n_{inu}} & l \le l_n\cdot\mu \\ \int_{\mu\cdot l_n\cdot\tau_0}^{l\cdot\tau_0} e^{\mathbf{A}_{n_x\times n_x}(l\cdot\tau_0-\tau)}\mathbf{B}_{in_{nx}\times n_{inu}}d\tau & l_n\cdot\mu < l \le l_n\cdot(\mu+1) \\ \int_{\mu\cdot l_n\cdot\tau_0}^{(\mu+1)\cdot l_n\cdot\tau_0} e^{\mathbf{A}_{n_x\times n_x}(l\cdot\tau_0-\tau)}\mathbf{B}_{in_{nx}\times n_{inu}}d\tau & l_n\cdot(\mu+1) < l \end{cases}$$

$(i=1,2,3)$

$$\Longleftrightarrow$$

$$\mathbf{b}_{D_{1n,l\mu_{12\times1}}} = \begin{cases} \mathbf{0}_{12\times1} & l \le 8\cdot\mu = 0 \\ \int_{\mu\cdot8\cdot\tau_0}^{l\cdot\tau_0} e^{\mathbf{A}_{12\times12}(l\cdot\tau_0-\tau)}\mathbf{B}_{1n_{12\times1}}d\tau & 8\cdot\mu = 0 < l \le 8\cdot(\mu+1) = 8 \\ \int_{\mu\cdot8\cdot\tau_0}^{(\mu+1)\cdot8\cdot\tau_0} e^{\mathbf{A}_{12\times12}(l\cdot\tau_0-\tau)}\mathbf{B}_{1n_{12\times1}}d\tau & 8\cdot(\mu+1) = 8 < l \end{cases}$$

$$\mathbf{b}_{D_{2n,l\mu_{12\times1}}} = \begin{cases} \mathbf{0}_{12\times1} & l \le 8\cdot\mu = 0 \\ \int_{\mu\cdot8\cdot\tau_0}^{l\cdot\tau_0} e^{\mathbf{A}_{12\times12}(l\cdot\tau_0-\tau)}\mathbf{B}_{2n_{12\times1}}d\tau & 8\cdot\mu = 0 < l \le 8\cdot(\mu+1) = 8 \\ \int_{\mu\cdot8\cdot\tau_0}^{(\mu+1)\cdot8\cdot\tau_0} e^{\mathbf{A}_{12\times12}(l\cdot\tau_0-\tau)}\mathbf{B}_{2n_{12\times1}}d\tau & 8\cdot(\mu+1) = 8 < l \end{cases}$$

$$\mathbf{b}_{D_{3n,l\mu_{12\times1}}} = \begin{cases} \mathbf{0}_{12\times1} & l \le 8\cdot\mu = 0 \\ \int_{\mu\cdot8\cdot\tau_0}^{l\cdot\tau_0} e^{\mathbf{A}_{12\times12}(l\cdot\tau_0-\tau)}\mathbf{B}_{3n_{12\times1}}d\tau & 8\cdot\mu = 0 < l \le 8\cdot(\mu+1) = 8 \\ \int_{\mu\cdot8\cdot\tau_0}^{(\mu+1)\cdot8\cdot\tau_0} e^{\mathbf{A}_{12\times12}(l\cdot\tau_0-\tau)}\mathbf{B}_{3n_{12\times1}}d\tau & 8\cdot(\mu+1) = 8 < l \end{cases}$$

(A.57)

For the simplified version we get:

$$\begin{aligned}
\mathbf{b}_{D_{1n,l\mu_{12\times1}}} &= \int_{\mu\cdot8\cdot\tau_0}^{l\cdot\tau_0} e^{\mathbf{A}_{12\times12}(l\cdot\tau_0-\tau)}\mathbf{B}_{1n_{12\times1}}d\tau \qquad 0<l\leq8\\
\mathbf{b}_{D_{2n,l\mu_{12\times1}}} &= \int_{\mu\cdot8\cdot\tau_0}^{l\cdot\tau_0} e^{\mathbf{A}_{12\times12}(l\cdot\tau_0-\tau)}\mathbf{B}_{2n_{12\times1}}d\tau \qquad 0<l\leq8\\
\mathbf{b}_{D_{3n,l\mu_{12\times1}}} &= \int_{\mu\cdot8\cdot\tau_0}^{l\cdot\tau_0} e^{\mathbf{A}_{12\times12}(l\cdot\tau_0-\tau)}\mathbf{B}_{3n_{12\times1}}d\tau \qquad 0<l\leq8
\end{aligned} \tag{A.58}$$

Hence:

$$\begin{aligned}
\mathbf{B}_{D_{n_{N_0\cdot n_x\times N_n\cdot n_{nu}=8\cdot12\times1\cdot3=96\times3}}} &= \begin{bmatrix}\mathbf{b}_{D_{n,10_{12\times3}}}\\ \mathbf{b}_{D_{n,20_{12\times3}}}\\ \vdots\\ \mathbf{b}_{D_{n,70_{12\times3}}}\\ \mathbf{b}_{D_{n,80_{12\times3}}}\end{bmatrix} = \begin{bmatrix}\mathbf{b}_{D_{1n,10_{12\times1}}} & \mathbf{b}_{D_{2n,10_{12\times1}}} & \mathbf{b}_{D_{3n,10_{12\times1}}}\\ \mathbf{b}_{D_{1n,20_{12\times1}}} & \mathbf{b}_{D_{2n,20_{12\times1}}} & \mathbf{b}_{D_{3n,20_{12\times1}}}\\ \vdots & & \\ \mathbf{b}_{D_{1n,70_{12\times1}}} & \mathbf{b}_{D_{2n,70_{12\times1}}} & \mathbf{b}_{D_{3n,70_{12\times1}}}\\ \mathbf{b}_{D_{1n,80_{12\times1}}} & \mathbf{b}_{D_{2n,80_{12\times1}}} & \mathbf{b}_{D_{3n,80_{12\times1}}}\end{bmatrix}\\
&= \begin{bmatrix}\mathbf{b}_{D_{n,0_{96\times3}}}\end{bmatrix} = \begin{bmatrix}\mathbf{b}_{D_{1n,0_{96\times1}}} & \mathbf{b}_{D_{2n,0_{96\times1}}} & \mathbf{b}_{D_{3n,0_{96\times1}}}\end{bmatrix}
\end{aligned} \tag{A.59}$$

$$\begin{aligned}
\mathbf{C}_{D_{(N_c\cdot n_{cy}+N_n\cdot n_{ny})\times N_0\cdot n_x}} &= \begin{bmatrix}\mathbf{C}_{D_{c_{N_c\cdot n_{cy}\times N_0\cdot n_x}}}\\ \mathbf{C}_{D_{n_{N_n\cdot n_{ny}\times N_0\cdot n_x}}}\end{bmatrix}\\
\Longleftrightarrow \mathbf{C}_{D_{(8\cdot12+1\cdot6)\times8\cdot12}} &= \begin{bmatrix}\mathbf{C}_{D_{c_{8\cdot12\times8\cdot12}}}\\ \mathbf{C}_{D_{n_{1\cdot6\times8\cdot12}}}\end{bmatrix}\\
\Longleftrightarrow \mathbf{C}_{D_{102\times96}} &= \begin{bmatrix}\mathbf{C}_{D_{c_{96\times96}}}\\ \mathbf{C}_{D_{n_{6\times96}}}\end{bmatrix}
\end{aligned} \tag{A.60}$$

The $\mathbf{C}_{D_{c_{96\times 96}}}$ matrix is an $N_c \times N_0 = 8 \times 8$ block matrix:

$$\begin{aligned}
\mathbf{C}_{D_{c_{N_c \cdot n_{cy} \times N_0 \cdot n_x}}} &= \left[\mathbf{c}_{D_{c,\nu l_{n_{cy}\times n_x}}}\right] = \left[\begin{pmatrix} \mathbf{c}_{D_{1c,\nu l_{n_{1cy}\times n_x}}} \\ \mathbf{c}_{D_{2c,\nu l_{n_{2cy}\times n_x}}} \\ \mathbf{c}_{D_{3c,\nu l_{n_{3cy}\times n_x}}} \end{pmatrix}\right] \\
\nu &= 0, \ldots, N_c - 1;\ l = 1, \ldots, N_0 \\
&\Longleftrightarrow \\
\mathbf{C}_{D_{c_{96\times 96}}} &= \left[\mathbf{c}_{D_{c,\nu l_{12\times 12}}}\right] = \left[\begin{pmatrix} \mathbf{c}_{D_{1c,\nu l_{4\times 12}}} \\ \mathbf{c}_{D_{2c,\nu l_{4\times 12}}} \\ \mathbf{c}_{D_{3c,\nu l_{4\times 12}}} \end{pmatrix}\right] \\
\nu &= 0, \ldots, 7;\ l = 1, \ldots, 8
\end{aligned} \tag{A.61}$$

with the νl block computed via:

$$\mathbf{c}_{D_{ic,\nu l}{}_{n_{icy}\times n_x}} = \begin{cases} \mathbf{C}_{ic_{n_{icy}\times n_x}} & \nu = 0, l = N_0 \quad or \quad l_c \cdot \nu = l \\ \\ \mathbf{0}_{n_{icy}\times n_x} & otherwise \end{cases}$$

$$\Longleftrightarrow$$

$(i = 1, 2, 3)$

$$\mathbf{c}_{D_{1c,\nu l}{}_{4\times 12}} = \begin{cases} \mathbf{C}_{1c_{4\times 12}} & \nu = 0, l = 8 \quad or \quad 1 \cdot \nu = l \\ \\ \mathbf{0}_{4\times 12} & otherwise \end{cases},$$

$$\mathbf{c}_{D_{2c,\nu l}{}_{4\times 12}} = \begin{cases} \mathbf{C}_{2c_{4\times 12}} & \nu = 0, l = 8 \quad or \quad 1 \cdot \nu = l \\ \\ \mathbf{0}_{4\times 12} & otherwise \end{cases}$$

$$\mathbf{c}_{D_{3c,\nu l}{}_{4\times 12}} = \begin{cases} \mathbf{C}_{3c_{4\times 12}} & \nu = 0, l = 8 \quad or \quad 1 \cdot \nu = l \\ \\ \mathbf{0}_{4\times 12} & otherwise \end{cases} \tag{A.62}$$

Hence:

$$\mathbf{C}_{D_{c_{N_c \cdot n_{cy} \times N_0 \cdot n_x = 8 \cdot 12 \times 8 \cdot 12 = 96 \times 96}}}$$

$$= \begin{bmatrix} \mathbf{0}_{12\times12} & \mathbf{0}_{12\times12} & \mathbf{0}_{12\times12} & \mathbf{0}_{12\times12} & \mathbf{0}_{12\times12} & \mathbf{0}_{12\times12} & \mathbf{0}_{12\times12} & \mathbf{C}_{c_{12\times12}} \\ \mathbf{C}_{c_{12\times12}} & \mathbf{0}_{12\times12} & \mathbf{0}_{12\times12} & \mathbf{0}_{12\times12} & \mathbf{0}_{12\times12} & \mathbf{0}_{12\times12} & \mathbf{0}_{12\times12} & \mathbf{0}_{12\times12} \\ \mathbf{0}_{12\times12} & \mathbf{C}_{c_{12\times12}} & \mathbf{0}_{12\times12} & \mathbf{0}_{12\times12} & \mathbf{0}_{12\times12} & \mathbf{0}_{12\times12} & \mathbf{0}_{12\times12} & \mathbf{0}_{12\times12} \\ \mathbf{0}_{12\times12} & \mathbf{0}_{12\times12} & \mathbf{C}_{c_{12\times12}} & \mathbf{0}_{12\times12} & \mathbf{0}_{12\times12} & \mathbf{0}_{12\times12} & \mathbf{0}_{12\times12} & \mathbf{0}_{12\times12} \\ \mathbf{0}_{12\times12} & \mathbf{0}_{12\times12} & \mathbf{0}_{12\times12} & \mathbf{C}_{c_{12\times12}} & \mathbf{0}_{12\times12} & \mathbf{0}_{12\times12} & \mathbf{0}_{12\times12} & \mathbf{0}_{12\times12} \\ \mathbf{0}_{12\times12} & \mathbf{0}_{12\times12} & \mathbf{0}_{12\times12} & \mathbf{0}_{12\times12} & \mathbf{C}_{c_{12\times12}} & \mathbf{0}_{12\times12} & \mathbf{0}_{12\times12} & \mathbf{0}_{12\times12} \\ \mathbf{0}_{12\times12} & \mathbf{0}_{12\times12} & \mathbf{0}_{12\times12} & \mathbf{0}_{12\times12} & \mathbf{0}_{12\times12} & \mathbf{C}_{c_{12\times12}} & \mathbf{0}_{12\times12} & \mathbf{0}_{12\times12} \\ \mathbf{0}_{12\times12} & \mathbf{0}_{12\times12} & \mathbf{0}_{12\times12} & \mathbf{0}_{12\times12} & \mathbf{0}_{12\times12} & \mathbf{0}_{12\times12} & \mathbf{C}_{c_{12\times12}} & \mathbf{0}_{12\times12} \end{bmatrix} \tag{A.63}$$

where

$$\mathbf{C}_{c_{12\times12}} = \begin{pmatrix} \mathbf{C}_{1c_{4\times12}} \\ \mathbf{C}_{2c_{4\times12}} \\ \mathbf{C}_{3c_{4\times12}} \end{pmatrix} \tag{A.64}$$

The $\mathbf{C}_{D_{n_{6\times96}}}$ matrix is a $N_n \times N_0 = 1 \times 8$ block matrix:

$$
\begin{aligned}
\mathbf{C}_{D_{n_{N_n \cdot n_{ny} \times N_0 \cdot n_x}}} &= \left[\mathbf{c}_{D_{n,\nu l_{n_{ny} \times n_x}}}\right] = \left[\begin{pmatrix} \mathbf{c}_{D_{1n,\nu l_{n_{1ny} \times n_x}}} \\ \mathbf{c}_{D_{2n,\nu l_{n_{2ny} \times n_x}}} \\ \mathbf{c}_{D_{3n,\nu l_{n_{3ny} \times n_x}}} \end{pmatrix}\right] \\
\nu &= 0, \ldots, N_n - 1;\, l = 1, \ldots, N_0 \\
&\Longleftrightarrow \\
\mathbf{C}_{D_{n_{6 \times 96}}} &= \left[\mathbf{c}_{D_{n,\nu l_{6 \times 12}}}\right] = \left[\begin{pmatrix} \mathbf{c}_{D_{1n,\nu l_{2 \times 12}}} \\ \mathbf{c}_{D_{2n,\nu l_{2 \times 12}}} \\ \mathbf{c}_{D_{3n,\nu l_{2 \times 12}}} \end{pmatrix}\right] \\
\nu &= 0;\, l = 1, \ldots, 8
\end{aligned}
\tag{A.65}
$$

with the νl block computed via:

$$\mathbf{c}_{D_{in,l\nu_{n_{iny}\times n_x}}} = \begin{cases} \mathbf{C}_{in_{n_{iny}\times n_x}} & \nu = 0, l = N_0 \quad or \quad l_n \cdot \nu = l \\ \\ \mathbf{0}_{n_{iny}\times n_x} & otherwise \end{cases} \qquad (i = 1, 2, 3)$$

$$\Longleftrightarrow$$

$$\mathbf{c}_{D_{1n,l\nu_{2\times 12}}} = \begin{cases} \mathbf{C}_{1n_{2\times 12}} & \nu = 0, l = 8 \quad or \quad 8 \cdot \nu = l \\ \\ \mathbf{0}_{2\times 12} & otherwise \end{cases}$$

$$\mathbf{c}_{D_{2n,l\nu_{2\times 12}}} = \begin{cases} \mathbf{C}_{2n_{2\times 12}} & \nu = 0, l = 8 \quad or \quad 8 \cdot \nu = l \\ \\ \mathbf{0}_{2\times 12} & otherwise \end{cases}$$

$$\mathbf{c}_{D_{3n,l\nu_{2\times 12}}} = \begin{cases} \mathbf{C}_{3n_{2\times 12}} & \nu = 0, l = 8 \quad or \quad 8 \cdot \nu = l \\ \\ \mathbf{0}_{2\times 12} & otherwise \end{cases} \qquad (A.66)$$

Thus:

$$\mathbf{C}_{D_{n_{N_n}\cdot n_{ny}\times N_0\cdot n_x = 1\cdot 6\times 8\cdot 12 = 6\times 96}} = \begin{bmatrix} \mathbf{0}_{6\times 12} & \mathbf{0}_{6\times 12} & \mathbf{0}_{6\times 12} & \mathbf{0}_{6\times 12} & \mathbf{0}_{6\times 12} & \mathbf{0}_{6\times 12} & \mathbf{0}_{6\times 12} & \mathbf{C}_{n_{6\times 12}} \end{bmatrix} \qquad (A.67)$$

Where

$$\mathbf{C}_{n_{6\times 12}} = \begin{pmatrix} \mathbf{C}_{1n_{2\times 12}} \\ \mathbf{C}_{2n_{2\times 12}} \\ \mathbf{C}_{3n_{2\times 12}} \end{pmatrix} \tag{A.68}$$

$\mathbf{U}1_{N_0\cdot n_x \times N_0\cdot n_x = 8\cdot 12\times 8\cdot 12 = 96\times 96}$ and $\mathbf{U}2_{N_0\cdot n_x \times N_0\cdot n_x = 8\cdot 12\times 8\cdot 12 = 96\times 96}$ are $N_0 \times N_0 = 8$ blocks diagonal matrices having the following $n_x \times n_x = 12 \times 12$ blocks on their diagonals:

$$\begin{cases} \mathbf{U}1_{N_0\cdot n_x \times N_0\cdot n_x} &= blockdiag\left(\mathbf{I}_{n_x\times n_x}, \ldots, \mathbf{I}_{n_x\times n_x}, \mathbf{0}_{n_x\times n_x}\right) \\ \mathbf{U}2_{N_0\cdot n_x \times N_0\cdot n_x} &= blockdiag\left(\mathbf{0}_{n_x\times n_x}, \ldots, \mathbf{0}_{n_x\times n_x}, \mathbf{I}_{n_x\times n_x}\right) \end{cases}$$
$$\Longleftrightarrow$$
$$\begin{cases} \mathbf{U}1_{8\cdot 12\times 8\cdot 12} &= \mathbf{U}1_{96\times 96} = blockdiag\left(\mathbf{I}_{12\times 12}, \ldots, \mathbf{I}_{12\times 12}, \mathbf{0}_{12\times 12}\right) \\ \mathbf{U}2_{8\cdot 12\times 8\cdot 12} &= \mathbf{U}2_{96\times 96} = blockdiag\left(\mathbf{0}_{12\times 12}, \ldots, \mathbf{0}_{12\times 12}, \mathbf{I}_{12\times 12}\right) \end{cases} \tag{A.69}$$

Therefore,

$$\begin{aligned} \hat{\mathbf{C}}_{D_{102\times 96}} &= \mathbf{C}_{D_{102\times 96}} \cdot \mathbf{U}1_{96\times 96} \cdot \mathbf{A}_{D_{96\times 96}} + \mathbf{C}_{D_{102\times 96}} \cdot \mathbf{U}2_{96\times 96} \\ \hat{\mathbf{D}}_{D_{102\times 51}} &= \mathbf{C}_{D_{102\times 96}} \cdot \mathbf{U}1_{96\times 96} \cdot \mathbf{B}_{D_{96\times 51}} \end{aligned} \tag{A.70}$$

Deploying the feedback law, the closed-loop dynamics can be obtained from the open-loop discrete-time difference equations:

$$\begin{aligned} \mathbf{u}_{D_{(N_c \cdot n_{cu} + N_n \cdot n_{nu}) \times 1}} &= \mathbf{F}_{D_{(N_c \cdot n_{cu} + N_n \cdot n_{nu}) \times (N_c \cdot n_{cy} + N_n \cdot n_{ny})}} \mathbf{y}_{D_{(N_c \cdot n_{cy} + N_n \cdot n_{ny}) \times 1}} \iff \\ \mathbf{u}_{D_{51 \times 1}} &= \mathbf{F}_{D_{(8 \cdot 6 + 1 \cdot 3) \times (8 \cdot 12 + 1 \cdot 6)}} \mathbf{y}_{D_{(8 \cdot 12 + 1 \cdot 6) \times 1}} = \mathbf{F}_{D_{51 \times 102}} \mathbf{y}_{D_{102 \times 1}} \end{aligned} \tag{A.71}$$

According to feedback equations, given:

$$
\begin{aligned}
\mathbf{F}_{cc_{N_c \cdot n_{cu} \times N_c \cdot n_{cy}}} = \mathbf{F}_{cc_{8\cdot 6 \times 8 \cdot 12}} &= \begin{bmatrix} \mathbf{F}_{1c_{n_{1cu} \times n_{1cy}}} & \mathbf{0}_{n_{1cu} \times n_{2cy}} & \mathbf{0}_{n_{1cu} \times n_{3cy}} \\ \mathbf{0}_{n_{2cu} \times n_{1cy}} & \mathbf{F}_{2c_{n_{2cu} \times n_{2cy}}} & \mathbf{0}_{n_{2cu} \times n_{3cy}} \\ \mathbf{0}_{n_{3cu} \times n_{1cy}} & \mathbf{0}_{n_{3cu} \times n_{2cy}} & \mathbf{F}_{3c_{n_{3cu} \times n_{3cy}}} \end{bmatrix} \\
&= \begin{bmatrix} \mathbf{F}_{1c_{2\times 4}} & \mathbf{0}_{2\times 4} & \mathbf{0}_{2\times 4} \\ \mathbf{0}_{2\times 4} & \mathbf{F}_{2c_{2\times 4}} & \mathbf{0}_{2\times 4} \\ \mathbf{0}_{2\times 4} & \mathbf{0}_{2\times 4} & \mathbf{F}_{3c_{2\times 4}} \end{bmatrix} \\
\mathbf{F}_{cn_{N_c \cdot n_{cu} \times N_n \cdot n_{ny}}} = \mathbf{F}_{cn_{8\cdot 6 \times 1 \cdot 6}} &= \begin{bmatrix} \mathbf{0}_{n_{1cu} \times n_{1ny}} & \mathbf{0}_{n_{1cu} \times n_{2ny}} & \mathbf{0}_{n_{1cu} \times n_{3ny}} \\ \mathbf{0}_{n_{2cu} \times n_{1ny}} & \mathbf{0}_{n_{2cu} \times n_{2ny}} & \mathbf{0}_{n_{2cu} \times n_{3ny}} \\ \mathbf{0}_{n_{3cu} \times n_{1ny}} & \mathbf{0}_{n_{3cu} \times n_{2ny}} & \mathbf{0}_{n_{3cu} \times n_{3ny}} \end{bmatrix} \\
&= \begin{bmatrix} \mathbf{0}_{2\times 2} & \mathbf{0}_{2\times 2} & \mathbf{0}_{2\times 2} \\ \mathbf{0}_{2\times 2} & \mathbf{0}_{2\times 2} & \mathbf{0}_{2\times 2} \\ \mathbf{0}_{2\times 2} & \mathbf{0}_{2\times 2} & \mathbf{0}_{2\times 2} \end{bmatrix} \\
\mathbf{F}_{nc_{N_n \cdot n_{nu} \times N_c \cdot n_{cy}}} = \mathbf{F}_{nc_{1\cdot 3 \times 8 \cdot 12}} &= \begin{bmatrix} \mathbf{0}_{n_{1nu} \times n_{1cy}} & \mathbf{0}_{n_{1nu} \times n_{2cy}} & \mathbf{0}_{n_{1nu} \times n_{3cy}} \\ \mathbf{0}_{n_{2nu} \times n_{1cy}} & \mathbf{0}_{n_{2nu} \times n_{2cy}} & \mathbf{0}_{n_{2nu} \times n_{3cy}} \\ \mathbf{0}_{n_{3nu} \times n_{1cy}} & \mathbf{0}_{n_{3nu} \times n_{2cy}} & \mathbf{0}_{n_{3nu} \times n_{3cy}} \end{bmatrix} \\
&= \begin{bmatrix} \mathbf{0}_{1\times 4} & \mathbf{0}_{1\times 4} & \mathbf{0}_{1\times 4} \\ \mathbf{0}_{1\times 4} & \mathbf{0}_{1\times 4} & \mathbf{0}_{1\times 4} \\ \mathbf{0}_{1\times 4} & \mathbf{0}_{1\times 4} & \mathbf{0}_{1\times 4} \end{bmatrix} \\
\mathbf{F}_{nn_{N_n \cdot n_{nu} \times N_n \cdot n_{ny}}} = \mathbf{F}_{nn_{1\cdot 3 \times 1 \cdot 6}} &= \begin{bmatrix} \mathbf{F}_{1n_{n_{1nu} \times n_{1ny}}} & \mathbf{0}_{n_{1nu} \times n_{2ny}} & \mathbf{0}_{n_{1nu} \times n_{3ny}} \\ \mathbf{0}_{n_{2nu} \times n_{1ny}} & \mathbf{F}_{2n_{n_{2nu} \times n_{2ny}}} & \mathbf{0}_{n_{2nu} \times n_{3ny}} \\ \mathbf{0}_{n_{3nu} \times n_{1ny}} & \mathbf{0}_{n_{3nu} \times n_{2ny}} & \mathbf{F}_{3n_{n_{3nu} \times n_{3ny}}} \end{bmatrix} \\
&= \begin{bmatrix} \mathbf{F}_{1n_{1\times 2}} & \mathbf{0}_{1\times 2} & \mathbf{0}_{1\times 2} \\ \mathbf{0}_{1\times 2} & \mathbf{F}_{2n_{1\times 2}} & \mathbf{0}_{1\times 2} \\ \mathbf{0}_{1\times 2} & \mathbf{0}_{1\times 2} & \mathbf{F}_{3n_{1\times 2}} \end{bmatrix}
\end{aligned}
\tag{A.72}
$$

The discrete-time feedback matrix $\mathbf{F}_{D_{(N_c \cdot n_{cu}+N_n \cdot n_{nu})\times\left(N_c \cdot n_{cy}+N_n \cdot n_{ny}\right)=(8\cdot 6+1\cdot 3)\times(8\cdot 12+1\cdot 6)=51\times 102}}$ is:

$$\mathbf{F}_{D_{(N_c \cdot n_{cu}+N_n \cdot n_{nu})\times\left(N_c \cdot n_{cy}+N_n \cdot n_{ny}\right)}} = \begin{bmatrix} \mathbf{F}_{D_{cc_{N_c \cdot n_{cu}\times N_c \cdot n_{cy}}}} & \mathbf{F}_{D_{cn_{N_c \cdot n_{cu}\times N_n \cdot n_{ny}}}} \\ \mathbf{F}_{D_{nc_{N_n \cdot n_{nu}\times N_c \cdot n_{cy}}}} & \mathbf{F}_{D_{nn_{N_n \cdot n_{nu}\times N_n \cdot n_{ny}}}} \end{bmatrix} \Longleftrightarrow$$

$$\mathbf{F}_{D_{(48+3)\times(96+6)}} = \begin{bmatrix} \mathbf{F}_{D_{cc_{48\times 96}}} & \mathbf{F}_{D_{cn_{48\times 6}}} \\ \mathbf{F}_{D_{nc_{3\times 96}}} & \mathbf{F}_{D_{nn_{3\times 6}}} \end{bmatrix} = \begin{bmatrix} \mathbf{F}_{D_{cc_{48\times 96}}} & \mathbf{0}_{48\times 8} \\ \mathbf{0}_{3\times 96} & \mathbf{F}_{D_{nn_{3\times 6}}} \end{bmatrix} \tag{A.73}$$

$\mathbf{F}_{D_{cc_{N_c \cdot n_{cu}\times N_c \cdot n_{cy}}}}$ has $N_c \times N_c = 8 \times 8$ blocks of dimension $n_{cu} \times n_{cy} = 6 \times 12$:

$$\begin{aligned} \mathbf{F}_{D_{cc_{N_c \cdot n_{cu}\times N_c \cdot n_{cy}}}} &= \left[\mathbf{f}_{D_{cc,\mu\nu_{n_{cu}\times n_{cy}}}}\right] \quad \mu = 0,\ldots,N_c-1;\ \nu = 0,\ldots,N_c-1 \\ &\Longleftrightarrow \\ \mathbf{F}_{D_{cc_{8\cdot 6\times 8\cdot 12=48\times 96}}} &= \left[\mathbf{f}_{D_{cc,\mu\nu_{6\times 12}}}\right] \quad \mu = 0,\ldots,7;\ \nu = 0,\ldots,7 \end{aligned} \tag{A.74}$$

with the $\mu\nu$ block computed via:

$$\mathbf{f}_{D_{cc,\mu\nu_{n_{cu}\times n_{cy}}}} = \begin{cases} \mathbf{F}_{cc_{n_{cu}\times n_{cy}}} & \nu l_c \leq \mu l_c < (\nu+1)\, l_c \\ \\ \mathbf{0}_{n_{cu}\times n_{cy}} & otherwise. \end{cases}$$

$$\Longleftrightarrow$$

$$\mathbf{f}_{D_{cc,\mu\nu_{6\times 12}}} = \begin{cases} \mathbf{F}_{cc_{6\times 12}} & \nu \leq \mu < (\nu+1) \\ \\ \mathbf{0}_{6\times 12} & otherwise. \end{cases} \tag{A.75}$$

Thus:

$$\mathbf{F}_{D_{cc_{48\times 96}}} = \begin{bmatrix} \mathbf{F}_{cc_{6\times 12}} & \mathbf{0}_{6\times 12} & \mathbf{0}_{6\times 12} & \mathbf{0}_{6\times 12} & \mathbf{0}_{6\times 12} & \mathbf{0}_{6\times 12} & \mathbf{0}_{6\times 12} & \mathbf{0}_{6\times 12} \\ \mathbf{0}_{6\times 12} & \mathbf{F}_{cc_{6\times 12}} & \mathbf{0}_{6\times 12} & \mathbf{0}_{6\times 12} & \mathbf{0}_{6\times 12} & \mathbf{0}_{6\times 12} & \mathbf{0}_{6\times 12} & \mathbf{0}_{6\times 12} \\ \mathbf{0}_{6\times 12} & \mathbf{0}_{6\times 12} & \mathbf{F}_{cc_{6\times 12}} & \mathbf{0}_{6\times 12} & \mathbf{0}_{6\times 12} & \mathbf{0}_{6\times 12} & \mathbf{0}_{6\times 12} & \mathbf{0}_{6\times 12} \\ \mathbf{0}_{6\times 12} & \mathbf{0}_{6\times 12} & \mathbf{0}_{6\times 12} & \mathbf{F}_{cc_{6\times 12}} & \mathbf{0}_{6\times 12} & \mathbf{0}_{6\times 12} & \mathbf{0}_{6\times 12} & \mathbf{0}_{6\times 12} \\ \mathbf{0}_{6\times 12} & \mathbf{0}_{6\times 12} & \mathbf{0}_{6\times 12} & \mathbf{0}_{6\times 12} & \mathbf{F}_{cc_{6\times 12}} & \mathbf{0}_{6\times 12} & \mathbf{0}_{6\times 12} & \mathbf{0}_{6\times 12} \\ \mathbf{0}_{6\times 12} & \mathbf{0}_{6\times 12} & \mathbf{0}_{6\times 12} & \mathbf{0}_{6\times 12} & \mathbf{0}_{6\times 12} & \mathbf{F}_{cc_{6\times 12}} & \mathbf{0}_{6\times 12} & \mathbf{0}_{6\times 12} \\ \mathbf{0}_{6\times 12} & \mathbf{0}_{6\times 12} & \mathbf{0}_{6\times 12} & \mathbf{0}_{6\times 12} & \mathbf{0}_{6\times 12} & \mathbf{0}_{6\times 12} & \mathbf{F}_{cc_{6\times 12}} & \mathbf{0}_{6\times 12} \\ \mathbf{0}_{6\times 12} & \mathbf{0}_{6\times 12} & \mathbf{0}_{6\times 12} & \mathbf{0}_{6\times 12} & \mathbf{0}_{6\times 12} & \mathbf{0}_{6\times 12} & \mathbf{0}_{6\times 12} & \mathbf{F}_{cc_{6\times 12}} \end{bmatrix} \tag{A.76}$$

The $\mathbf{F}_{D_{nn_{N_n \cdot n_{nu} \times N_n \cdot n_{ny}}}}$ has $N_n \times N_n = 1 \times 1$ blocks of dimension $n_{nu} \times n_{ny} = 3 \times 6$:

$$\begin{aligned} \mathbf{F}_{D_{nn_{N_n \cdot n_{nu} \times N_n \cdot n_{ny}}}} &= \left[\mathbf{f}_{D_{nn,\mu\nu_{n_{nu} \times n_{ny}}}} \right] \quad \mu = 0, \ldots, N_n - 1;\, \nu = 0, \ldots, N_n - 1 \\ &\Longleftrightarrow \\ \mathbf{F}_{D_{nn_{1 \cdot 3 \times 1 \cdot 6 = 3 \times 6}}} &= \left[\mathbf{f}_{D_{nn,\mu\nu_{3 \times 6}}} \right] \quad \mu = 0;\, \nu = 0 \end{aligned} \tag{A.77}$$

with the $\mu\nu$-th block computed via:

$$\begin{aligned} \mathbf{f}_{D_{nn,\mu\nu_{n_{cu} \times n_{cy}}}} &= \begin{cases} \mathbf{F}_{nn_{n_{nu} \times n_{ny}}} & \nu l_n \leq \mu l_n < (\nu + 1)\, l_n \\ \\ \mathbf{0}_{n_{nu} \times n_{cny}} & otherwise. \end{cases} \\ &\Longleftrightarrow \\ \mathbf{f}_{D_{nn,\mu\nu_{3 \times 6}}} &= \begin{cases} \mathbf{F}_{nn_{3 \times 6}} & 8\nu \leq 8\mu < 8\,(\nu + 1) \\ \\ \mathbf{0}_{3 \times 6} & otherwise. \end{cases} \end{aligned} \tag{A.78}$$

Hence:

$$\mathbf{F}_{D_{nn_{3 \times 6}}} = \mathbf{F}_{nn_{3 \times 6}} \tag{A.79}$$

A.2 Passive wave-based communication channel with constant time delay

Let $T_d^{ij} = k_d^{ij} T$ denote the communication delay from site i to site j (see Figure 4.1). By using Equation (4.3), the energy stored in the transmission channel up to time instant $\overline{k}$ is:

$$\begin{aligned} E_{ij}(\bar{k}T) &= T \sum\nolimits_{k=0}^{\bar{k}} P_{ij}(kT) \\ &= \frac{T}{2} \sum\nolimits_{k=0}^{\bar{k}} \Big(v_{ij}^2(kT) - u_{ij}^2(kT) + v_{ji}^2(kT) - u_{ji}^2(kT) \Big) \end{aligned} \tag{A.80}$$

Knowing the fact that $u_{ij}(kT) = v_{ji}(kT - T_d^{ji})$ and $u_{ji}(kT) = v_{ij}(kT - T_d^{ij})$, Equation (A.80) turns to:

$$\begin{aligned} E_{ij}(\bar{k}T) &= \frac{T}{2} \sum\nolimits_{k=0}^{\bar{k}} \Big(v_{ij}^2(kT) - v_{ji}^2(kT - T_d^{ji}) + v_{ji}^2(kT) - v_{ij}^2(kT - T_d^{ij}) \Big) \\ &= \frac{T}{2} \sum\nolimits_{k=\overline{k}-k_d^{ji}+1}^{\bar{k}} v_{ji}^2(kT) + \frac{T}{2} \sum\nolimits_{k=\overline{k}-k_d^{ij}+1}^{\bar{k}} v_{ij}^2(kT) \\ &\geq 0, \end{aligned} \tag{A.81}$$

which implies the passivity of the wave-based communication channel independent of the magnitude of constant time delay.

A.3

This section explains why Equation (4.43) holds. At port j of node i, the corresponding decoded force can be calculated using Equation (4.21):

$$f_{ij}(t) = \sqrt{\frac{b_w}{2}} \Big(u_{ij}(t) - v_{ij}(t) \Big), \tag{A.82}$$

From Equation (4.26), u_{ij} can be replaced as:

$$f_{ij}(t) = \sqrt{\frac{b_w}{2}}\Big(v_{ji}(t - T_d^{ji}) - v_{ij}(t)\Big), \tag{A.83}$$

Application of Laplace transformation onto the Equation (A.83) yields:

$$F_{ij}(s) = \sqrt{\frac{b_w}{2}}\left(e^{-sT_d^{ji}}V_{ji}(s) - V_{ij}(s)\right) \tag{A.84}$$

By taking the $\lim_{s\to 0}$ from Equation (A.84) we have:

$$\begin{aligned}\lim_{s\to 0}\ F_{ij}(s) &= \lim_{s\to 0}\ \sqrt{\frac{b_w}{2}}\left(\big(e^{-sT_d^{ji}}\big)V_{ji}(s) - V_{ij}(s)\right)\\ &= \lim_{s\to 0}\ \sqrt{\frac{b_w}{2}}\left(V_{ji}(s) - V_{ij}(s)\right)\end{aligned} \tag{A.85}$$

Similarly, at port i of node j, the decoded force is:

$$\begin{aligned}f_{ji}(t) &= \sqrt{\frac{b_w}{2}}\Big(u_{ji}(t) - v_{ji}(t)\Big)\\ &= \sqrt{\frac{b_w}{2}}\Big(v_{ij}(t - T_d^{ij}) - v_{ji}(t)\Big),\end{aligned} \tag{A.86}$$

In Laplace domain, Equation (A.86) gives:

$$F_{ji}(s) = \sqrt{\frac{b_w}{2}}\left(\big(e^{-sT_d^{ij}}\big)V_{ij}(s) - V_{ji}(s)\right) \tag{A.87}$$

Application of $\lim_{s\to 0}$ on both sides of Equation (A.88) yields:

$$\lim_{s\to 0}\ F_{ji}(s) = \lim_{s\to 0}\ \sqrt{\frac{b_w}{2}}\left(V_{ij}(s) - V_{ji}(s)\right) \tag{A.88}$$

Comparing Equations (A.85) and (A.88) yields to Equation (4.43).

A.4 Taylor's theorem

If function $\mathcal{H} : \mathbb{R}^n \to \mathbb{R}$ belongs to $\mathcal{C}^2$ in a region containing the line segment $[\mathbf{y}_1, \mathbf{y}_2]$ with $\mathbf{y}_1, \mathbf{y}_2 \in \mathbb{R}^n$, there is a θ, $0 \leq \theta \leq 1$ such that:

$$\begin{aligned} \mathcal{H}(\mathbf{y}_2) &= \mathcal{H}(\mathbf{y}_1) + \nabla\mathcal{H}(\mathbf{y}_1)(\mathbf{y}_2 - \mathbf{y}_1) \\ &+ \frac{1}{2}(\mathbf{y}_2 - \mathbf{y}_1)^\top \nabla^2\mathcal{H}(\theta\mathbf{y}_1 + (1-\theta)\mathbf{y}_2)(\mathbf{y}_2 - \mathbf{y}_1) \end{aligned} \tag{A.89}$$

in which $\nabla\mathcal{H}$ and $\nabla^2\mathcal{H}$ denote for gradient vector and Hessian matrix of $\mathcal{H}$ respectively.

A.5 Continiuous- and discrete-time port-Hamiltonian systems

Port-Hamiltonian formulation combines the port-based network modelling technique with the Hamiltonian framework, by employing the interconnection structure of the network model called *Dirac structure*. The Dirac structure represents a power preserving[1] relation between the internal power variables (corresponding to energy-storing elements), energy-dissipative elements and, external power port variables.

Let $\mathscr{F} \times \mathscr{F}^*$ be the space of *power variables*. For mechanical systems, power variables are conjugated pairs of velocities (flows) and forces (efforts). With $\mathscr{F}$ being the linear space of *flows* $\dot{x}$, and $\mathscr{F}^*$ being the dual space of *efforts* f, the *power* can then be defined with effort-flow pair as:

$$P = \langle f, \dot{x} \rangle, \quad (\dot{x}, f) \in \mathscr{F} \times \mathscr{F}^* \tag{A.90}$$

[1] In power-preserving interconnections, energy can only be transferred and not be produced nor be dissipated.

where $\langle f, \dot{x} \rangle$ denotes the duality product of pair $(\dot{x}, f) \in \mathscr{F} \times \mathscr{F}^*$.

Let $\mathtt{x}$ be the vector of energy variables on a space $\mathcal{X} := \mathbb{R}$ associated to the energy-storing elements in the system, and function $\mathtt{H} : \mathcal{X} \to \mathbb{R}$ (Hamiltonian) represents the total energy stored in the system. A port-Hamiltonian system interacts with other systems by exchanging energy via the power ports defined on the vector spaces $\mathscr{F}$ and $\mathscr{F}^*$. For instance in mechanical systems, power variables are conjugated pairs of velocities (flows) and forces (efforts). Table A.1 provides a list of power-conjugate variables for different physical domains.

Systems	Flow	Effort
Electrical	Current	Voltage
Translational mechanical	Velocity	Force
Rotational mechanical	Angular velocity	Torque

Table A.1: Power conjugate variables for different physical system.

The following terms are required to model a physical system as a port-Hamiltonian system:

- A state space $\mathcal{X}$;
- The space of flow variables, $\mathscr{F}$, and its dual space of effort variables, $\mathscr{F}^*$;
- The Dirac structure $\mathcal{D}$ which is the internal power-preserving interconnection of different components of the system. Dirac structure defines how the energy flows in between the various elements of the system;
- The Hamiltonian (energy) function $\mathtt{H}$ that corresponds to the total energy stored in the system.

Power-conserving interconnections of port-Hamiltonian systems can be studied in terms of the composition of the Dirac structures of various parts of the system. For

mechanical systems, the space of flow variables for the Dirac structure $\mathcal{D}$ can be split into $\mathcal{X} \times \mathscr{F}$:

- $\dot{x}_{\mathcal{X}} \in \mathcal{X}$, comprising the flows corresponding to the energy-storing elements in the system (i.e, mass in this thesis);
- $\dot{x}_{\mathcal{F}} \in \mathscr{F}$, including the flows of the dissipative elements $\dot{x}_{ds}$, plus the flows $\dot{x}_{ext}$ corresponding to the external ports of the system.

Dually, the space of effort variables of the Dirac structure is split into $\mathcal{X}^* \times \mathscr{F}^*$:

- $f_{\mathcal{X}} \in \mathcal{X}^*$, comprising the efforts corresponding to the energy-storing elements in the system;
- $f_{\mathcal{F}} \in \mathscr{F}^*$, including the effort of the dissipative elements f_{ds}, plus the effort f_{ext} corresponding to the external ports of the system.

From [94], one can show that the Dirac structure $\mathcal{D}$ possesses the *power-preserving* property, that it:

$$\langle \dot{x}_{\mathcal{X}}, f_{\mathcal{X}} \rangle + \langle \dot{x}_{ds}, f_{ds} \rangle + \langle \dot{x}_{ext}, f_{ext} \rangle = 0 \tag{A.91}$$

Equation (A.91) can be written in the form of the following power balance:

$$\begin{aligned} \dot{\mathtt{H}} &= \langle \frac{\partial \mathtt{H}}{\partial \mathtt{x}}, \dot{\mathtt{x}} \rangle \\ &= -\langle f_{\mathcal{X}}, \dot{x}_{\mathcal{X}} \rangle = \langle f_{ext}, \dot{x}_{ext} \rangle + \langle f_{ds}, \dot{x}_{ds} \rangle. \end{aligned} \tag{A.92}$$

in which, in order to have a consistent power flow direction, a minus sign is included. Since the dissipative elements supply negative power to the system, i.e.:

$$\langle f_{ds}, \dot{x}_{ds} \rangle \leq 0. \tag{A.93}$$

Substitution of Equation (A.93) into Equation (A.92) gives:

$$\dot{\mathtt{H}} = \langle \dot{x}_{ext}, f_{ext} \rangle + \langle \dot{x}_{ds}, f_{ds} \rangle \leq \langle \dot{x}_{ext}, f_{ext} \rangle. \tag{A.94}$$

Equation (A.94) implies the *passivity* of the port-Hamiltonian system, namely, the externally supplied power into the port-Hamiltonian system is either stored or dissipated. Generic demonstration and a deep discussion of port-Hamiltonian systems and their passivity properties can be found in [100].

A.5.1 Explicit port-Hamiltonian formulation

In analogy to state-space representation, an input-state-output port-Hamiltonian system can be described by:

$$\begin{aligned} \dot{\mathtt{x}} &= \left(J(\mathtt{x}) - R(\mathtt{x}) \right) \frac{\partial \mathtt{H}}{\partial \mathtt{x}} + g(\mathtt{x})\mathtt{u} \\ \mathtt{y} &= g^{\top}(\mathtt{x}) \frac{\partial \mathtt{H}}{\partial \mathtt{x}}, \end{aligned} \tag{A.95}$$

that satisfies:

$$\dot{\mathtt{H}} = -\frac{\partial^{\top} \mathtt{H}}{\partial \mathtt{x}} R(\mathtt{x}) \frac{\partial \mathtt{H}}{\partial \mathtt{x}} + \mathtt{y}^{\top} \mathtt{x}, \tag{A.96}$$

where $\mathtt{x} \in \mathcal{X}$ is the vector of energy variables corresponding to the energy-storing elements of the system; the flow and effort variables are split into power-conjugate input-output pairs $(\mathtt{u}, \mathtt{y})$; $R(\mathtt{x}) = R^{\top}(\mathtt{x}) \geq 0$ is the dissipation matrix; $J(\mathtt{x}) = -J^{\top}(\mathtt{x})$ is the internal power-preserving interconnection matrix; and $g(\mathtt{x})$ represents the input-output matrix.

Example A.1. (*Mass-spring-damper*)
The mass-spring-damper shown in Fig. A.1 can be formulated in port-Hamiltonian form in continuous-time as:

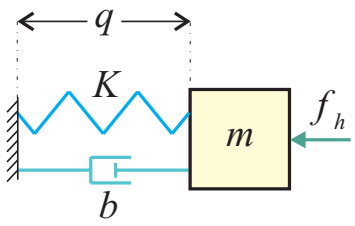

Figure A.1: The mass-spring-damper system.

$$\begin{aligned} \dot{\mathtt{x}}(t) = \begin{pmatrix} \dot{q}(t) \\ \dot{p}(t) \end{pmatrix} &= \left(\begin{bmatrix} 0 & 1 \\ -1 & 0 \end{bmatrix} - \begin{bmatrix} 0 & 0 \\ 0 & b \end{bmatrix} \right) \begin{pmatrix} Kq(t) \\ \frac{P(t)}{m} \end{pmatrix} + \begin{bmatrix} 0 \\ 1 \end{bmatrix} f_h(t), \\ y(t) &= \begin{bmatrix} 0 \\ 1 \end{bmatrix}^\top \begin{pmatrix} Kq(t) \\ \frac{P(t)}{m} \end{pmatrix} \end{aligned} \tag{A.97}$$

for which the energy function is described as:

$$\mathtt{H}(\mathtt{x}) = \mathtt{H}\Big(q(t), p(t)\Big) = \frac{1}{2} K q(t)^2 + \frac{P(t)^2}{2m} \tag{A.98}$$

where p and q are the momentum of the mass and the spring elongation respectively; K is the spring stiffness; m is the mass; b presents the local damping; and f_h is the external force applied onto the mass.

A.5.2 Discrete-time port-Hamiltonian formalism

Real-time simulation is crucial for haptic applications. Virtual environments implemented in digital computers demand discrete-time integration algorithms that should satisfy two main characteristics for real-time applications: (i) *fixed execution time* and; (ii) *explicit nature*. Forward Euler integration technique endows these requirements however, it does not preserve the passivity properties when applied onto the continuous-time systems. In fact, discretizatoin of continuous-time integrators $1/s$ characterizes non-passive behaviour in discrete-time descreibed in $\mathtt{z}$-transform do-

main, that is, $\frac{T}{z-1}$. A numerical algorithm is however introduced in [13, 94] which modifies the discrete-time states such that the discretized port-Hamiltonian system resembles the energetic evolution of its continuous-time counterpart and thus, preserving the passivity properties.

In Appendices A.6 and A.7, mass and spring as two fundamental elements for modelling of any mechanical systems are formulated in port-Hamiltonian framework in discrete-time and their passivity is discussed in details.

A.6 Discrete-time port-Hamiltonian spring

Let $\mathcal{D}_s$ be the Dirac structure of a spring as shown in Figure A.2. Let $q(t) = q_1(t) -$

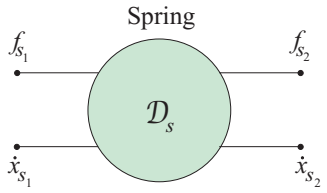

Figure A.2: The Dirac structure of a spring. f_{s_i} and $\dot{x}_{s_i}$ are the effort and flow variables at port $i = 1, 2$ respectively.

$q_2(t)$ denote the spring elongation with $q_i(t)$ being the displacement at end-side i of the spring at time instant t. The potential energy stored in the spring is:

$$\mathtt{H}_s(t) = \frac{1}{2} K q(t)^2 \tag{A.99}$$

with K being the spring stiffness. The continuous-time port-Hamiltonian formulation of the spring is:

$$\begin{aligned} \dot{q}(t) &= \Big([0] - [0]\Big) Kq(t) + \begin{bmatrix} 1 & -1 \end{bmatrix} \begin{pmatrix} \dot{x}_{s_1}(t) \\ \dot{x}_{s_2}(t) \end{pmatrix} \\ \mathbf{y}(t) &= \begin{pmatrix} f_{s_1}(t) \\ f_{s_2}(t) \end{pmatrix} = \begin{bmatrix} 1 \\ -1 \end{bmatrix} Kq(t). \end{aligned} \tag{A.100}$$

Equation (A.100) can be discretized with sampling time T as:

$$\begin{aligned} \frac{\Delta q(k)}{T} &= \Big([0] - [0]\Big) Kq(k) + \begin{bmatrix} 1 & -1 \end{bmatrix} \begin{pmatrix} \dot{x}_{s_1}(k) \\ \dot{x}_{s_2}(k) \end{pmatrix} \\ y &= \begin{pmatrix} Kq(k) \\ -Kq(k) \end{pmatrix}. \end{aligned} \tag{A.101}$$

The state evolution of the spring can be computed using forward Euler integration:

$$q(k+1) = q(k) + \Delta q(k), \tag{A.102}$$

for which, $\Delta q(k)$ can be substituted from Equation (A.101). Let $H_s(k)$ denote the energy of the spring in discrete-time and $\Delta H_s(k)$ be the variation of energy of the spring during the time interval $[kT, (k+1)T]$. Using Taylor's Theorem (Appendix

A.4), one can show:

$$\begin{aligned}\Delta H_s(k) &= H_s(k+1) - H_s(k) = \frac{1}{2}Kq^2(k+1) - \frac{1}{2}Kq^2(k) \\ &= \nabla\Big(\frac{K}{2}q^2(k)\Big)\big(q(k+1) - q(k)\big) + \frac{1}{2}\nabla^2\Big(\frac{K}{2}q^2(k)\Big)\big(q(k+1) - q(k)\big)^2 \\ &= Kq(k)\Delta q(k) + \frac{K}{2}\Delta q(k)^2\end{aligned} \tag{A.103}$$

Substitution of $\Delta q(k)$ from Equation (A.101) into Equation (A.103) gives:

$$\Delta H_s(k) \;\; = \;\; Kq(k)\big(f_{s_1}(k) - f_{s_2}(k)\big)T + \frac{KT^2}{2}\big(f_{s_1}(k) - f_{s_2}(k)\big)^2. \tag{A.104}$$

The last term in Equation (A.104) is the energy injected into the spring by the forward Euler integration at each simulation step. The state update algorithm [13,97], can be used to make the variation of energy of the discrete-time spring equal to the variation of energy of the continuous-time spring, i. e., to make the discrete-time spring passive. Let $\tilde{q}(k+1)$ be the state updated using [13,97] and substitute it in Equation (A.103). Thus, the variation of energy in Equation (A.104) becomes:

$$\begin{aligned}\Delta\tilde{H}_s(k) &= \frac{1}{2}K\tilde{q}^2(k+1) - \frac{1}{2}K\tilde{q}^2(k) \\ &= K\tilde{q}(k)\big(f_{s_1}(k) - f_{s_2}(k)\big)T\end{aligned} \tag{A.105}$$

For two-port passivity of the discrete-time spring we need to show:

$$\sum_{k=0}^{\bar{k}}\Big(f_{s_1}(k)\dot{x}_{s_1}(k) + f_{s_2}(k)\dot{x}_{s_2}(k)\Big)\,T \geq -E(0) \tag{A.106}$$

where $E(0)$ is the initial energy stored into the system. Thus, by summing up the terms in Equation (A.105) over time up to $\bar{k} \in \mathbb{Z}^+$, the discrete-time passivity condi-

tion of the spring is satisfied as:

$$\begin{aligned}\sum_{k=0}^{\bar{k}} K\tilde{q}(k)\big(\dot{x}_{s_1}(k)-\dot{x}_{s_2}(k)\big)T &= \sum_{k=0}^{\bar{k}}\Big(\frac{1}{2}K\tilde{q}^2(k+1)-\frac{1}{2}K\tilde{q}^2(k)\Big)\\ &\geq -\frac{1}{2}K\tilde{q}^2(0)\end{aligned} \tag{A.107}$$

where $-\frac{1}{2}K\tilde{q}^2(0)$ is the initial energy stored in the spring. The spring effort variables are $f_{s_1}(k) = K\big(\bar{q}_1(k)-\bar{q}_2(k)\big)$ and $f_{s_2}(k) = K\big(\tilde{q}_2(k)-\tilde{q}_1(k)\big)$ at ports 1 and 2 respectively. Thus Equation (A.107) can be written as:

$$\sum_{k=0}^{\bar{k}}\Big(\dot{x}_{s_1}(k)f_{s_1}(k)+\dot{x}_{s_2}(k)f_{s_2}(k)\Big)T \;\geq\; -\frac{1}{2}K\tilde{q}^2(0), \tag{A.108}$$

which proves the passivity of the discrete-time spring shown in Figure A.2.

A.7 Discrete-time port-Hamiltonian mass

Let $\mathcal{D}_m$ represent the Dirac structure of a mass as shown in Figure A.3. Consider

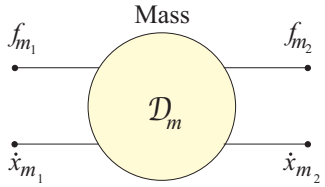

Figure A.3: The Dirac structure of a mass. $\dot{x}_{m_i}$ and f_{m_i} are the flow and effort variables at port $i = 1, 2$ respectively.

$p(t)$ be the momentum of the mass m. The kinetic energy function of the mass is:

$$\mathtt{H}_m(t) = \frac{p^2(t)}{2m} \tag{A.109}$$

Following the Equation (A.96), the system shown in Fig. A.3 can be presented in continuous-time port-Hamiltonian formulation as:

$$\begin{aligned} \dot{p}(t) &= \Big([0] - [b]\Big)\frac{p(t)}{m} + \begin{bmatrix} 1 & 1 \end{bmatrix} \begin{pmatrix} f_{m_1}(t) \\ f_{m_2}(t) \end{pmatrix} \\ y(t) &= \begin{pmatrix} \dot{x}_{m_1}(t) \\ \dot{x}_{m_2}(t) \end{pmatrix} = \begin{bmatrix} \frac{p(t)}{m} \\ \frac{p(t)}{m} \end{bmatrix} \end{aligned} \tag{A.110}$$

in which, $\dot{x}_{m_i}$ and f_{m_i} are the flow and effort variables at port $i = 1, 2$ respectively; $p(t)$ is the momentum of the mass m; and b is the local damping connected to the mass. Assuming $b = 0$, Equation (A.110) can the be discretized with sampling time T as:

$$\begin{aligned} \frac{\Delta p(k)}{T} &= \Big([0] - [0]\Big)\frac{p(k)}{m} + \begin{bmatrix} 1 & 1 \end{bmatrix} \begin{pmatrix} f_{m_1}(k) \\ f_{m_2}(k) \end{pmatrix} \\ y(k) &= \begin{pmatrix} \frac{p}{m}(k) \\ \frac{p}{m}(k) \end{pmatrix}. \end{aligned} \tag{A.111}$$

Similar to the previous section, the forward Euler integration technique is employed to compute the state evolution as:

$$p(k+1) = p(k) + \Delta p(k) \tag{A.112}$$

in which, $\Delta p(k)$ can be substituted from Equation (A.111). Let $\Delta H_m(k)$ be the variation of energy of the mass in discrete-time during the time interval $[kT, (k+1)T]$. Then,

$$\Delta H_m(k) = \frac{p^2(k+1)}{2m} - \frac{p^2(k)}{2m}. \tag{A.113}$$

Substituting Equation (A.112) into Equation (A.113) gives:

$$\Delta H_m(k) = \frac{p(k)}{m}\Big(f_{m_1}(k) + f_{m_2}(k)\Big)T + \frac{T^2}{2m}\Big(f_{m_1}(k) + f_{m_2}(k)\Big)^2 \tag{A.114}$$

where, the last term is the extra energy injected into the system due to the forward Euler integration. State update algorithm [13, 97] is then employed and the new updated state $\tilde{p}(k+1)$ is substituted in Equation (A.113). Thus, the variation of energy in Equation (A.114) becomes:

$$\begin{aligned} \Delta \tilde{H}_m(k) &= \frac{\tilde{p}^2(k+1)}{2m} - \frac{\tilde{p}^2(k)}{2m} \\ &= \frac{\tilde{p}(k)}{m}\Big(f_{m_1}(k) + f_{m_2}(k)\Big)T. \end{aligned} \tag{A.115}$$

By taking the summation over time from Equation (A.115), the discrete-time passivity condition of the mass is satisfied as:

$$\begin{aligned} \sum_{k=0}^{\bar{t}} \Big(\dot{x}_{m_1}(k) f_{m_1}(k) + \dot{x}_{m_2}(k) f_{m_2}(k)\Big)T &= \sum_{k=0}^{\bar{t}} \frac{\tilde{p}(k)}{m}\Big(f_{m_1}(k) + f_{m_2}(k)\Big)T \\ &= \sum_{k=0}^{\bar{t}} \frac{\tilde{p}^2(k+1)}{2m} - \frac{\tilde{p}^2(k)}{2m}\Big) \\ &\geq -\frac{\tilde{p}^2(0)}{2m} \end{aligned} \tag{A.116}$$

where $-\frac{\tilde{p}^2(0)}{2m}$ is the initial kinetic energy of the mass. Equation (A.116) does prove the passivity of the discrete-time mass shown in Fig. A.3.

A.8 Variation of the mass as a passive action

This section verifies that the variation of a mass value does not violate the passivity if simulated via the numerical algorithm introduced [94]. Let the value of mass $\underline{m}$

change to $\bar{m}$ at time instant $\underline{k}$. Therefore, for the energy flow entering the mass system we have:

$$\begin{aligned} T\sum_{k=0}^{\underline{k}} f_h(k)\dot{x}(k) &= \frac{1}{2}\underline{m}\dot{x}(\underline{k})^2 - \frac{1}{2}\underline{m}\dot{x}(0)^2 \\ T\sum_{k=\underline{k}+1}^{\bar{k}} f_h(k)\dot{x}(k) &= \frac{1}{2}\bar{m}\dot{x}(\bar{k})^2 - \frac{1}{2}\bar{m}\dot{x}(\underline{k}+1)^2 \end{aligned} \tag{A.117}$$

where $\bar{k}$ is the final simulation time, f_h is the external force; and $\dot{x}$ is the velocity. Therefore, summing up the terms on both sides of Equation (A.119) gives:

$$\begin{aligned} T\sum_{k=0}^{\underline{k}} f_h(k)\dot{x}(k) + T\sum_{k=\underline{k}+1}^{\bar{k}} f_h(k)\dot{x}(k) = \frac{1}{2}\underline{m}\dot{x}(\underline{k})^2 - \frac{1}{2}\underline{m}\dot{x}(0)^2 \\ + \frac{1}{2}\bar{m}\dot{x}(\bar{k})^2 - \frac{1}{2}\bar{m}\dot{x}(\underline{k}+1)^2 \end{aligned} \tag{A.118}$$

which can be further simplified to:

$$T\sum_{k=0}^{\bar{k}} f_h(k)\dot{x}(k) \geq -\frac{1}{2}\underline{m}\dot{x}(0)^2 - \frac{1}{2}\bar{m}\dot{x}(\underline{k}+1)^2. \tag{A.119}$$

The above equation implies that variation in the value of the mass is a passive action and does not violate the passivity of the discrete-time simulation.

A.9 Technical Specifications for Novint Falcon haptic interfaces

In [101], the damping (mainly by friction) and inertia (apparent mass) of the Falcon devices is identified via performing a frequency domain system identification. Other specifications of this device is given in Table A.2.

Workspace	$10 \times 10 \times 10$ cm
Force Capabilities	> 2 lbs
Position Resolution	> 400 dpi
Communication Interface	USB 2.0
Size	$23 \times 23 \times 23$ cm
Weight	6 lbs
Power 30 watts	$100 - 240$ V, $50 - 60$ Hz

Table A.2: Technical specifications for Novint Falcon haptic device.

Bibliography

[1] R.J. Adams and B. Hannaford. Stable haptic interaction with virtual environments. *IEEE Transactions on Robotics and Automation*, 15(3):465–474, jun. 1999.

[2] M. Alhalabi and S. Horiguchi. Tele-handshake: A cooperative shared haptic virtual environment. In *Eurographics*, pages 60–64, Birmingham, UK, 2001.

[3] M. Alhalabi, S. Horiguchi, and S. Kunifuji. An experimental study on the effects of network delay in cooperative shared haptic virtual environment. *Computers and Graphics*, 27(2):205–213, 2003.

[4] R. S. Allison, J. E. Zacher, D. Wang, and J. Shu. Effects of network delay on a collaborative motor task with telehaptic and televisual feedback. In *ACM SIGGRAPH International Conference on Virtual Reality Continuum and its Applications in Industry*, pages 375–381, Singapore, 2004.

[5] R. J. Anderson and M. W. Spong. Bilateral control of teleoperators with time delay. *IEEE Transactions on Automatic Control*, 34(5):494–501, 1989.

[6] Robert J. Anderson and Mark W. Spong. Asymptotic stability for force reflecting teleoperators with time delay. *The International Journal of Robotics Research*, 11(2):135–149, 1992.

[7] R.J. Ansari, M. Zareinejad, S.M. Rezaei, K. Baghestan, and N. Sarli. Stable multi-user interaction with cooperative haptic virtual environments by a modification of passive set-position modulation. *IET Control Theory Applications*, 6(16):2538–2548, 2012.

[8] M. Araki and K. Yamamoto. Multivariable multirate sampled-data systems: state-space description, transfer characteristics, and nyquist criterion. *IEEE Transactions on Automatic Control*, 31(2):145–154, 1986.

[9] M. Arbabtafti, M. Moghaddam, A. Nahvi, M. Mahvash, B. Richardson, and B. Shirinzadeh. Physics-based haptic simulation of bone machining. *IEEE Transactions on Haptics*, 4(1):39–50, 2011.

[10] M. Arcak. Passivity as a design tool for group coordination. *IEEE Transactions on Automatic Control*, 52(8):1380 –1390, Aug. 2007.

[11] J. Artigas, C. Preusche, G. Hirzinger, G. Borghesan, and C. Melchiorri. Bilateral energy transfer in delayed teleoperation on the time domain. In *IEEE International Conference on Robotics and Automation (ICRA)*, pages 671–676, May 2008.

[12] G. Bianchini, M. Orlandesi, and D. Prattichizzo. Passivity-based analysis and design of multi-contact haptic systems via lmis. In M. Hosseini Zadeh, editor, *Advances in Haptics*, pages 155–170. InTech, 2010.

[13] G. Borghesan, A. Macchelli, and C. Melchiorri. Interconnection and simulation issues in haptics. *IEEE Transactions on Haptics*, 3(4):266–279, 2010.

[14] J. M. Brown and J. E. Colgate. Minimum mass for haptic display simulations. In *ASME Dynamic Systems and Control Conference*, pages 249–256, Anaheim, CA, 1998.

[15] P. Buttolo, R. Oboe, and B. Hannaford. Architectures for shared haptic virtual environments. *Computers and Graphics*, 21(4):421–429, 1997.

[16] Y. Cao, W. Yu, W. Ren, and Ch. Chen. An overview of recent progress in the study of distributed multi-agent coordination. *IEEE Transactions on Industrial Informatics*, 9(1):427–438, Feb 2013.

[17] J. Cheong, S. I. Niculescu, A. Annaswamy, and M. A. Srinivasan. Motion synchronization in virtual environments with shared haptics and large time delays. In *World Haptics Conference*, pages 277–282, Pisa, Italy, 2005.

[18] H. Ching and W. J. Book. Internet-based bilateral teleoperation based on wave variable with adaptive predictor and direct drift control. *Journal of Dynamic Systems, Measurement, and Control*, 128(1):86–93, 2006.

[19] N. Chopra, P. Berestesky, and M.W. Spong. Bilateral teleoperation over unreliable communication networks. *IEEE Transactions on Control Systems Technology*, 16(2):304 –313, mar. 2008.

[20] N. Chopra and M. W. Spong. *Passivity-Based Control of Multi-Agent Systems*. Springer Berlin Heidelberg, 2006.

[21] N. Chopra and M. W. Spong. Adaptive synchronization of bilateral teleoperators with time delay. In Manuel Ferre, Martin Buss, Rafael Aracil, Claudio Melchiorri, and Carlos Balaguer, editors, *Advances in Telerobotics*, volume 31 of *Springer Tracts in Advanced Robotics*, pages 257–270. Springer Berlin Heidelberg, 2007.

[22] N. Chopra, M.W. Spong, R. Ortega, and N.E. Barabanov. On position tracking in bilateral teleoperation. In *Proceedings of the American Control Conference (ACC)*, volume 6, pages 5244 – 5249 vol.6, jun. 2004.

[23] J. E. Colgate and J. M. Brown. Factors affecting the z-width of a haptic display. In *IEEE International Conference on Robotics and Automation*, pages 3205–3210, San Diego, CA, 1994.

[24] J. E. Colgate and G. Schenkel. Passivity of a class of sampled-data systems: application to haptic interfaces. *Journal of Robotic Systems*, 14(1):37–47, 1997.

[25] B. Daunay, A. Abbaci, A. Micaelli, and S. Regnier. The wave variables, a solution for stable haptic feedback in molecular docking simulations. In Tarek Sobh, Khaled Elleithy, Ausif Mahmood, and Mohammed Karim, editors, *Innovative Algorithms and Techniques in Automation, Industrial Electronics and Telecommunications*, pages 67–73. Springer Netherlands, 2007.

[26] N. Diolaiti, G. Niemeyer, and N. A. Tanner. Wave haptics: Building stiff controllers from the natural motor dynamics. *The International Journal of Robotics Research*, 26(1):5–21, 2007.

[27] P. Fong. Sensing, acquisition, and interactive playback of data-based models for elastic deformable objects. *The International Journal of Robotics Research*, 28(5):630–655, 2009.

[28] M. Fotoohi, S. Sirouspour, and D. Capson. Stability and performance analysis of centralized and distributed multi-rate control architectures for multi-user haptic interaction. *International Journal of Robotics Research*, 26(9):977–994, 2007.

[29] A. Franchi, C. Secchi, Hyoung Il Son, H.H. Bulthoff, and P.R. Giordano. Bilateral teleoperation of groups of mobile robots with time-varying topology. *IEEE Transactions on Robotics*, 28(5):1019–1033, Oct 2012.

[30] M. Franken, S. Stramigioli, S. Misra, C. Secchi, and A. Macchelli. Bilateral telemanipulation with time delays: A two-layer approach combining passivity and transparency. *IEEE Transactions on Robotics*, 27(4):741–756, Aug 2011.

[31] A. Haddadi and K. Hashtrudi-Zaad. Delay-robust transparent bilateral teleoperation control design. In *IEEE/RSJ International Conference on Intelligent Robots and Systems, IROS*, pages 438–444, sep. 2008.

[32] A. Haddadi and K. Hashtrudi-Zaad. A new robust stability analysis and design tool for bilateral teleoperation control systems. In *IEEE International Conference on Robotics and Automation, ICRA*, pages 663–670, may. 2008.

[33] B. Hannaford and J. H. Ryu. Time-domain passivity control of haptic interfaces. *IEEE Transactions on Robotics and Automation*, 18(1):1 –10, feb. 2002.

[34] K. Hashtrudi-Zaad and S.E. Salcudean. Adaptive transparent impedance reflecting teleoperation. In *International Conference on Robotics and Automation, ICRA*, volume 2, pages 1369–1374 vol.2, Apr 1996.

[35] S. Haykin. *Active Network Theory*. Addison-Wesley, 1970.

[36] K. Hikichi, H. Morino, I. Arimoto, K. Sezaki, and Y. Yasuda. Evaluation of delay jitter for haptics collaboration over the internet. In *IEEE Global Telecommunications Conference*, pages 1492–1496, San Francisco, CA, 2002.

[37] S. Hirche and M. Buss. Packet-loss effects in passive telepresence systems. In *43rd IEEE Conference on Decision and Control*, pages 4010–4015, Paradise Islands, Bahamas, 2004.

[38] N. Hogan. Impedance control: An approach to manipulation: Parts i-iii. *Journal of Dynamic Systems, Measurement, and Control*, 107(1):1–24, 1985.

[39] K. Huang and D. Lee. Consensus-based peer-to-peer control architecture for multiuser haptic interaction over the internet. *IEEE Transactions on Robotics*, 29(2):417–431, 2013.

[40] M. Ishii, M. Nakata, and M. Sato. Networked spidar: A networked virtual environment with visual, auditory, and haptic interactions. *Presence*, 3(4):351–359, jul. 1994.

[41] P. Jacobs, M. J. Fu, and M. C. Cavusoglu. High fidelity haptic rendering of frictional contact with deformable objects in virtual environments using multi-rate simulation. *The International Journal of Robotics Research*, 29(14):1778–1792, 2010.

[42] C. Jay, M. Glencross, and R. Hubbold. Modeling the effects of delayed haptic and visual feedback in a collaborative virtual environment. *ACM Transactions on Computer-Human Interaction*, 14(2):8, 2007.

[43] K. Jeffay, T. Hudson, and M. Parris. Beyond audio and video: Multimedia networking support for distributed, immersive virtual environments. In *27th Euromicro Conference*, pages 300–307, Warsaw, Poland, 2001.

[44] T. Kanno and Y. Yokokohji. Multilateral teleoperation control over time-delayed computer networks using wave variables. In *Haptics Symposium (Haptics), IEEE*, pages 125–131, 2012.

[45] H. Kawada and T. Namerikawa. Bilateral control of nonlinear teleoperation with time varying communication delays. In *American Control Conference*, pages 189–194, Seattle, WA, 2008.

[46] B. Khademian and K. Hashtrudi-Zaad. Shared control architectures for haptic training: Performance and coupled stability analysis. *The International Journal of Robotics Research*, 30(13):1627–1642, 2011.

[47] B. Khademian and K. Hashtrudi-Zaad. Dual-user teleoperation systems: New multilateral shared control architecture and kinesthetic performance measures. *IEEE/ASME Transactions on Mechatronics*, 17(5):895–906, Oct 2012.

[48] J. Kim, H. Kim, B. K. Tay, M. Muniyandi, M. A. Srinivasan, J. Jordan, J. Mortensen, M. Oliveira, and M. Slater. Transatlantic touch: A study of haptic collaboration over long distance. *Presence: Teleoperators and Virtual Environments*, 13(3):328–337, 2004.

[49] J. P. Kim and J. Ryu. Robustly stable haptic interaction control using an energy-bounding algorithm. *The International Journal of Robotics Research*, 29(6):666–679, 2010.

[50] Y Kim, M Otaduy, M Lin, and D Manocha. Six-degree-of-freedom haptic rendering using incremental and localized computations. *Presence*, 12(3):277–295, June 2003.

[51] Y-B. Kim, S-H. Han, S-J. Kim, E. Kim, and C-G. Song. Multi-player virtual ping-pong game. In *17th International Conference on Artificial Reality and Telexistence*, pages 269 –273, Nov. 2007.

[52] N. Kottenstette, Joseph F. Hall, III, X. Koutsoukos, Panos Antsaklis, and J. Sztipanovits. Digital control of multiple discrete passive plants over networks. *International Journal of Systems, Control and Communications*, 3(2):194–228, April 2011.

[53] D.A. Lawrence. Stability and transparency in bilateral teleoperation. *IEEE Transactions on Robotics and Automation*, 9(5):624–637, 1993.

[54] H. LeBlanc, E. Eyisi, N. Kottenstette, X. Koutsoukos, and J. Sztipanovits. *A Passivity-Based Approach to Group Coordination in Multi-Agent Networks*, volume 89 of *Lecture Notes in Electrical Engineering*, pages 135–149. Springer, 1 edition, 2011.

[55] D.J. Lee and K. Huang. On passive non-iterative variable-step numerical integration of mechanical systems for haptic rendering. In *ASME Dynamic Systems and Control Conference*, pages 1147–1154, 2008.

[56] D.J. Lee and K. Huang. Passive-set-position-modulation framework for interactive robotic systems. *IEEE Transactions on Robotics*, 26(2):354–369, 2010.

[57] J-H. Lee, C-H Cho, M. Kim, and J-B Song. Haptic interface through wave transformation using delayed reflection: application to a passive haptic device. *Advanced Robotics*, 20(3):305–322, 2006.

[58] Z. Li and D. Constantinescu. Comparison of power- and wave-based control of remote dynamic proxies for networked haptic cooperation. In *International Conference on Mechatronics and Automation, ICMA*, pages 66–71, Aug 2009.

[59] Z. Li and D. Constantinescu. Networked haptic cooperation using remote dynamic proxies. In *Second International Conferences on Advances in Computer-Human Interactions, ACHI*, pages 243–248, Feb 2009.

[60] Z. Li and D. Constantinescu. Remote dynamic proxies for wave-based peer-to-peer haptic interaction. In *Third Joint Symposium on Haptic Interfaces for Virtual Environment and Teleoperator Systems, World Haptics*, pages 553–558, March 2009.

[61] P. Lin and Y. Jia. Consensus of second-order discrete-time multi-agent systems with nonuniform time-delays and dynamically changing topologies. *Automatica*, 45(9):2154 – 2158, 2009.

[62] L.J. Love and W.J. Book. Force reflecting teleoperation with adaptive impedance control. *IEEE Transactions on Systems, Man, and Cybernetics, Part B: Cybernetics*, 34(1):159–165, Feb 2004.

[63] M. Mahvash and V. Hayward. High-fidelity passive force-reflecting virtual environments. *IEEE Transactions on Robotics*, 21(1):38–46, Feb 2005.

[64] A. Marshall, M. K. Yap, and W. Yu. Providing qos for networked peers in distributed haptic virtual environments. *Advances in Multimedia*, 2008, 2008.

[65] S. Matsumoto, I. Fukuda, H. Morino, K. Hikichi, K. Sezaki, and Y. Yasuda. Influences of network issues on haptic collaboration in shared virtual environments. In *5th Phantom Users' Group Workshop*, pages 22–24, Aspen, Colo, 2000.

[66] V. Mendez, M. Tavakoli, and J. Li. A method for passivity analysis of multilateral haptic systems. *Advanced Robotics*, 28(18):1205–1219, 2014.

[67] B.E. Miller, J.E. Colgate, and R.A. Freeman. Guaranteed stability of haptic systems with nonlinear virtual environments. *IEEE Transactions on Robotics and Automation*, 16(6):712–719, Dec 2000.

[68] B.E. Miller, J.E. Colgate, and R.A. Freeman. On the role of dissipation in haptic systems. *IEEE Transactions on Robotics*, 20(4):768 – 771, aug. 2004.

[69] E. M. Navarro-Lpez. Several dissipativity and passivity implications in the linear discrete-time setting. *Mathematical Problems in Engineering*, 2005(6):599–616, 2005.

[70] S. Niakosari and S. Sirouspour. Improving transparency in network-based haptics. In *The Third Joint EuroHaptics Conference and Symposium on Haptic Interfaces for Virtual Environment and Teleoperator Systems*, pages 547 –552, Salt Lake City, USA, 2009.

[71] S. Niakosari and S. Sirouspour. An iterative approach to optimizing multi-user networked haptic simulations. In *Haptics Symposium, IEEE*, pages 167–174, Waltham, MA, 2010.

[72] G. Niemeyer and J.-J. E. Slotine. Stable adaptive teleoperation. *IEEE Journal of Oceanic Engineering*, 16(1):152–162, 1991.

[73] G. Niemeyer and J.-J. E. Slotine. Telemanipulation with time delays. *The International Journal of Robotics Research*, 23(9):873–890, 2004.

[74] S.S. Nudehi, R. Mukherjee, and M. Ghodoussi. A shared-control approach to haptic interface design for minimally invasive telesurgical training. *IEEE Transactions on Control Systems Technology*, 13(4):588–592, July 2005.

[75] E. Nuno, R. Ortega, N. Barabanov, and L. Basanez. A globally stable pd controller for bilateral teleoperators. *IEEE Transactions on Robotics*, 24(3):753 –758, jun. 2008.

[76] J. H. Park and H. C. Cho. Sliding-mode controller for bilateral teleoperation with varying time delay. In *International Conference on Advanced Intelligent Mechatronics*, pages 311–316, 1999.

[77] K.S. Park and R.V. Kenyon. Effects of network characteristics on human performance in a collaborative virtual environment. In *Virtual Reality, IEEE*, pages 104–111, Houston, TX, 1999.

[78] I. G. Polushin and H. J. Marquez. Stabilization of bilaterally controlled teleoperators with communication delay: an iss approach. *International Journal of Control*, 76(8):858 – 870, January. 2003.

[79] G. Raisbeck. A definition of passive linear networks in terms of time and energy. *Journal of Applied Physics*, 25(12):1510–1514, Dec 1954.

[80] R. Rakhsha and D. Constantinescu. Enhanced stability of three-users multirate distributed haptic cooperation via coordination to average peer position. In *The Fourth International Conference on Advances in Computer-Human Interactions, ACHI*, pages 136–141, Gosier, Guadeloupe, France, 2011.

[81] R. Rakhsha and D. Constantinescu. Distributed haptic cooperation with passive multirate wave communications. In *Haptics Symposium (HAPTICS), 2012 IEEE*, pages 117–123, March 2012.

[82] R. Rakhsha and D. Constantinescu. On distributed multirate control of direct user-to-user touch in networked haptic systems with passive wave-domain communications. *International Journal of Advanced Robotic Systems*, 9(52):1–10, 2012.

[83] R. Rakhsha and D. Constantinescu. Passive shared virtual environment for distributed haptic cooperation. In *Haptics Symposium (HAPTICS), 2014 IEEE*, pages 221–226, Feb 2014.

[84] R. Rakhsha and D. Constantinescu. Average-position coordination for distributed multiuser networked haptic cooperation. *Human-Robot Interaction*, to appear, 2015.

[85] J. H. Ryu, J. Artigas, and C Preusche. A passive bilateral control scheme for a teleoperator with time-varying communication delay. *Mechatronics*, 20(7):812 – 823, 2010.

[86] J. H. Ryu, Y. S. Kim, and B. Hannaford. Sampled- and continuous-time passivity and stability of virtual environments. *IEEE Transactions on Robotics*, 20(4):772–776, Aug 2004.

[87] J. H. Ryu, D. S. Kwon, and B. Hannaford. Stable teleoperation with time-domain passivity control. *IEEE Transactions on Robotics and Automation*, 20(2):365–373, 2004.

[88] J. H. Ryu and C. Preusche. Stable bilateral control of teleoperators under time-varying communication delay: Time domain passivity approach. In *IEEE International Conference on Robotics and Automation (ICRA)*, pages 3508–3513, April 2007.

[89] J. H. Ryu, C. Preusche, B. Hannaford, and G. Hirzinger. Time domain passivity control with reference energy following. *IEEE Transactions on Control Systems Technology*, 13(5):737–742, sept. 2005.

[90] M. S. Sadeghi, H. R. Momeni, and R. Amirifar. h_∞ and l_1 control of a teleoperation system via lmis. *Applied Mathematics and Computation*, 206(2):669 – 677, 2008.

[91] G. Sankaranarayanan and B. Hannaford. Virtual coupling schemes for position coherency in networked haptic environments. In *1st IEEE/RAS-EMBS International Conference on Biomedical Robotics and Biomechatronics*, pages 853–858, Pisa, Italy, 2006.

[92] G. Sankaranarayanan and B. Hannaford. Experimental comparison of internet haptic collaboration with time-delay compensation techniques. In *IEEE International Conference on Robotics and Automation*, pages 206–211, Pasadena, CA, may. 2008.

[93] G. Sankaranarayanan and B. Hannaford. Experimental internet haptic collaboration using virtual coupling schemes. In *Symposium on haptic interfaces for virtual environment and teleoperator systems*, pages 259–266, Reno, NE, 2008.

[94] C. Secchi, S. Stramigioli, and C. Fantuzzi. *Control of Interactive Robotic Interfaces*. Springer, 2007.

[95] A Shahdi and S. Sirouspour. Adaptive/robust control for time-delay teleoperation. *Robotics, IEEE Transactions on*, 25(1):196–205, Feb 2009.

[96] X. Shen, F. Bogsanyi, Liya Ni, and N.D. Georganas. A heterogeneous scalable architecture for collaborative haptics environments. In *The 2nd IEEE Internatioal Workshop on Haptic, Audio and Visual Environments and Their Applications*, pages 113–118, Ottawa, Ontario, 2003.

[97] S. Stramigioli, C. Secchi, A. J. vanderSchaft, and C. Fantuzzi. Sampled data systems passivity and discrete port-hamiltonian systems. *IEEE Transactions on Robotics*, 21(4):574 – 587, aug. 2005.

[98] H. Sugarman, E. Dayan, A. Weisel-Eichler, and J. Tiran. The jerusalem telerehabilitation system, a new, low-cost, haptic rehabilitation approach. *CyberPsychology & Behavior*, 9(2):178–182, 2006.

[99] H.G. Tanner, A. Jadbabaie, and G.J. Pappas. Flocking in fixed and switching networks. *IEEE Transactions on Automatic Control*, 52(5):863–868, May 2007.

[100] A. van der Schaft. *L_2-Gain and Passivity in Nonlinear Control*. Springer, 1999.

[101] Lode Vanacken, Joan De Boeck, and Karin Coninx. The phantom versus the falcon: Force feedback magnitude effects on user's performance during target acquisition. In Rolf Nordahl, Stefania Serafin, Federico Fontana, and Stephen Brewster, editors, *Haptic and Audio Interaction Design*, volume 6306 of *Lecture Notes in Computer Science*, pages 179–188. Springer Berlin Heidelberg, 2010.

[102] N. Yasrebi and D. Constantinescu. Centralized multi-user multi-rate haptic cooperation using wave transformation. In *International Conference on Mechatronics and Automation, ICMA*, pages 3816–3821, Aug 2009.

[103] N. Yasrebi and D. Constantinescu. Passive multirate wave communications for haptic interaction in slow virtual environments. *IEEE/ASME Transactions on Mechatronics*, 18(1):328–336, Feb 2013.

[104] Y. Yokokohji, T. Tsujioka, and T. Yoshikawa. Bilateral control with time-varying delay including communication blackout. In *10th Symposium on Haptic Interfaces for Virtual Environment and Teleoperator Systems*, pages 285–292, 2002.

[105] W. H. Zhu and S.E. Salcudean. Stability guaranteed teleoperation: an adaptive motion/force control approach. *IEEE Transactions on Automatic Control*, 45(11):1951 – 1969, nov. 2000.